Delivering Molecules to the Brain using Blood-Brain Barrier Modulators: Mechanism of Action and Activity of Cyclic and Linear Peptides from E-cadherin

By

Ahmed L. Alaofi

Submitted to the graduate degree program in Pharmaceutical Chemistry and the Graduate Faculty of the University of Kansas in partial fulfillment of the requirements for the degree of Doctor of Philosophy.

_____

Chairperson Teruna J. Siahaan

_____

Sue Lunte

_____

Cory Berkland

_____

Thomas Tolbert

_____

Krzysztof Kuczera

Date Defended: Nov.30.2015

The Dissertation Committee for Ahmed L. Alaofi

certifies that this is the approved version of the following dissertation:

Delivering Molecules to the Brain using Blood-Brain Barrier Modulators: Mechanism of Action and Activity of Cyclic and Linear Peptides from E-cadherin

_____

Chairperson Teruna Siahaan

Date approved: Nov.30.2015

Delivering Molecules to the Brain using Blood-Brain Barrier Modulators: Mechanism of Action and Activity of Cyclic and Linear Peptides from E-cadherin

Ahmed L. Alaofi

The University of Kansas, 2015

The goals of this work are to (a) compare the blood-brain barrier (BBB) modulatory activities of cyclic cHAVc3 (cyclo(1,6)Ac-CSHAVC-NH_2) and linear HAV4 (Ac-SHAVAS-NH_2) peptides, (b) compare the rat plasma stability of HAV4 and cHAVc3, and (c) probe the mechanism of binding of HAV peptides (i.e., HAV6, cHAVc3) and ADT peptides (i.e., ADTc5, ADTc7, ADTc9) to the EC1 domain of E-cadherin. The cyclic and linear HAV and ADT peptides were derived from the EC1 domain of human E-cadherin. Cyclic cHAVc3 was more effective than linear HAV4 in modulating MDCK cell monolayers and in improving in vivo brain delivery of Gd-DTPA upon i.v. administration in Balb/c mice. In vivo, the duration of the BBB modulation was longer for cyclic cHAVc3 (2–4 h) than for linear HAV4 (<1 h). Both HAV4 and cHAVc3 peptides also enhanced the in vivo brain delivery of IRdye800cw-PEG (25 kDa) as detected by near IR imaging. Cyclic cHAVc3 ($t_{1/2}$ = 12.95 h) has better plasma stability compared to linear HAV4 ($t_{1/2}$ = 2.4 h). Using 2D ^{1}H,-^{15}N-HSQC NMR, molecular dynamics, and molecular docking simulations, cyclic cHAVc3 peptide was shown to bind at residues Y36, S37, I38, I53, F77, S78, H79, and I94 on the EC1 domain of human E-cadherin. Using chemical shift perturbations of several residues, the

dissociation constants (K_d values) of cHAVc3 peptide to EC1 were estimated to be between 0.5×10^{-5} and 7.0×10^{-5} M. In summary, cyclic cHAVc3 peptide has better plasma stability and in vitro and in vivo activities to modulate BBB than linear HAV4 peptide. The proposed mechanism of modulatory activity of HAV and ADT peptides is due to binding to the EC1 domain of E-cadherin. Using NMR and molecular docking techniques, HAV and ADT peptides were found to bind to the EC1 domain and the binding site of HAV peptides in EC1 was different from ADT peptides. The ADT and HAV peptides bind to the EC1 domain with different affinities. ADTc5 and ADTc7 peptides showed lower dissociation constants (K_d ~ 10 μM) than ADTc9 peptide that showed a higher K_d values (K_d ~ 190 μM). HAV6 peptide showed similar binding site for cHAVc3 peptide on the EC1 domain with higher K_d values (K_d ~ 190 μM) in comparison to cHAVc3 peptide (K_d ~ 5 μM).

This Thesis Dedicated to:

My Father: Lafi Alaofi

My Wife: Noura Alharbi

My Sons: Ibrahim & Ziyad

ACKNOWLEDGMENTS

During my journey for seeking and completing my Ph.D. dissertation I am gratefully thankful for my advisor Dr. Teruna Siahaan for his guidance, his helpful suggestions, his righteous encouragements and his generously open door policy. I appreciate the opportunities that he provided to me to select and conduct my projects while he was always there for comments and corrections. I learned from him not only sciences, but also many helpful skills to be successful inside and outside the lab.

I would like to thank my dissertation committee members, Dr. Sue Lunte, Dr. Cory Berkland, Dr. Thomas Tolbert, and Dr. Krzysztof Kuczera for their helpful comments and suggestions. I appreciate and thank Dr. Berkland and Dr. Kuczera as the readers for my dissertation.

I am deeply thankful for Dr. Kuczera for his helpful comments, discussion and suggestions. I appreciate his generosity to allow me using his lab tools to finish and complete my projects. I am thankful for Siahaan's previous and current lab members for their great suggestions and helpful comments. I thank current lab members Dr. Paul Kiptoo, Dr. Mario and Kavisha. I am especially thankful for Dr. Kiptoo for his time, efforts, patience and suggestions that he provided to help me conducting my research experiments. I will always remember from him the discussion and right decisions that we have made to do the experiments successfully. I would like to thank Pharmaceutical Chemistry Department faculty, post docs, students and staff.

I would like to extend my thanks to King Saud University and Saudi Arabia Culture Mission (SACM) as they were my financial supportive during my graduate school.

Finally, I would like to thank my father and my family. My sincere thanks go for my father from my heart as he supported me to continue my graduate education. Noura Alharbi started early with me in this wonderful journey as a wife and later as a mother for my kids. I appreciate her support, her sacrificing, her kind assistance and her lovely statement " you can do it". Thank you Noura so much.

Table of Contents

Chapter 2: Comparison of Linear and Cyclic HAV Peptides in Modulating the Blood-Brain Barrier Permeability: Impact on Delivery of Molecules to the Brain

CHAPTER 1

Delivery to the Brain using Intercellular Junction Modulators and Prodrugs

1.1 The Biological Barriers to Delivery of Drugs to the Brain

1.1.1 The Blood Brain Barrier (BBB)

Many brain diseases are difficult to treat because it is challenging to deliver drugs to the brain. This is due to the presence of the blood–brain barrier (BBB), which restricts transport of drugs into the brain. The BBB in the human brain consists of microvessel endothelium with a surface area of approximately 20 m^2 [1]. The BBB acts as a physical, enzymatic, and transporter barrier to allow nutrients and prevent unwanted molecules from entering the brain [2-4]. Therefore, it is difficult to design and develop drugs that can readily enter the brain for pharmacological effects. To improve drug delivery to the brain, it is necessary to understand how drugs can cross the BBB. Drugs can pass through the BBB via the transcellular pathway by partitioning into the cell membranes of the BBB endothelial cells; the drugs then enter the cytoplasmic domain and cross into the brain [3, 5]. This route is limited by the presence of efflux pumps and/or poor physicochemical properties of the drugs. Alternatively, drugs can percolate through the paracellular pathways of the BBB; unfortunately, the paracellular (intercellular) pathways have tight junctions that limit the ability of molecules to cross the paracellular pathways [3, 5]. The blood–brain barrier presents physical, chemical and metabolic barriers to drugs entering the brain (Figure 1).

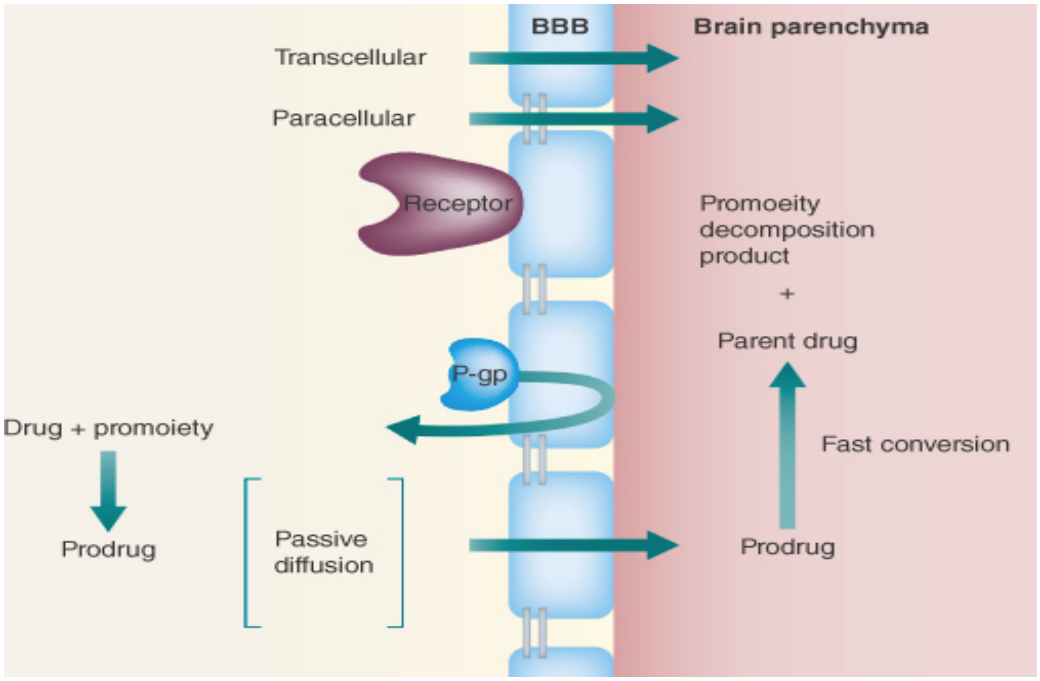

Figure 1. Drug molecules can enter the brain via paracellular and transcellular pathways. Paracellular (intercellular junction) pathway can be modulated by using synthetic intercellular junctions peptides such occludin, claudin and cadherin peptides. Transcellular passive diffusion can be modified or inhibited by efflux pumps (i.e., P-gp). Prodrugs have been used to improve the physicochemical properties of drugs for favorable passive diffusion through the BBB.

1.1.2 Intercellular Junction in Biological Barriers

1.1.2.1 Tight Junctions

The junctional complex in paracellular pathway of epithelial and endothelial cells responsible for the cell-cell adhesion function, maintain tissues integrity and

polarity. This complex is comprised of and aligned from apical to basolateral- tight junction (TJ), adherens junction, and desmosomes. The TJ are mediated by protein–protein interactions, including occludins, claudins, junctional adhesion molecules (JAM), and zonula occludins-1, -2 and -3. The TJ region, in paracellular pathway, works as a gate that controls the passage of molecules such as ions and maintains polarization of epithelial and endothelial cells by preventing the passive diffusion of lipids and proteins. Occludin and claudin are integral membrane proteins of the TJ working as a backbone for the TJ. The third integral membrane protein JAM suggested to be more important as a barrier regulator for T-cells during immune and inflammatory responses in epithelial and endothelial tissues [6, 7].

1.1.2.1.1 Tight Junction Structure

Occludin structure, a 62 kDa integral protein, showed two extracellular loops, four transmembrane domains with long C- and short N- termini intracellular domains [6]. Although occludin is known to be involved in the formation of TJ strands, some cells such as endothelial and non-neural tissues, can form tight-junction strands in gene knock out occludin that makes occludin function still unclear [8]. The claudin family consist of 24 members, 20-27 kDa, are involved in formation of TJ strands. Claudin structure as in occludin has two extracellular loops, four transmembrane domains and intracellular short C- and long N-termini. Claudin integral membrane proteins express more than two claudin species for TJ tightness. Claudin expression in different cells may vary based on claudin species and then their intercellular junction selectivity for

ions and their electrical resistance can vary. For example, in kidney almost all claudins were found and the transepithelial electrical resistance (TEER) values of nephron are low in proximal segments but in collecting duct of kidney TEER values are high that suggest different claudins can vary in their tightness. Moreover, claudins expression can be specific in some tissues such as claudin-5 is expressed specifically in endothelial cells of the blood vessels [8, 9]. JAM structure, 43 kDa protein belong to Ca^{2+} independent immunoglobulin family (IgG), has a single extracellular region consisting of two IgG domains linked by a disulfide bond (one domain form homophilic adhesion for adjacent cells), a one transmembrane domain and intracellular short C-terminus.

1.1.2.2 Adherens Junctions

Adherens junctions that are below the tight junctions are mediated by cadherins and nectins. Desmosomes are beneath the adherens junctions and connected by desmocollins and desmogleins. Classical cadherin proteins are Ca^{2+} dependent transmembrane glycoproteins that dimerize and cluster to mediate the cell-cell adhesion located in adhesion junctions. Cadherins are expressed specifically in different tissues such as epithelial (E-cadherin), neural (N-cadherin), placental (P-cadherin) and vascular endothelial (VE-cadherin) tissues [10]. In addition to cell adhesion function, cadherins are involved in other biological functions such as signaling in tissues, cell morphogenesis, migration, and cytoskeletal organization. For example, signaling can be explained by the ability of cadherins (via adhesion property) to bring membranes of

opposite cells in close to each other allowing induction of juxtacrine signaling and by maintaining the cells polarization [11].

1.1.2.2.1 Adherens Junctions Structure

Cadherins structure is composed of five extracellular domains (EC1–EC5) that mediate the adhesion function with homophilic interaction, a single transmembrane and intracellular conserved region that link cadherins to cytoplasmic proteins. For example, N- and E-cadherin intracellular region links to β-catenin and the latter links to α-catenin and then to actin cytoskeleton network to strength the adhesion of cadherins protein. Other catenins include p-120 catenin that is claimed to be responsible for lateral clustering of cis-dimer [10, 11].

1.1.2.2.2 Mechanism Action of Cadherin in the Formation and Maintaining the Integrity of the BBB

Different mechanisms have been proposed for homophilic cadherins interaction in extracellular domains (EC). For instance, zipper model for N-cadherin interaction suggests that N-terminus cis-dimer from one cell interact with N-terminus cis-dimer of opposing cell in a trans-interaction manner (i.e. EC1 domain from cis-dimer to EC1 domain from opposite cis-dimer) [12]. The monomeric E-cadherin of NMR experiments showed a similar cadherin interaction mechanism to the N-cadherin. The C-cadherin interaction can be trans-interaction but the EC1 from one cis-dimer of one cell interacts with EC2 domain cis-dimer from the opposite cell. Moreover, the C-cadherin show

trans-interaction involves more than one EC domains such as EC1 from one cell (A) to EC3 from opposite cell (B), EC2 (A) to EC2 (B), and EC3 (A) to EC1 (B) of cis-dimers (A and B) of the opposite cells [12, 13].

1.1.2.3 Desmosomal Cadherins

Desmosomal cadherins, similar to classical cadherins, have five extracellular domains that mediate the adhesion function with homophilic or heterophilic interactions. The desomosomal cadherins have two Ca^{2+} dependent subfamilies: desmocollin (DSC) and desmoglein (DSG) proteins. The adhesion mechanism for desmosome could be by trans-interaction of the adhesive surface of EC1 domains or N-terminal hydrophobic pocket for conserved residue Trp2 [14]. For adhesion function of desmosomes, at least DSC, DSG, and plakoglobin components are required. DSC and DSG showed basic extracellular domains of the classical cadherin. Both DSC and DSG peptides are required to block the desmosome adhesion, in contrast to E-cadherin as one E-cadherin peptide can block adhesion of E-cadherin. The desmosome plaques are associated with cytoskeleton intermediate filaments (IFs). The link between the cytoplasmic part of the desmosomes and IFs is complex with high-organized protein network. Based on tissues type there is specific IF system, for example, in epithelial tissue desmosomal cytoplasmic plaque bind to cytokeratin filaments while in cardiac tissues desmosomal cytoplasmic plaque bind to desmin filament. This suggests the cytoplasmic domain of desmosome participate in junctional formation [14, 15].

1.2 Using Synthetic Intercellular Junction Peptides to Enhance Drug Delivery via the Biological Barriers

1.2.1 The Disruption of Intercellular Junctions in the BBB

Many approaches used to improve drug delivery to the brain have been investigated with limited success such as disruption of the BBB (e.g. using pharmacological molecules) or non-disruption of the BBB methods (e.g. using prodrugs). There are many potential hydrophilic drugs such as peptides and proteins that cannot readily cross the BBB via the transcellular pathway due to their physicochemical properties (i.e., size, hydrogen-bond potential). One way to improve their delivery is to increase their permeation through the paracellular pathways of the BBB. The porosities of the paracellular pathways can be increased via disruption of the cell-cell adhesion in the intercellular junctions of the BBB. Peptides derived from occludins, claudins, and cadherins have been shown to improve delivery of drug and marker molecules through the BBB.

1.2.2 Cadherin Peptides

Cadherin peptides such as HAV- and ADT peptides derived from the extracellular domain of E-cadherin have been shown to disrupt the intercellular junctions of biological barriers in cell culture monolayers and in vivo models. HAV peptides improved the brain delivery of ^{14}C-mannitol and ^{3}H-daunomycin in an in-situ rat brain perfusion model [16]. In addition, the HAV- and ADT-peptides improved BBB

permeation of a magnetic resonance imaging (MRI) contrasting agent called gadolinium-diethylenetriaminopentaacetic (Gd-DTPA) in mouse and rat as detected by MRI.

1.2.3 Occludin Peptides

Occludin and claudin peptides have also been shown to improve delivery of marker and drug molecules through an in vitro model of the BBB as well as in in vivo animal models [17-21]. Occludin peptides derived from extracellular loops of occludin in TJ showed ability to perturb the TJ and enhance the paracellular flux for large molecules. OCC2 peptide represent second extracellular loop of occludin, able to perturb the A6 cell monolayer by decreasing their TEER values in a reversible manner and increase the flux of molecules of different sizes such as inulin (5.2 kDa) and dextran (40 kDa) [17]. Synthetic occludin peptides (OP) from extracellular loops with different sequence numbers showed ability to enhance the ^{14}C-mannitol using Caco-2 cell monolayer as a model [18]. For example, C1C2 peptide derived from occludin can improve the in vivo delivery of tetrodotoxin (TTX) and opioid peptide (DAMGO) through the BBB in the mouse model [20].

1.2.4 Claudin Peptides

The barrier function of claudins in TJ suggested to be more connected to TJ barrier permeability than occludins, as knock out occludins in some tissues did not change the TJ function. The modulation of claudins in TJ may result in toxic risks, as

claudins are target for bacterial toxin, for example, claudin-3 and -4 are targets for Clostridium Perfringens enterotoxin [18]. Based on claudin species, claudins derived peptidomimetics can be used either to enhance the permeability of the TJ or prevent unwanted viruses or toxin entry via TJ. For example, extracellular loop peptidomimetics of claudin-1 showed compromise the intestinal barrier in vitro and in vivo and a modified peptidomimetic (C1C2; Claudin-1^{58-81}) from same region of claudin-1 can reversibly decrease the TEER in Caco-2 cell monolayer and enhance the MOR-agonists DAMGO or morphine via blood-nerve barrier (BNB) for analgesic effects in in vivo model [22]. Differently, CL58 (MANAGLQLLGFILAFLGW) and CL59 (AFLGWIGAIVSTALPQWR) derived from N-terminus and first transmembrane regions of claudin-1 able to minimize the entry of hepatitis C virus (HIV) in in vitro model [23]. A synthetic peptides derived from second loop of extracellular domain of claudin-4 showed ability to prevent the action of Clostridium Perfringens enterotoxin in Caco-2 and in vivo models [24].

1.2.5 Effect of Cyclization on Peptides.

Conformational flexibility of linear peptides can be restricted through cyclization processes that might increase the biological activity of these peptides. The high affinity of cyclic peptides than linear analogues to receptors might be a result from better structural-activity relationships and more favorable entropic effects or increasing in the cyclic peptides biological rigidity [25]. Cyclic peptides gain more structural rigidity in comparison to linear analogues that may enhance their stability against proteolytic

enzymes [26, 27]. Peptides or peptide analogues can be cyclized (intermolecular cyclization) by different methods such as making a disulfide bond between two thiol groups in cysteine residues, an amide bond between C-terminus and N-terminus or a lactam bridge between aspartic or glutamic acid and lysine residues. Moreover, the disulfide bridge that can be made by oxidizing thiol groups of the cysteine residues occur naturally in proteins or peptides (e.g. insulin and somatostatin) [27, 28].

1.3 Mechanism of Action of Agents used to Modulate the BBB and Improve the Delivery of Molecules through the BBB

1.3.1 Binding Studies of Peptides and Proteins

The cell macromolecular components such as proteins are responsible and/or involved in many biological functions of the cells. The biological interaction process of ligands to proteins may affect on the biological activity of these proteins as some of the pharmacological actions occur by binding between ligands and their receptors (i.e. proteins) [29, 30]. Exploring ligands interaction to proteins may serve as a basis to design bioactive molecules, evaluate the ligands binding affinity to their receptors and understanding the proteins biological activity. For example, the interruption of protein-protein interaction by peptides (ligands) can help to understand the biological function of these proteins. Another example, the binding affinity studies usually aims to evaluate ligands affinity to their receptors and analyze receptor-ligands mechanism interaction [29]. One of the fundamental binding studies is the saturation binding assays as

dissociation constant at equilibrium is evaluated by a series of ligand concentrations titrated against its receptor. Competition binding assays are used to evaluate the cooperativity between two ligands to a receptor [29].

1.3.2 Methods

There are numerous experimental methods to study the binding assays as some of them use labeled ligand or receptors either by radioactive, fluorophores, chromophores or isotopes labeling and the other methods do not need to label ligands or receptors to perform the assay.

1.3.2.1 NMR Technique

Nuclear magnetic resonance (NMR) spectroscopy is a fast and a powerful technique to study intermolecular interactions (e.g. receptor-ligand) due to different NMR parameters like chemical shifts, linewidths, coupling constants and signal intensities are sensitive for nuclei environment. In addition, NMR can measure one or more NMR parameters for the binding action as nuclei, residues or secondary structure of proteins can be affected. The 1D NMR resolution spectra can be improved by using one or two of NMR active isotopes such as ^{13}C, ^{15}N, ^{19}F or ^{31}P for 2D or 3D-NMR assays [31].

1.3.2.2 Other Techniques

Radioreceptor assays (RRA) require labeling ligands with radioactive isotopes such as ^{3}H, ^{125}I or ^{32}P. Although RRA provides sensitivity and specificity, it uses a hazardous labeling while fluorescence resonance energy transfer (FRET) requires a non-radioactive labeling (fluorophore labeling). Isothermal titration calorimetry (ITC) and optical biosensors are binding assays methods that do not require labeling for either ligands or receptors [32]. In addition to energetics and kinetics information that can be provided by pervious binding assays methods, NMR and X-ray spectroscopies can provide spatial arrangement of the receptor-ligand complex, which is important to identify binding sites and how receptors, for example proteins, structures can be altered and changed.

1.4 Other Strategies used to Improve Delivery of Drugs to the Brain

1.4.1 Clinical Methods

1.4.1.1 Osmotic modifiers

Hypertonic mannitol solution can disrupt the BBB. Studies have shown 25% hyperosmolar mannitol solution or hyperosmolar solutions of arabinose, and lactamide can be used to temporarily modify the BBB permeability and improve delivery of drug molecules.

1.4.1.2 Intracerebral implantation

One of the direct methods to bypass or avoid the BBB is to implant biodegradable polymers contain drugs in brain tissues (brain parenchyma) that give a sustain release for drugs in brain tissues. For example Gliadel wafers used for delivering chemotherapeutic agents to treat recurrence glioma brain cancer [33].

1.4.2 Prodrugs

Hydrophobic drugs can cross the BBB via the transcellular pathway because they can partition to cell membranes [3, 34]. In contrast, hydrophilic drugs cannot cross the BBB because they cannot readily partition into the cell membranes [35]. To improve the transcellular permeation of hydrophilic drugs, their physicochemical properties have to be altered and make them more lipophilic with lower hydrogen-bonding potential to favor membrane partition. Pardridge et al. proposed that there is a relationship between BBB transport and H-bond potential and/or membrane partition coefficient (PC; i.e., 1-octanol/Ringer's buffer PC) [36]. For example, progesterone (PC = 1800) with two potential hydrogen bonds (H bonds) has higher BBB permeation than cortisol (PC = 35), which has eight potential H bonds [36]. It was suggested that each pair of hydrogen bonds in a given molecule could decrease BBB permeation by 1 log unit [4]. Later, the rule of five was proposed by Lipinski in an attempt to predict successful delivery of drugs through the biological barriers; this is based on H-bond potential, molecular weight and logP value [37]. Drug molecules with more than five H-bond donors, ten H-bond acceptors, a molecular weight >500 and a logP of 5 are less likely to be absorbed

and/or penetrate the biological barriers [37][10]. Hydrophobic molecules with a high molecular weight such as epipodophyllotoxin (MW: 588 Da) and vincristine (MW: 842 Da) exhibit low brain uptake [38].

The formation of a prodrug is one way to alter the physicochemical properties of a drug to increase transcellular passive diffusion [34]. In this case, the charged and/or polar functional group on the drug can be transiently masked with ester, amide or acetylated groups in the prodrug (Figure 1) [34, 39]. The expectation is that the prodrug can be converted back to the parent drug by enzymatic and/or chemical reaction within the CNS to produce the desired biological activity [39]. Many ester prodrugs have been developed to improve brain delivery of drugs; the abundance of esterase enzymes in tissues can readily convert the prodrug to drug to exhibit biological activity. Heroin is a classic example of a morphine prodrug in which the OH groups in morphine are derivatized with acetyl esters. This derivatization gives heroin higher lipophilicity than morphine. Enhancement of morphine lipophilicity by masking OH groups with acetyl ester gives heroin a brain uptake that is 100-fold higher than morphine, thus a higher potency of heroin compared with that of morphine [39]. A similar idea has been attempted in which one of the OH groups in morphine is converted to methyl ethers – this generates codeine and its brain delivery increased tenfold compared with morphine. Both heroin and codeine can be converted to morphine by enzymes in the brain parenchyma [39]. In another example, mouse brain uptake of the phenyl ester prodrug of nipecotic acid is enhanced compared with that of the parent nipecotic acid

(Figure 2) [40]. Similarly, acetorphan, an ester prodrug of thiorphan (enkephalinase inhibitor), more effectively crosses the BBB than thiorphan (Figure 2) [41]. Upon delivering acetorphan, the parent thiorphan was detected in the rat brain, suggesting that the ester prodrug was converted to the drug in the brain [41]. The brain delivery of peptides is also hampered by the presence of the BBB because peptides have physicochemical properties that are not conducive to partitioning to cell membranes for transcellular delivery [35]. Some peptides have charges at the N- and C-termini, and most peptides have a high hydrogen-bonding potential to water molecules. To improve delivery of peptides through the BBB, their physicochemical properties have to be altered to favor membrane partition. One way to alter the physicochemical properties is to form cyclic peptide prodrugs (Figure 3). By increasing lipophilicity, lowering hydrogen-bonding potential, lowering hydrodynamic radii and increasing secondary structure, the formation of cyclic prodrugs of opioid peptides [35] and RGD peptidomimetics [42, 43] has been shown to increase transport though the biological barriers compared with that of their parent peptides or peptidomimetics. The cyclic peptide prodrugs can be converted to the parent opioid peptide or RGD peptidomimetic by esterases. In some cases, the formation of cyclic peptide prodrugs can also cause recognition by efflux pumps in the biological barriers; this is due to the recognition of the chemical linker or the promoiety by the efflux pumps [44]. Important considerations for blood-to-brain transport of prodrugs are the rate of prodrug-to-drug conversion and the site-selective conversion. This bioconversion in the brain tissues

should be fast to allow accumulation or trapping of the parent drug in the brain [39]. By contrast, the prodrug-to-drug bioconversion should be slow in the blood to maintain a high blood concentration of the prodrug for crossing the BBB. For therapeutic activity in the brain, sufficient pharmacological concentration of the parent drug in the brain is required; thus, the clearance rate of the prodrug should be close to the rate of bioconversion in the brain [39]. The chemical delivery system (CDS) is derived from a prodrug technology and it is a conjugate between a targeting moiety (T) and the drug (D) to make a T–D conjugate [45]. The chemical delivery system uses a redox conversion system as a chemical pathway to trap the T–D conjugate in the brain. The targeting moiety increased the lipophilicity of the T–D conjugate to enhance transcellular transport across the BBB. After entering the brain, the T in T–D is converted by metabolic enzyme to a charged moiety T to give a T–D conjugate. The concentration gradient drives the T–D conjugates to cross the BBB and metabolic conversion in the brain produces T–D conjugates. Because the T–D conjugate cannot partition to BBB cell membranes, the conjugate is trapped and accumulated in the brain. Finally, another enzyme reaction converts T–D to release the D and T.

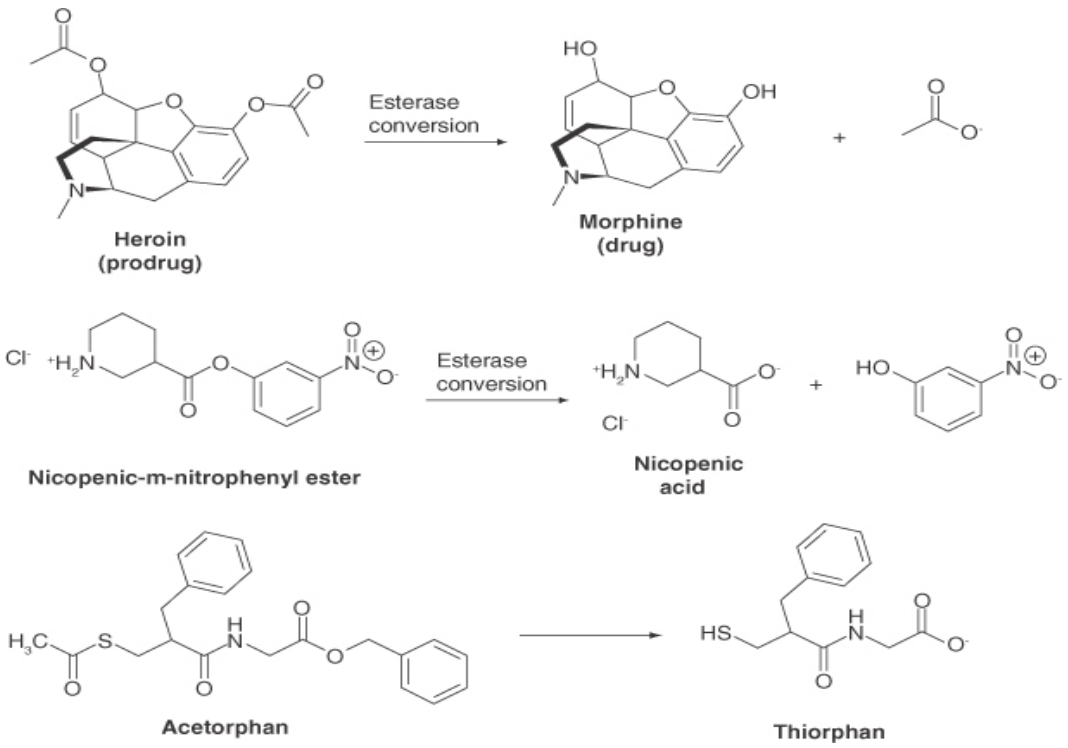

Figure 2. Formation of ester prodrugs to improve blood–brain barrier membrane permeation of morphine, nipecotic acid and thiorphan. The alcohol group of morphine was acetylated to make heroin, which is a 100-fold greater ability to permeate the blood–brain barrier than morphine. The carboxylic acid of nipecotic acid was converted to phenyl ester with m-nitrophenol to increase its blood–brain barrier permeation. The esters can be converted to their parent drugs by esterases in the brain. Acetorphan, the phenyl and acetyl ester prodrug of thiorphan, is able to cross the blood–brain barrier; the parent drug thiorphan is released and detected in the brain after crossing the blood–brain barrier.

1.4.3 Efflux transporters and their inhibition

Although the increase in lipophilicity of a prodrug increases brain uptake, the increase in lipophilicity can also affect the pharmacokinetic properties of the drug. The increase in lipophilicity can lower the plasma concentration owing to the increase protein binding and/or drug uptake by peripheral tissues. Therefore, lowering the plasma concentration can then proportionally decrease the drug brain uptake [46]. Additionally, increasing lipophilicity may increase recognition by efflux pumps such as P-glycoprotein (P-gp) receptors [47]. The energy dependent ATP-binding cassette family of efflux transporters (i.e., P-gp and MRPs) are localized at the BBB endothelial cells and prevent drug molecules from entering the brain [48]. P-gp efflux pumps have broad structural recognition, and one potential way to avoid P-gp recognition is to remove the P-gp recognition feature(s) on the drug when designing it [48]. However, this is difficult to accomplish without altering the biological activity of the drug. A prodrug method has been investigated to mask the functional group(s) that is responsible for P-gp recognition [39]. One option for overcoming the efflux transporters is utilizing P-gp inhibitors such as verapamil. Drug co-administration with inhibitors can enhance drug permeation into the brain [39, 48, 49]. It should be noted that these inhibitors could induce side effects. As an example, because verapamil is a calcium channel blocker for treatment of hypertension, its use for blocking P-gp to enhance BBB drug delivery may generate side effects caused by blocking the calcium channel. It should be noted that efflux transporters play an important role in clearing brain

metabolites and toxic molecules from the brain; therefore, prolonged treatment with the efflux inhibitors may lead to unfavorable side effects [48]. A better way to use a P-gp inhibitor is by designing out the other biological activity. A good example of this is cyclosporine D; it inhibits P-gp without immunosuppressive activity. By contrast, cyclosporine A has both immunosuppressive activity and efflux pump inhibitory activity [50, 51]. Recently, a dimer prodrug of an HIV protease inhibitor (abacavir) was designed to inhibit P-gp as well as to increase BBB drug permeation for treating accumulated HIV in the brain [52]. The abacavir dimer was conjugated via a disulfide bond through a promoiety that can release the abacavir after reduction of the disulfide bond (**Figure 4**). The rationale to form a dimer was that P-gp has multiple substrate recognition sites. The idea is that each unit of the dimer fills two different sites on P-gp to effectively block its activity while allowing the unbound dimer molecules to penetrate the BBB. The hope is that after the dimer prodrug enters the brain it can be converted to a monomer upon reduction of the disulfide bond. The abacavir dimer improved the uptake of NBD-abacavir, calcein-AM, and I-iodoarylazidoprazosin in T-lymphoblastiod cells that have overexpression of P-gp. This suggests that the abacavir dimer binds to P-gp. The concept of prodrug dimers has been used in galantamine [53] for potential treatment of Alzheimer's disease; its mechanism of action to block P-gp was evaluated in a cell culture system similar to that of the abacavir dimer.

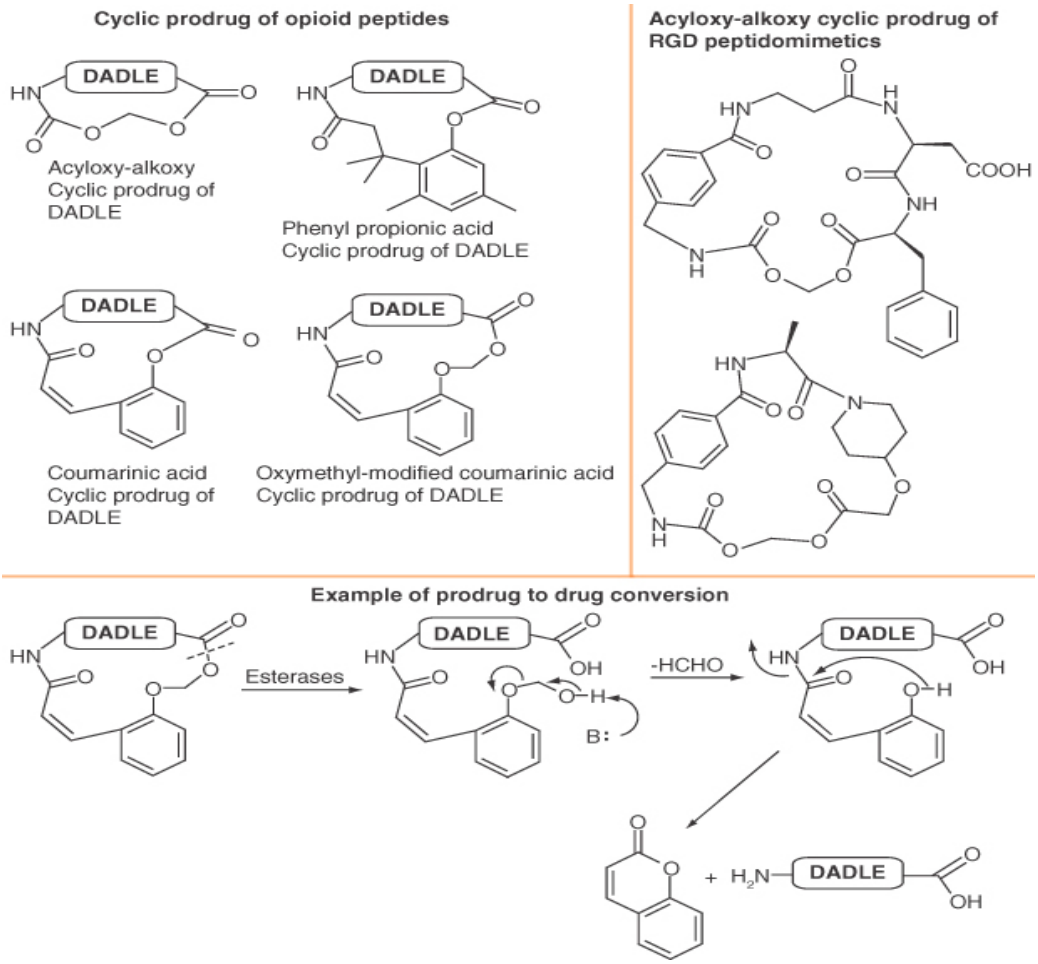

Figure 3. The cyclic prodrugs were formed using acyloxy-alkoxy, phenyl propionic acid, coumarinic acid and oxymethyl-modified coumarinic acid promoieties. The prodrugs can be converted to the parent drugs upon esterase cleavage reaction followed by chemical reactions. DADLE: (D-Ala, D-Leu) Enkephalin

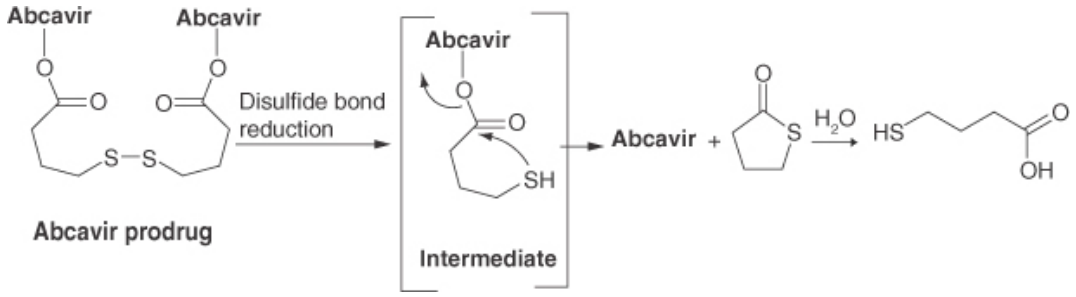

Figure 4. The conversion of the abacavir dimer prodrug for effective inhibition of P-glycoprotein to improve delivery of abacavir into thebrain. The dimer can be converted into the abacavir monomer upon reduction of the disulfide bond followed by a cyclization reaction of the promoiety.

1.4.4 Utilizing carrier-mediated transport system

Most nutrients (i.e., glucose, mannose, amino acids, nucleosides and vitamins) that are essential for the brain are polar molecules that cannot pass through the BBB via passive diffusion. These nutrients utilize specific transporter(s) at both the luminal and abluminal sides of the BBB for their entry into the brain [39, 54, 55]. These transporters have been exploited to enhance drug delivery into the brain [54, 56]. A large neutral amino acid transporter (LAT1) [57-59] and a glucose transporter (GLUT1) [60-62] have been used to transport drugs across the BBB by conjugating the drug to an amino acid or glucose, respectively (Figure 5) [39, 56, 63]. Conjugates of ketoprofen and indomethacin with D-glucose were transported by GLUT1 receptors across biological barriers [61]. Ketoprofen-lysine and 6-mercaptopurine-L-Cys were used to target LAT1 transporters for improving brain delivery of ketoprofen and 6-mercaptopurine,

respectively (Figure 5) [57, 58]. An in situ rat brain perfusion study showed that the ketoprofen-lysine prodrug crossed the BBB via a LAT1-mediated transport mechanism. 6-mercaptopurine-L-Cys can also inhibit the cellular uptake of C-L-Leu, a substrate for LAT1 transporters; this suggests that LAT1 transporters mediate the uptake of 6-mercaptopurine-L-Cys. Similarly, acyclovir and zanamivir were linked to valine to give valacyclovir and Zan-L-Val prodrugs, and they have been shown to cross the intestinal mucosa barrier utilizing an hPepT1 receptor [64, 65].

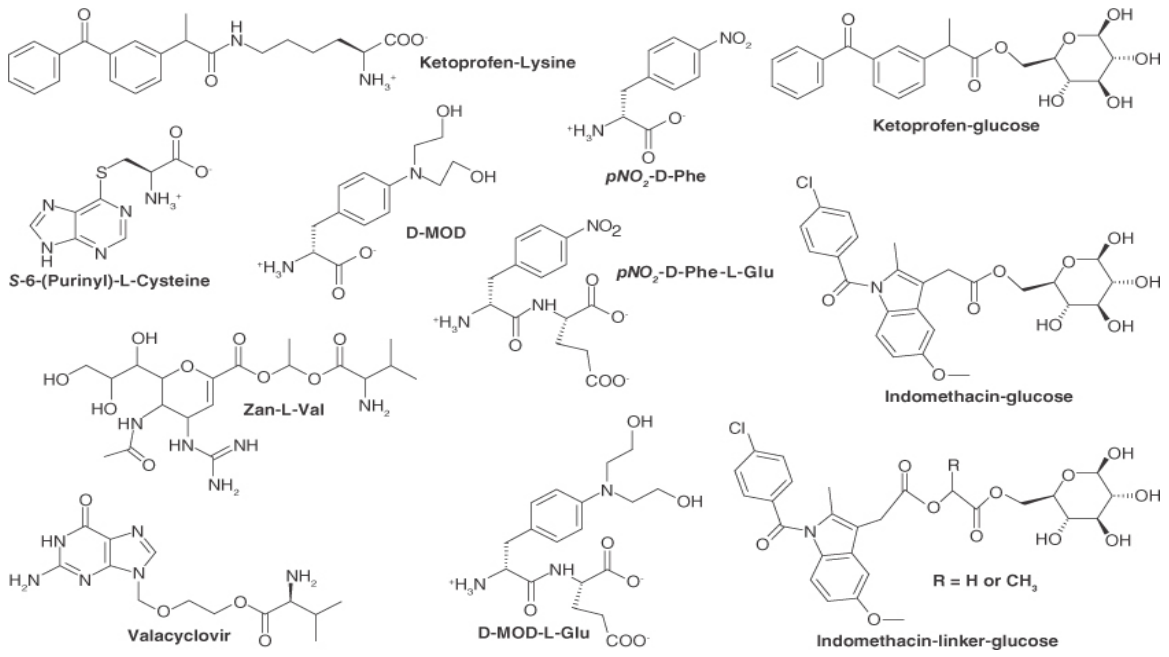

Figure 5. The formation of prodrugs with ligands to target cell surface receptors such as amino acid and glucose transporters Some of the prodrugs have a linker between the drug and targeting ligand as shown in Zan-L-Val, valacyclovir and indomethacin-linker-glucose. Some prodrugs, such as ketoprofen-lysine, S-6-(purinyl)-L-cysteine,

pNO2-Phe-L-Glu, d-MOD-L-Glu, ketoprofen-glucose and indomethacin-glucose,have a direct connection between the drug and targeting ligand.

1.5. Thesis and Chapters Goals

1.5.1 Overall goals of the thesis

The overall goals of the thesis are to deliver marker, diagnostic or drug molecules to the brain by modulating the BBB using synthetic cadherin peptides, understand how might these modulator peptides can work, bind and evaluate their affinity to first domain of E-cadherin.

1.5.2 Chapter 2

The goal of this project is to make more active and stable synthetic cadherin peptides for the BBB modulating purposes by cyclization linear synthetic cadherin peptides that showed modulation activity in different BBB models. The cyclic HAV (cHAVc3) peptide showed better activity and stability than linear HAV (HAV4) peptide for enhancing marker molecules delivery to the brain using in vitro and in vivo models of the BBB.

1.5.3 Chapter 3

The goals of this project are to probe cHAVc3 peptide interaction with EC1 domain of human E-cadherin by determining the affinity and potential binding sites of cHAVc3 peptide to the EC1 domain using NMR and moleucular modeling (i.e.,

molecular dynamics and molecular docking simulations). Cyclic cHAVc3 peptide binds to residues F77, S78 on EC1 with intermediate dissociation constant (0.5–7.0 X 10^{-5} M).

1.5.4 Chapter 4

The goals of this project are to investigate the binding sites and dissociation constants (K_d) for ADT and HAV peptides (synthetic cadherin peptides) using docking technique and NMR data. The binding sites of three ADT peptides on the EC1 domain are approximately in one region while HAV6 peptide showed binding to a different region, which was around to the binding region of cyclic HAVc3 site. Although these synthetic cadherin peptides fall in weak binding range to EC1 domain, ADTc7 and ADTc5 peptides showed higher in binding affinity ten times than ADTc9 and HAV6 peptides.

1.6 References

1. Zlokovic, B.V., *The blood-brain barrier in health and chronic neurodegenerative disorders.* Neuron, 2008. **57**(2): p. 178-201.
2. Vlieghe, P. and M. Khrestchatisky, *Medicinal chemistry based approaches and nanotechnology-based systems to improve CNS drug targeting and delivery.* Med Res Rev, 2013. **33**(3): p. 457-516.
3. Gabathuler, R., *Approaches to transport therapeutic drugs across the blood-brain barrier to treat brain diseases.* Neurobiol Dis, 2010. **37**(1): p. 48-57.
4. Pardridge, W.M., *Blood-brain barrier delivery.* Drug Discov Today, 2007. **12**(1-2): p. 54-61.
5. Zheng, K., M. Trivedi, and T.J. Siahaan, *Structure and function of the intercellular junctions: barrier of paracellular drug delivery.* Curr Pharm Des, 2006. **12**(22): p. 2813-24.
6. Furuse, M., et al., *Overexpression of occludin, a tight junction-associated integral membrane protein, induces the formation of intracellular multilamellar bodies bearing tight junction-like structures.* Journal of Cell Science, 1996. **109**(2): p. 429-435.
7. Denker, B.M. and S.K. Nigam, *Molecular structure and assembly of the tight junction.* American Journal of Physiology-Renal Physiology, 1998. **274**(1): p. F1-F9.
8. Tsukita, S., M. Furuse, and M. Itoh, *Multifunctional strands in tight junctions.* Nature Reviews Molecular Cell Biology, 2001. **2**(4): p. 285-293.

9. Gonzalez-Mariscal, L., et al., *Tight junction proteins.* Progress in biophysics and molecular biology, 2003. **81**(1): p. 1-44.

10. Provost, E. and D.L. Rimm, *Controversies at the cytoplasmic face of the cadherin-based adhesion complex.* Curr Opin Cell Biol, 1999. **11**(5): p. 567-72.

11. Angst, B.D., C. Marcozzi, and A.I. Magee, *The cadherin superfamily: diversity in form and function.* J Cell Sci, 2001. **114**(Pt 4): p. 629-41.

12. van Roy, F. and G. Berx, *The cell-cell adhesion molecule E-cadherin.* Cell Mol Life Sci, 2008. **65**(23): p. 3756-88.

13. Koch, A.W., K.L. Manzur, and W. Shan, *Structure-based models of cadherin-mediated cell adhesion: the evolution continues.* Cell Mol Life Sci, 2004. **61**(15): p. 1884-95.

14. Garrod, D.R., A.J. Merritt, and Z. Nie, *Desmosomal cadherins.* Curr Opin Cell Biol, 2002. **14**(5): p. 537-45.

15. Huber, O., *Structure and function of desmosomal proteins and their role in development and disease.* Cell Mol Life Sci, 2003. **60**(9): p. 1872-90.

16. Kiptoo, P., et al., *Enhancement of drug absorption through the blood-brain barrier and inhibition of intercellular tight junction resealing by E-cadherin peptides.* Molecular pharmaceutics, 2011. **8**(1): p. 239-49.

17. Wong, V. and B.M. Gumbiner, *A synthetic peptide corresponding to the extracellular domain of occludin perturbs the tight junction permeability barrier.* J Cell Biol, 1997. **136**(2): p. 399-409.

18. Tavelin, S., et al., *A new principle for tight junction modulation based on occludin peptides.* Mol Pharmacol, 2003. **64**(6): p. 1530-40.

19. Deli, M.A., *Potential use of tight junction modulators to reversibly open membranous barriers and improve drug delivery.* Biochim Biophys Acta, 2009. **1788**(4): p. 892-910.

20. Zwanziger, D., et al., *A peptidomimetic tight junction modulator to improve regional analgesia.* Mol Pharm, 2012. **9**(6): p. 1785-94.

21. Zwanziger, D., et al., *Claudin-derived peptides are internalized via specific endocytosis pathways.* Ann N Y Acad Sci, 2012. **1257**: p. 29-37.

22. Sauer, R.S., et al., *Safety, efficacy, and molecular mechanism of claudin-1-specific peptides to enhance blood-nerve-barrier permeability.* J Control Release, 2014. **185**: p. 88-98.

23. Si, Y., et al., *A human claudin-1-derived peptide inhibits hepatitis C virus entry.* Hepatology, 2012. **56**(2): p. 507-15.

24. Shrestha, A., et al., *A synthetic peptide corresponding to the extracellular loop 2 region of claudin-4 protects against Clostridium perfringens enterotoxin in vitro and in vivo.* Infect Immun, 2014. **82**(11): p. 4778-88.

25. Cala, O., F. Guilliere, and I. Krimm, *NMR-based analysis of protein-ligand interactions.* Anal Bioanal Chem, 2014. **406**(4): p. 943-56.

26. Ehrlich, A., et al., *Synthesis of cyclic peptides via efficient new coupling reagents.* Tetrahedron letters, 1993. **34**(30): p. 4781-4784.

27. Davies, J.S., *The cyclization of peptides and depsipeptides.* Journal of Peptide Science, 2003. **9**(8): p. 471-501.

28. Li, P. and P.P. Roller, *Cyclization strategies in peptide derived drug design.* Current topics in medicinal chemistry, 2002. **2**(3): p. 325-341.

29. Hulme, E.C. and M.A. Trevethick, *Ligand binding assays at equilibrium: validation and interpretation.* British journal of pharmacology, 2010. **161**(6): p. 1219-1237.

30. de Jong, L.A., et al., *Receptor-ligand binding assays: technologies and applications.* J Chromatogr B Analyt Technol Biomed Life Sci, 2005. **829**(1-2): p. 1-25.

31. Salvatella, X. and E. Giralt, *NMR-based methods and strategies for drug discovery.* Chem Soc Rev, 2003. **32**(6): p. 365-72.

32. Gesellchen, F., B. Zimmermann, and F.W. Herberg, *Direct optical detection of protein-ligand interactions.* Methods Mol Biol, 2005. **305**: p. 17-46.

33. Begley, D.J., *Delivery of therapeutic agents to the central nervous system: the problems and the possibilities.* Pharmacol Ther, 2004. **104**(1): p. 29-45.

34. Pathan, S.A., et al., *CNS drug delivery systems: novel approaches.* Recent Pat Drug Deliv Formul, 2009. **3**(1): p. 71-89.

35. R, T.B., et al., *Improvement of oral peptide bioavailability: Peptidomimetics and prodrug strategies.* Adv Drug Deliv Rev, 1997. **27**(2-3): p. 235-256.

36. Pardridge, W.M. and L.J. Mietus, *Transport of steroid hormones through the rat blood-brain barrier. Primary role of albumin-bound hormone.* J Clin Invest, 1979. **64**(1): p. 145-54.

37. Lipinski, C.A., et al., *Experimental and computational approaches to estimate solubility and permeability in drug discovery and development settings.* Adv Drug Deliv Rev, 2001. **46**(1-3): p. 3-26.

38. Levin, V.A., *Relationship of octanol/water partition coefficient and molecular weight to rat brain capillary permeability.* J Med Chem, 1980. **23**(6): p. 682-4.

39. Rautio, J., et al., *Prodrug approaches for CNS delivery.* AAPS J, 2008. **10**(1): p. 92-102.

40. Nassereddine-Sebaei, M., et al., *Determination of m-nitrophenol and nipecotic acid in mouse tissues by high-performance liquid chromatography after administration of the anticonvulsant m-nitrophenyl-3-piperidinecarboxylate hydrochloride.* J Pharm Sci, 1993. **82**(1): p. 39-43.

41. Lecomte, J.M., et al., *Pharmacological properties of acetorphan, a parenterally active "enkephalinase" inhibitor.* J Pharmacol Exp Ther, 1986. **237**(3): p. 937-44.

42. Wang, W., R.T. Borchardt, and B. Wang, *Orally active peptidomimetic RGD analogs that are glycoprotein IIb/IIIa antagonists.* Curr Med Chem, 2000. **7**(4): p. 437-53.

43. He, H.T., et al., *Syntheses of cyclic prodrugs of RGD peptidomimetics with various macrocyclic ring sizes: evaluation of physicochemical, transport and antithrombic properties.* J Pept Res, 2003. **61**(6): p. 331-42.

44. Ouyang, H., et al., *A comparison of the effects of p-glycoprotein inhibitors on the blood-brain barrier permeation of cyclic prodrugs of an opioid peptide (DADLE).* J Pharm Sci, 2009. **98**(6): p. 2227-36.

45. Bodor, N. and P. Buchwald, *Recent advances in the brain targeting of neuropharmaceuticals by chemical delivery systems.* Adv Drug Deliv Rev, 1999. **36**(2-3): p. 229-254.

46. Vytla, D., et al., *Prodrug approaches to reduce hyperexcitation in the CNS.* Adv Drug Deliv Rev, 2012. **64**(7): p. 666-85.

47. Pavan, B., et al., *Progress in drug delivery to the central nervous system by the prodrug approach.* Molecules, 2008. **13**(5): p. 1035-65.

48. Sun, H., et al., *Drug efflux transporters in the CNS.* Adv Drug Deliv Rev, 2003. **55**(1): p. 83-105.

49. Taylor, E.M., *The impact of efflux transporters in the brain on the development of drugs for CNS disorders.* Clin Pharmacokinet, 2002. **41**(2): p. 81-92.

50. Boote, D.J., et al., *Phase I study of etoposide with SDZ PSC 833 as a modulator of multidrug resistance in patients with cancer.* J Clin Oncol, 1996. **14**(2): p. 610-8.

51. Boesch, D., et al., *Restoration of daunomycin retention in multidrug-resistant P388 cells by submicromolar concentrations of SDZ PSC 833, a nonimmunosuppressive cyclosporin derivative.* Exp Cell Res, 1991. **196**(1): p. 26-32.

52. Namanja, H.A., et al., *Toward eradicating HIV reservoirs in the brain: inhibiting P-glycoprotein at the blood-brain barrier with prodrug abacavir dimers.* J Am Chem Soc, 2012. **134**(6): p. 2976-80.

53. Namanja, H.A., et al., *Inhibition of human P-glycoprotein transport and substrate binding using a galantamine dimer.* Biochem Biophys Res Commun, 2009. **388**(4): p. 672-6.

54. Pardridge, W.M., *Blood-brain barrier transport of nutrients.* Nutr Rev, 1986. **44 Suppl**: p. 15-25.

55. Pardridge, W.M., *Blood-brain barrier transport of glucose, free fatty acids, and ketone bodies.* Adv Exp Med Biol, 1991. **291**: p. 43-53.

56. Anderson, B.D., *Prodrug approaches for drug delivery to the brain*, in *Prodrugs*. 2007, Springer. p. 573-651.

57. Gynther, M., et al., *Brain uptake of ketoprofen-lysine prodrug in rats.* Int J Pharm, 2010. **399**(1-2): p. 121-8.

58. Killian, D.M., S. Hermeling, and P.J. Chikhale, *Targeting the cerebrovascular large neutral amino acid transporter (LAT1) isoform using a novel disulfide-based brain drug delivery system.* Drug Deliv, 2007. **14**(1): p. 25-31.

59. Peura, L., et al., *Design, Synthesis and Brain Uptake of LAT1-Targeted Amino Acid Prodrugs of Dopamine.* Pharm Res, 2013.

60. Cornford, E.M. and S. Hyman, *Localization of brain endothelial luminal and abluminal transporters with immunogold electron microscopy.* NeuroRx, 2005. **2**(1): p. 27-43.

61. Gynther, M., et al., *Glucose promoiety enables glucose transporter mediated brain uptake of ketoprofen and indomethacin prodrugs in rats.* J Med Chem, 2009. **52**(10): p. 3348-53.

62. Tserentsoodol, N., et al., *Immunolocalization of tight junction proteins, occludin and ZO-1, and glucose transporter GLUT1 in the cells of the blood-nerve barrier.* Arch Histol Cytol, 1999. **62**(5): p. 459-69.

63. Pardridge, W.M., R.J. Boado, and C.R. Farrell, *Brain-type glucose transporter (GLUT-1) is selectively localized to the blood-brain barrier. Studies with quantitative western blotting and in situ hybridization.* J Biol Chem, 1990. **265**(29): p. 18035-40.

64. Landowski, C.P., et al., *Gene expression in the human intestine and correlation with oral valacyclovir pharmacokinetic parameters.* J Pharmacol Exp Ther, 2003. **306**(2): p. 778-86.

65. Gupta, S.V., et al., *Enhancing the intestinal membrane permeability of zanamivir: a carrier mediated prodrug approach.* Mol Pharm, 2011. **8**(6): p. 2358-67.

CHAPTER 2

Comparison of Linear and Cyclic HAV Peptides in Modulating the Blood-Brain Barrier Permeability: Impact on Delivery of Molecules to the Brain

2.1 Introduction

It is challenging to treat brain diseases such as Alzheimer's and Parkinson's and brain tumors because drugs used to treat these disorders have difficulty in crossing the blood-brain barrier (BBB) [1-3]. The microvascular endothelial cells of the brain have tight junctions that limit paracellular diffusion [3] and there are various efflux transport proteins (P-glycoprotein, breast cancer resistance protein, multidrug resistance-associated proteins) and metabolic enzymes that reduce transcellular routes of entry to the brain [4-6]. To cross the BBB, the drug molecule must have optimal physicochemical properties; for example, many large molecules such as peptides and proteins cannot readily cross the BBB due to their size and hydrophilicity [1, 3, 7]. For example, nerve growth factor (NGF) and brain derived neurotrophic factor (BDNF) have been investigated to treat neurodegenerative diseases [8-13]. Unfortunately, as with other proteins, the brain delivery of NGF and BDNF is challenging. Therefore, there is a need for safe and effective methods to improve the delivery of proteins and peptides to the brain.

Modulation of the BBB paracellular pathway is one way to improve brain delivery of proteins and peptides. Blood-brain barrier modulation can be achieved in a variety of different ways; one example is the use of vasoactive agents (i.e., bradykinin, bradykinin analogs, histamine, lysophosphatidic acid) to disrupt the BBB [14]. However, these agents produce their effects through activation of receptors on the brain endothelial cells and can potentially cause rapid desensitization, pathological changes

in receptor density, and damage to the BBB [14]. Infusion of hyperosmolar mannitol (25% solution) has also been used to temporarily open the BBB tight junctions to allow both lower (i.e., methotrexate) and higher molecular weight (i.e., Evan blue-albumin) molecules to enter the brain [15, 16].

A more selective method to modulate the paracellular pathway of the BBB uses peptides to inhibit protein-protein interactions in the intercellular junctions of the BBB. Examples include inhibitory peptides targeting claudin-1 (i.e., C1C2 peptide) and occludin (i.e., OCC1 and OCC2 peptides) that modulate tight junctions in various *in vitro* models of the BBB [17, 18] and increase the brain delivery of the opioid receptor agonist [D-Ala^2, N-MePhe^4, Gly^5-ol]-enkephalin (DAMGO) [19]. In the case of C1C2 peptide, the mechanism of action involves relocalization of claudin-1 from the cell surface to cytosol, resulting in a long-lasting modulation of the BBB [20, 21]. Our work has focused on cadherin peptides that modulate cadherin interactions in the adherens junctions of both endothelial and epithelial cells. The His-Ala-Val (HAV) and Ala-Asp-Thr (ADT) peptides derived from the extracellular-1 (EC-1) domain of E-cadherin have been shown to enhance delivery of ^{14}C-mannitol *in vitro* in Madin-Darby canine kidney (MDCK) cell monolayers [22, 23]. Recently, both HAV6 (Table 1) and ADTC5 peptides have been shown to enhance the brain delivery of both small and large molecules into the brain of rats and mice [24-26].

In this study, cyclic HAV peptides (cHAVc1 and cHAVc3) were designed to improve BBB modulatory activity compared to that of linear HAV4 peptide (Table 1).

The hypothesis was that the increased backbone rigidity provided by cyclic HAV peptides would result in improved binding affinity for the extracellular domain of cadherin as well as improved plasma stability compared to that of the linear peptide. Therefore, cyclic HAV peptides (i.e., cHAVc1, cHAVc3) were synthesized by forming a disulfide bond between two cysteine residues added to the N- and C-termini of the original linear peptide (Table 1). The plasma stabilities of linear HAV4 and cyclic cHAVc3 peptides were determined in rat plasma, and the peptide degradation was detected and quantified by mass spectrometry. The adherens junction modulatory activity of cyclic cHAVc3 peptide was compared to that of linear HAV4 using *in vitro* MDCK cell monolayers, and the modulatory effects on BBB permeability were examined using the *in-situ* rat brain perfusion model as well as in the *in vivo* Balb/c mouse model. The results indicated that cyclic cHAVc3 peptide has better BBB modulatory activity and plasma stability than does the linear HAV4 peptide.

2.2 Material and Methods

2.2.1 Peptide Synthesis

Cyclic and linear HAV peptides were synthesized using solid-phase method with Fmoc chemistry in a Perceptive Pioneer Peptide synthesizer as previously described [22, 23]. HAV peptides were cleaved from resin and purified by reversed-phase HPLC using a C18 column. The disulfide bond in cyclic peptides was formed by

bubbling air into a dilute solution of precursor linear peptides in ammonium bicarbonate buffer at pH 8.5. The identity of each peptide was determined by mass spectroscopy.

2.2.2 In Vitro Peptide Modulatory Activity in MDCK Cell Monolayers

2.2.2.1 Cell Culture:

The *in vitro* modulatory activities of linear and cyclic HAV peptides were evaluated in MDCK cell monolayers and this model was selected to evaluate the effect of cadherin peptides in modulating the intercellular junctions of the cell monolayers. The MDCK-II cells **(**cat.# 00062107) were acquired from ECACC, Salisbury, UK and were seeded into Corning flasks until they reached 80% confluency as a monolayer. Then the cell monolayer was washed twice with PBS followed by treatment with trypsin-EDTA solution (0.25% trypsin, 1.0 mM EDTA in Hank's Balanced Salt Solution (HBSS)). The detached single cells were then resuspended, collected, and counted. They were then added into each well (75,000 cells/well) of a Transwell® plate (Permeable Supports, 0.4 μM polyester membrane, 12-well plates) and were incubated for 5–8 days. TEER values were measured before and at the day of the experiment to check the monolayer integrity.

2.2.2.2 Inhibition of Junction Resealing:

The inhibition of junction-resealing in MDCK-II cell monolayers was used to compare the modulatory activity of linear and cyclic HAV peptides [23]. In this study, the changes in TEER values were followed using an EVOM™ voltohmmeter (World Precision Instruments) in the presence and absence of HAV peptides. Each experiment was started at TEER values of 280–320 ohm.cm^2 for the monolayers. After the cell monolayers were confluent, they were washed with HBSS solution containing 25 mM glucose, 2 mM $CaCl_2$, 0.75 mM $MgSO_4$, and 10 mM HEPES**.** The cell monolayers were incubated with HBSS for 1.5 h, and the TEER values were recorded. Then the cell monolayers were washed and incubated with Ca^{2+}-free buffer to open the tight junctions. The intercellular junction opening caused a decrease in TEER values of 50–60%. The cells were then incubated in Ca^{2+}-sufficient medium to reseal the intercellular junctions in the presence and absence of HAV peptides (1.0 mM) on the apical and basolateral sides. During the resealing of the intercellular junctions, the TEER values were recorded every hour for 6–8 h.

.

2.2.2.3 Direct Junction Modulation:

The activities of HAV peptides were evaluated by directly modulating intact MDCK-II cell monolayers. In this assay, only Ca^{2+}-sufficient buffer was used. The Transwells were washed with HBSS buffer containing 25 mM glucose, 2 mM $CaCl_2$, 0.75 mM $MgSO_4$ and 10 mM HEPES**.** The MDCK cell monolayers were incubated with and

without HAV peptides (1.0 mM) on the apical and basolateral sides followed by measurement of TEER values every hour for 6–8 h.

.

2.2.3 Peptide Stability in Rat Plasma

The rat plasma (lot. no. 19595; NaHeparin) used for plasma stability studies was purchased from Innovative Research, Inc., Novi, Michigan. The plasma degradations of cyclic cHAVc3 and linear HAV4 were determined using LC-MS/MS, and the half-life of each peptide in plasma was calculated. Briefly, HAV4 or cHAVc3 peptide in 1.2 µL of DMSO was added into 200 µL of rat plasma to make the final concentration of DMSO 0.6%. Each peptide solution in rat plasma was incubated and agitated using an orbital shaker at 50 rpm at 37 °C for up to 2–3 half-lives, which were 72 h for cyclic cHAVc3 and 8 h for linear HAV4. The peptides were extracted from plasma using liquid-liquid extraction. In this case, 201.2 µL of plasma containing peptide was added into a 1.0 mL solvent mixture of ACN:H_2O:EtOAc (6:1:1) to precipitate plasma proteins; this was followed by centrifugation at 17226 g (12000 PRM) using Centrifuge-5415D (Eppendorf AG-22331 Hamburg, Germany). The supernatant was collected and evaporated under nitrogen at moderate temperature (35 °C). The resulting residue containing HAV peptide was resuspended in 1 mL of a solution mixture of 14% ACN and 1% formic acid (FA) in water. Then, 2% heptafluorobutyric acid (HFBA) was added as an ion-pairing agent to enhance the partitioning of HAV peptides in a C-18 column (dimensions: 150 ×

2 mm; pore size, 100 Å; particle size, 5.0 μm). The internal standard for cHAVc3 was HAV4 (~300 μM) while the internal standard for HAV4 was 58 μM cHAVc3.

2.2.4 In-Situ Rat Brain Perfusion

The *in-situ* rat brain perfusion studies were done following the previous method developed by Takasato et al. [27]. and using three groups of Sprague-Dawley rats for vehicle, linear HAV4 and cyclic cHAVc1 peptide. The protocol to perform the animal studies was approved by the IACUC at The University of Kansas (AUS#75-05). Before starting the animal surgery, the rats were anesthetized by administration of 100 mg/kg ketamine and 5 mg/kg xylazine via the intraperitoneal route. A cannula was inserted into the left common carotid artery (LCCA) for perfusion of the brain microvessels with vehicle or peptide solution (1.0 mM) at a flow rate of 5.0 mL/min. For ligation of the left common carotid artery (LCCA), a surgical silk thread was used to encircle the artery while the pterygopalatine, occipital, and superior thyroid arteries were coagulated and cut. Then the LCCA was catheterized with a polyethylene catheter (PE-50) for retrograde perfusion with a heparinized saline (100 IU/mL). The perfusion was started immediately after a cardiac puncture under anesthesia. The perfusion protocol was carried out as follows: 20-s pre-perfusion with saline, 240-s perfusion with peptide or vehicle, 240-s perfusion of ^{14}C-mannitol and 5-s post-perfusion of wash with saline. The perfusate was sterilized by filtration and placed in an incubator for oxygenation with 95% air and 5% CO_2 at 37 °C. Throughout the experiment, the rectal temperature was

kept at 36.5 ± 0.5 °C using a heat lamp with a monitoring device (YSI model 73 ATD indicating controller) [24].

2.2.5 In Vivo Studies

2.2.5.1 MRI Studies:

The activities of cyclic cHAVc3 and linear HAV4 peptides in modulating the BBB were compared in adult Balb/c mice. The animal study protocol to detect brain delivery and deposition of Gd-DTPA with and without HAV peptides followed with detection using MRI was approved by the IACUC at the University of Manitoba (Number 11-069). A previous MRI procedure by On et al. to monitor the BBB permeability was used in this study [28]. The enhancement of Gd-DTPA brain deposition caused by cHAVc3 or HAV4 peptides was determined using MRI pixel intensities of the brain images. Before administration of Gd-DTPA, T1- and T2-weighted brain images were obtained as background [25]. Then Gd-DTPA (0.4 mmol/kg) along with cHAVc3 (0.001–0.10 mmol/kg), HAV4 (0.001–0.10 mmol/kg), or PBS was administered via tail vein. Every 3 min, a T1-weighted image was obtained up to 21-min imaging session followed by a second dose of Gd-DTPA at 21 time; then, T1-weighted images were collected every 3 min for another 21-min. Marevisi 3.5 software (Institute for Biodiagnostics, National Research Council, Ottawa, Ontario, Canada) was used to quantified the intensity of Gd-DTPA in the brain at the outlined regions of interest (ROI) within coronal brain slices.

Paravision 3.0 software package was used to quantify the percent difference of Gd-DTPA in the images of brain slices using following equation:

[(post-Gd-DTPA T1-weighted images – T1-weighted images of pre-Gd-DTPA) /pre-Gd-DTPA T1-weighted images] × 100

The percent difference analysis was expressed as fold-enhancement of Gd-DTPA at different time intervals.

To determine the duration of BBB modulation achieved with the cadherin peptides, Gd-DTPA contrast MRI experiments were performed following various pretreatment periods. The dose of each peptide was 0.01 mmol/kg and the dose of Gd-DTPA was 0.4 mmol/kg. Three groups of mice were administered with vehicle, cHAVc3, or HAV4, respectively, via i.v. 1 h prior to administration of Gd-DTPA followed by an MRI imaging session. Another three groups of mice were injected i.v. with vehicle, cHAVc3, or HAV4, respectively, 2 h prior to i.v. administration of Gd-DTPA followed by MRI imaging of the brain. Finally, two groups of mice were administered vehicle and cHAVc3 via i.v. 4 h prior to the administration of Gd-DTPA followed by brain imaging with MRI.

2.2.5.2 NIR Imaging Studies:

The BBB permeability increases for a large molecular weight compound and a P-glycoprotein (P-gp)-sensitive agent cause by HAV peptide were also determined using NIRF imaging agents [25, 28, 29]. IRDye 800CW PEG (0.01 μmol/kg), a pegylated dye of approximately 25 kDa molecular weight, and R800 (0.032 μmol/kg) as P-gp substrate

were delivered and detected in the brain using NIRF [6, 30]. These marker molecules were delivered via i.v, route into mice in three different treatment regimens. In treatment regimen A, the mice received only vehicle injection (PBS); in treatment regimen B, they received 0.010 mmol/kg of cHAVc3; in treatment regime C, they received 0.010 mmol/kg of HAV4. Twenty minutes after treatment, cardiac perfusion of 10% formaldehyde solution was delivered to sacrifice the mice. Then, the brain was removed NIRF analysis and the deposition of NIRF dye in the brain was determined *ex vivo* using an Odyssey near-infrared imaging system (Licor, Lincoln, NE). For quantitative determination, the fluorescence intensity at ROI from the tissue was normalized to fluorescence from the blood sample at the same time point. The results were presented as relative fluorescence units per unit of tissue divided by relative fluorescence units per microliter of blood.

2.3 Results

2.3.1 Modulatory Activity Comparison between Linear HAV4 and Cyclic cHAVc1 Peptides

The activity of linear and cyclic peptides in inhibiting junction resealing was evaluated using MDCK cell monolayers. In this experiment, the cell monolayers were treated with calcium-free medium, resulting in the opening of intercellular junctions and a decrease in TEER values for the cell monolayers. After one hour, calcium-free medium was replaced with calcium-containing medium to reseal the intercellular

junctions. The junction resealing was reflected by the steady increase in the TEER values of the cell monolayers measured over time. To evaluate cadherin peptide activity, the peptide was added into the calcium-containing medium prior to addition into the disrupted cell monolayers. Both the linear HAV4 and cyclic cHAVc1 peptides at 1.0 mM significantly inhibited the resealing of the intercellular junction compared to HBSS control, and both peptides had the same activity (Figure 1A). At various concentrations (20 to 800 μM) and measuring %Δ TEER between the 2-h and 5-h time points, cHAVc1 inhibited the resealing in a concentration-dependent manner and significant inhibitory activity was observed as low as 40 μM (Figure 1B).

The *in-situ* rat brain perfusion studies were used to compare the efficacy of linear HAV4 and cyclic cHAVc1 in enhancing brain transport of ^{14}C-mannitol compared to vehicle (Figure 1C). Both linear HAV4 and cyclic cHAVc1 peptides significantly enhanced the passage of ^{14}C-mannitol into the rat brain compared to vehicle (Figure 1C). However, as observed in the *in vitro* junction annealing assay, there was no significant difference in the BBB permeability of ^{14}C-mannitol caused by linear HAV4 and cyclic cHAVc1 peptides.

Figure 1A

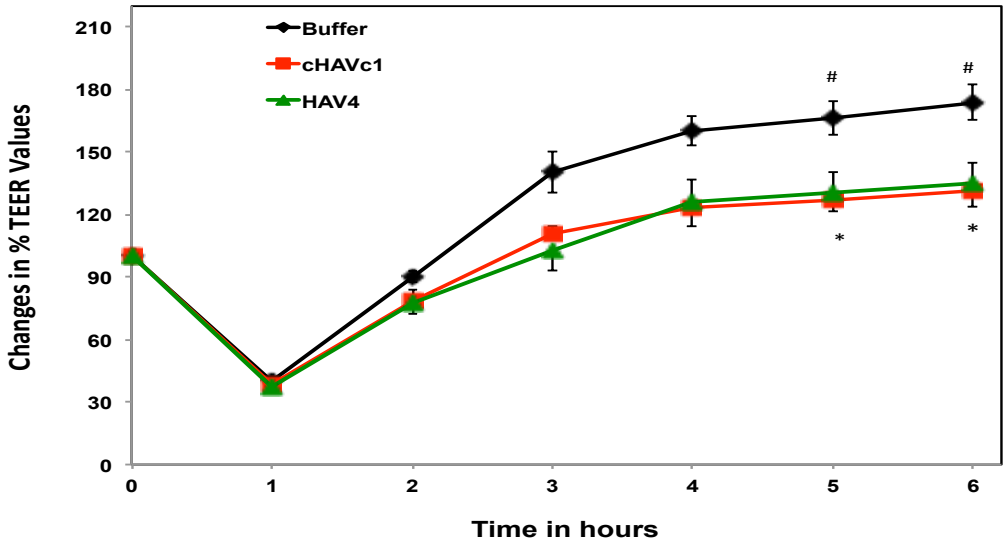

Figure 1B

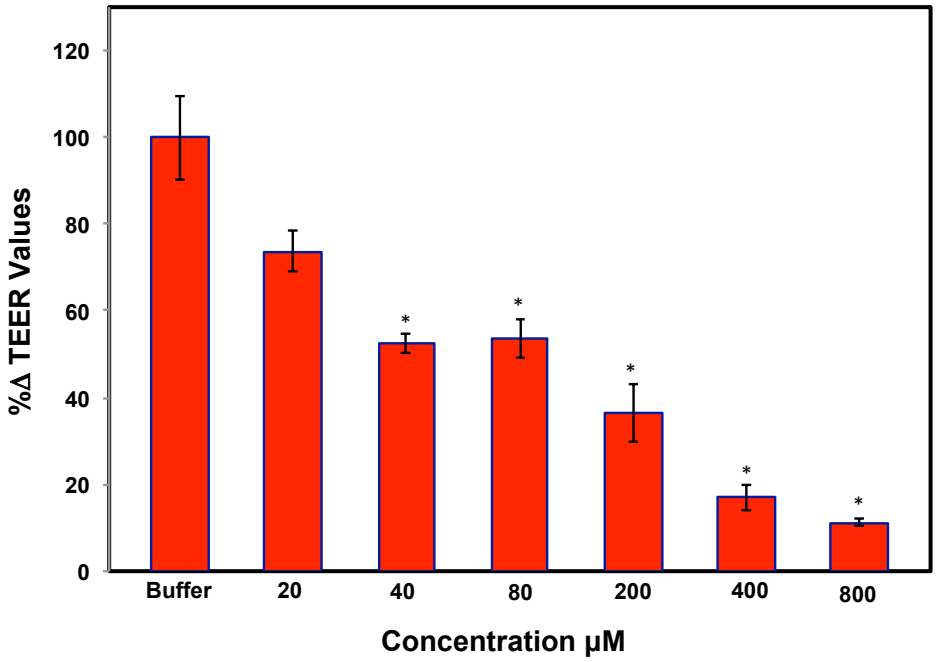

Figure 1C

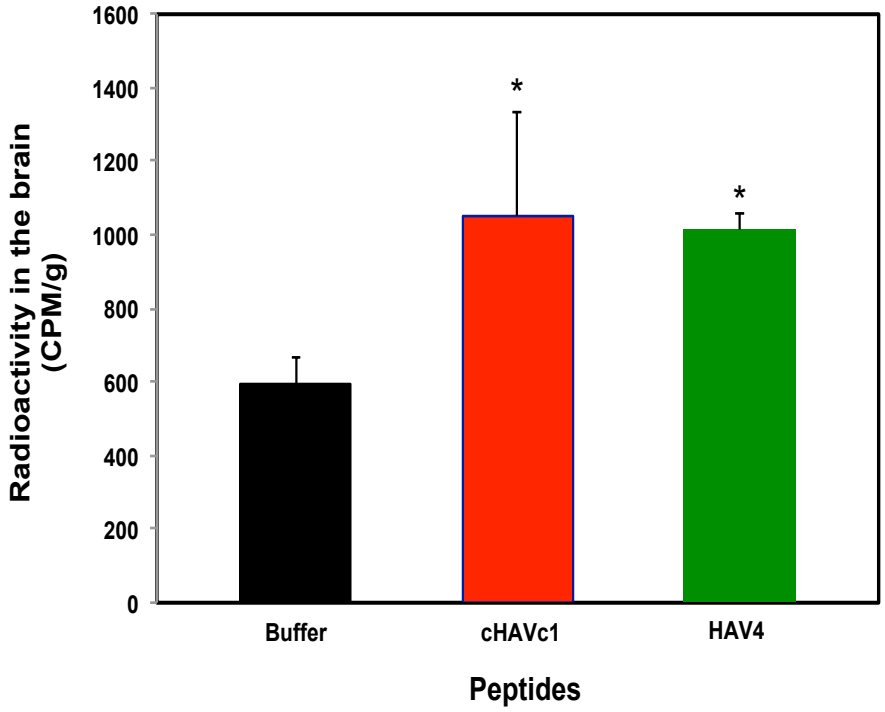

Figure 1: Modulatory activity comparison of linear HAV4, cyclic cHAVc1, and HBSS in MDCK cell monolayers. (A) Comparison of peptide activities to inhibit junction resealing. At 5- and 6-h time points, both linear HAV4 and cyclic cHAVc1 peptide significantly inhibited the junction resealing compared to HBSS (*, $p = 0.011$ for HAV4 vs. HBSS; #, $p = 0.035$ cHAVc1 vs. HBSS). There was no significant difference in the activity of linear HAV4 and cyclic cHAVc1 peptides. (B) The concentration-dependent activity of cHAVc1 peptide at 20–800 μM determined as %D TEER value. The %D TEER value was the difference of TEER values between 2-h and 5-h time points for each

concentration and %D TEER of HBSS was set at 100%. (*) considered significant change with $p < 0.013$. (C) The effect of cHAVc1 and HAV4 in increasing brain delivery of ^{14}C-mannitol in the in-situ rat brain perfusion model. Both linear HAV4 and cyclic cHAVc1 peptides significantly enhanced ^{14}C-mannitol transport to the brain compared to vehicle (*, $p < 0.05$). No difference was observed in the delivery enhancement of ^{14}C-manitol by HAV4 and cHAVc1.

2.3.2 Modulatory Activity Comparison between Linear HAV4 and Cyclic cHAVc3 Peptides

Both HAV4 and cyclic cHAVc3 peptides inhibited the junction resealing of MDCK cell monolayers compared to HBSS-treated controls (Figure 2A). However, cHAVc3 was a significantly better inhibitor of junction resealing than HAV4; at the 5- and 6-h time points, the cHAVc3-treated cells had lower TEER values than those of HAV4-treated cell monolayers. Next, the activities of these peptides were compared in the intact MDCK cell monolayers (Figure 2B). At the 7- and 8-h time points, both HAV4 and cHAVc3 peptides lowered the TEER values significantly compared to HBSS (Figure 2B). In addition, the cHAVc3 peptide had significantly better modulatory activity than HAV4 peptide at the 7- and 8-h time points. The cHAVc3 peptide was active in a concentration-dependent manner; the modulatory activity of 1000 μM peptide was significantly different from that of 500 μM peptide, and the activity of 500 μM peptide was significantly different than that of HBSS (Figure 2C).

Figure 2A

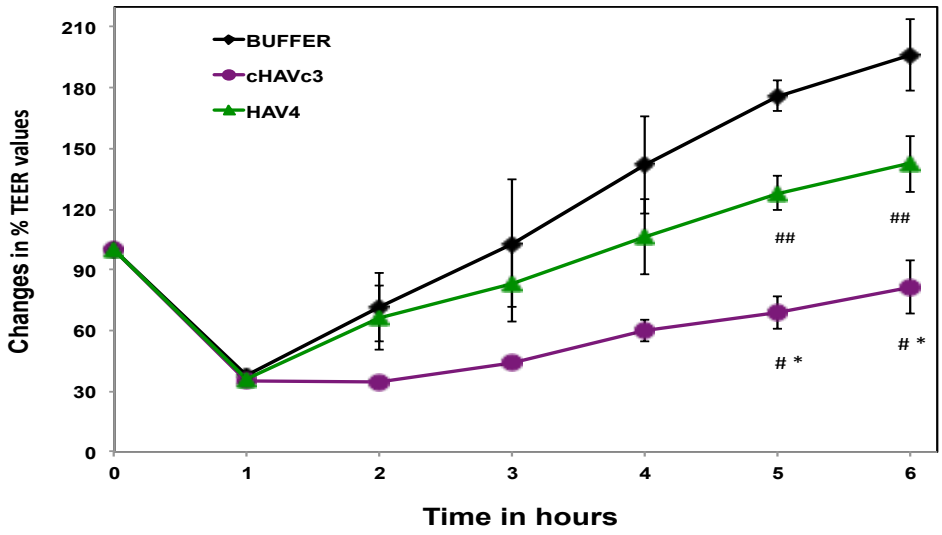

Figure 2B

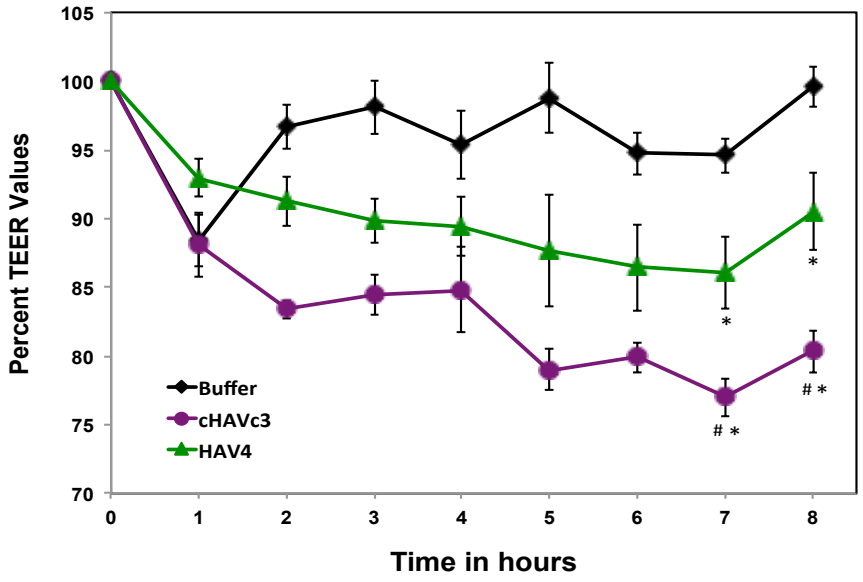

Figure 2C

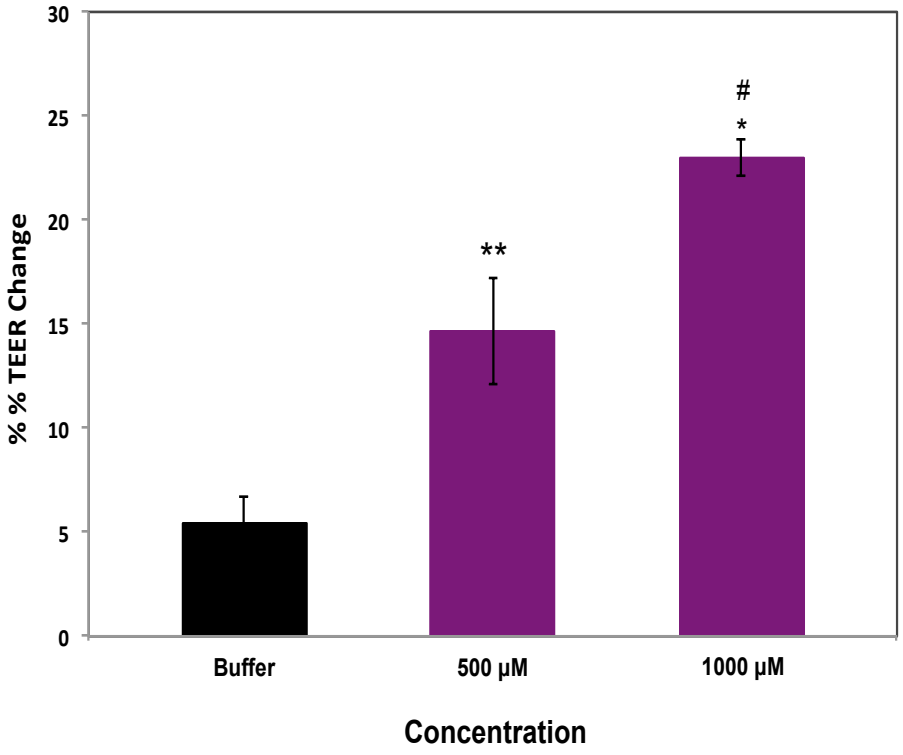

Figure 2: Modulatory activity comparison of linear HAV4, cyclic cHAVc3, and HBSS in MDCK cell monolayers. (A) Comparison of peptide activities to inhibit junction resealing. Cyclic cHAVc3 peptide has significantly higher activity than linear HAV4 peptide at the 6-h time point. (##) p = 0.029, cHAVc3 vs. HAV4; #, p = 0.002 cHAVc3 vs. HBSS. (B) Junction modulatory activity of linear HAV4 and cyclic cHAVc3 peptide in normal MDCK cell monolayers. Both peptides significantly decreased the TEER values compared to HBSS at time points 7- and 8-h. (*) considered significantly different, HAV4 vs. HBSS (7-h, p = 0.006; 8-h, p = 0.008) and cHAVc3 vs. HBSS (7-h and 8-h, p =

0.001). (#) considered significantly different, cHAVc3 vs. HAV4 (#, 7- and 8-h, p = 0.009). (C) The effect of concentrations of cHAVc3 in lowering the TEER values (% TEER change) at 7-h time point (*, p = 0.001 vs. 1000 μM; **, p = 0.003, 0 vs. 500 μM; #, p = 0.012 500 vs. 1000 μM).

2.3.3 Plasma Stability Comparison of Linear HAV4 and Cyclic cHAVc3 Peptides

The *in vitro* plasma stabilities of HAV4 and cHAVc3 peptides were determined in rat plasma using LC/MS-MS. Linear HAV4 degraded faster than cyclic cHAVc3—2.4 h and 12.95 h, respectively (Figure 3). These results suggest that cyclization increases peptide backbone rigidity, which suppresses enzymatic degradation of HAV peptides in plasma.

Figure 3

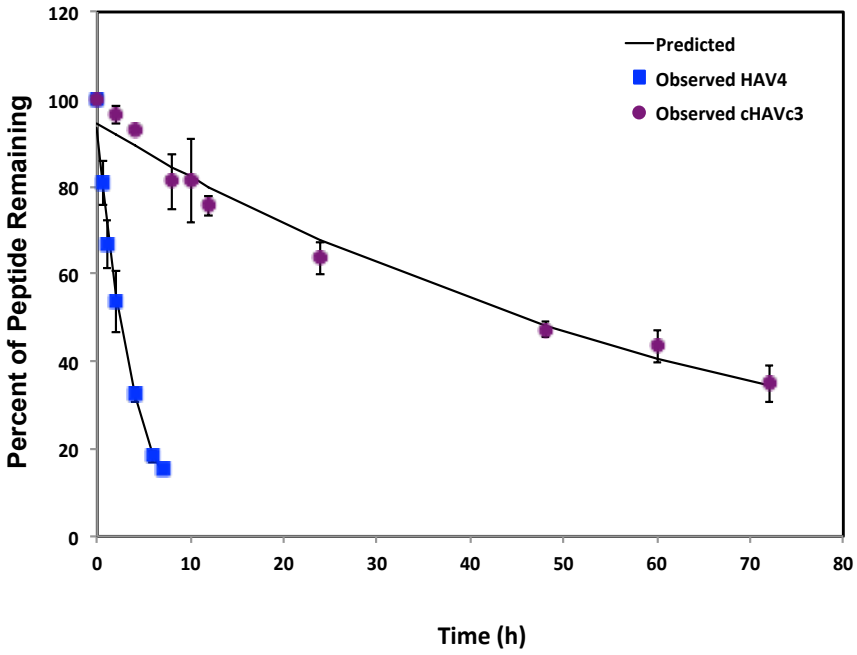

Figure 3: The stability of linear HAV4 (▲) and cyclic cHAVc3 (■) peptides in rat plasma. Peptides were detected using LC-MS/MS to quantify the half-lives. The results indicated that the half-life of linear HAV4 peptide (▲) is 2.4 h with k_d = 0.2858 ± 0.0162, and the half-life for cyclic cHAVc3 peptide (■) is 12.9 h with k_d = 0.053 ± 0.0016. The extraction efficiency for cHAVc3 is 92.94% and for HAV4 is 101.0%.

2.3.4 Comparison of HAV4 and cHAVc3 Peptides in Enhancing Brain Delivery of Gd-DTPA

The *in vivo* effects of HAV4 and cHAVc3 peptides on the brain delivery of Gd-DTPA were determined using MRI throughout a 42-min brain imaging session (Figure 4). Dose-dependent effects of the peptides (0.001, 0.0032, 0.01 mmol/kg) on Gd-DTPA

brain delivery were monitored in the posterior, midbrain, and anterior regions of the brain and were compared to those of mice receiving vehicle (PBS). In mice receiving vehicle, minimal amounts of Gd-DTPA were detected in the brain, resulting in mostly dark images except for the ventricle regions observed in mid-brain coronal slices (Figure 4A). The white/grey areas in the MRI images following peptide treatment represent areas of the brain having increased deposition of Gd-DTPA contrast agent (Figure 4A). Treatment with either the linear HAV4 or the cyclic cHAVc3 peptides rapidly enhanced the brain deposition of Gd-DTPA, with increases in brain deposition observed as early as 3 min following the Gd-DTPA+peptide administration (Figure 4B-G). The effect on BBB permeability was dose-dependent for both the linear and cyclic cadherin peptides. For both peptides, the highest brain deposition of Gd-DTPA was found in the posterior region followed by the midbrain and subsequently the anterior region (Figure 4B-G). At 0.010 mmol/kg in posterior region, the maximum enhancement of Gd-DTPA compared to the background at the 0 time point was up to fivefold for linear HAV4 peptide and about eightfold for cyclic cHAVc3 peptide while the maximum deposition when treated with vehicle was 2.5-fold.

Figure 4A

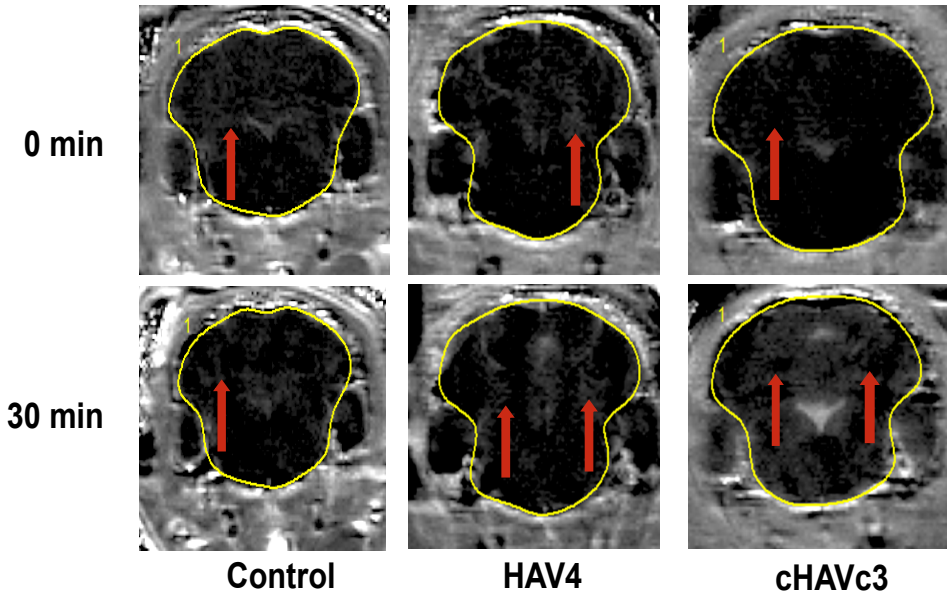

Figure 4B

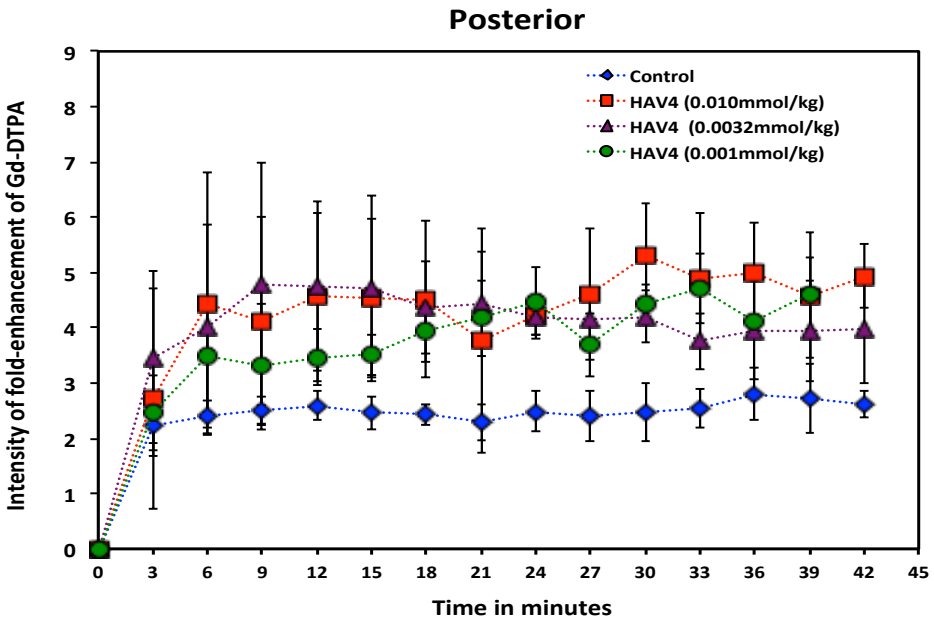

Figure 4C

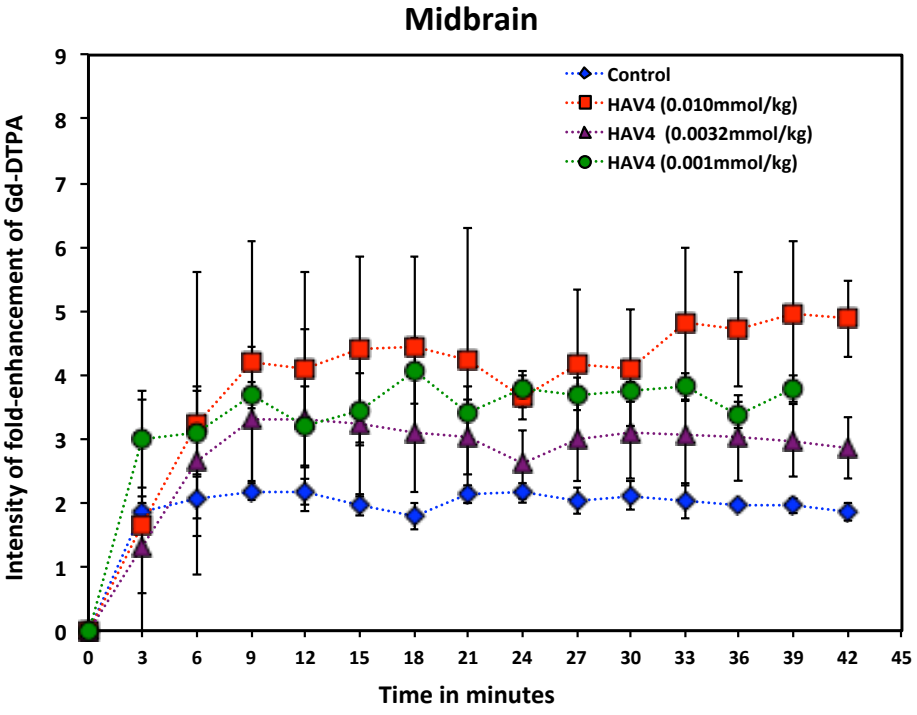

Figure 4D

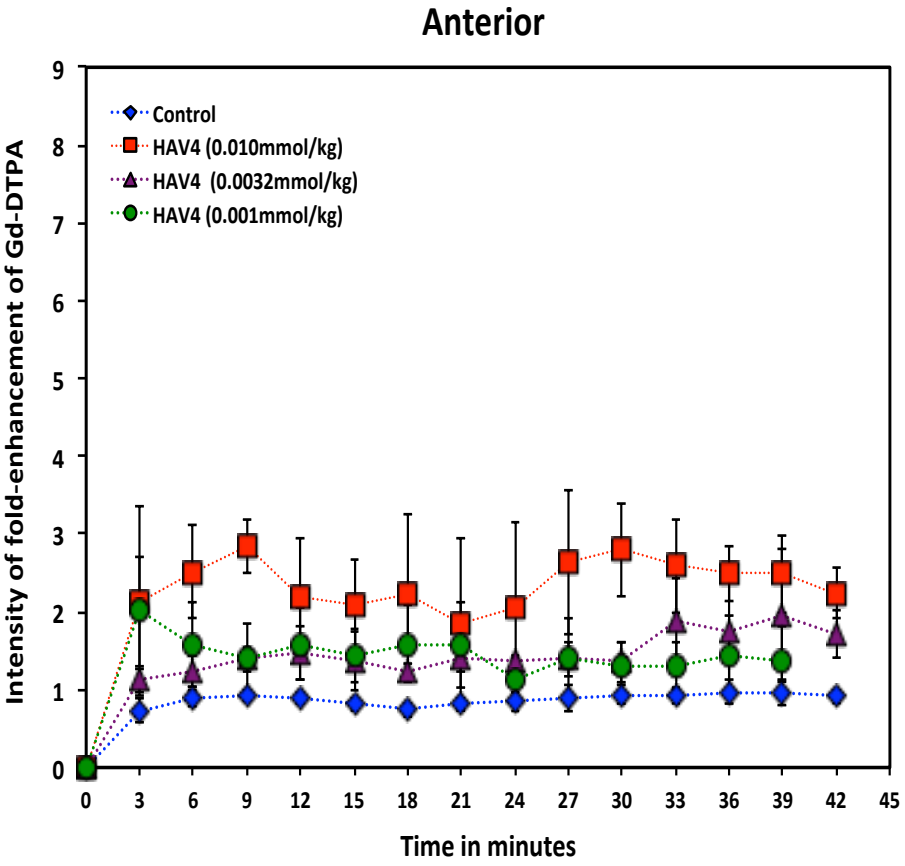

Figure 4E

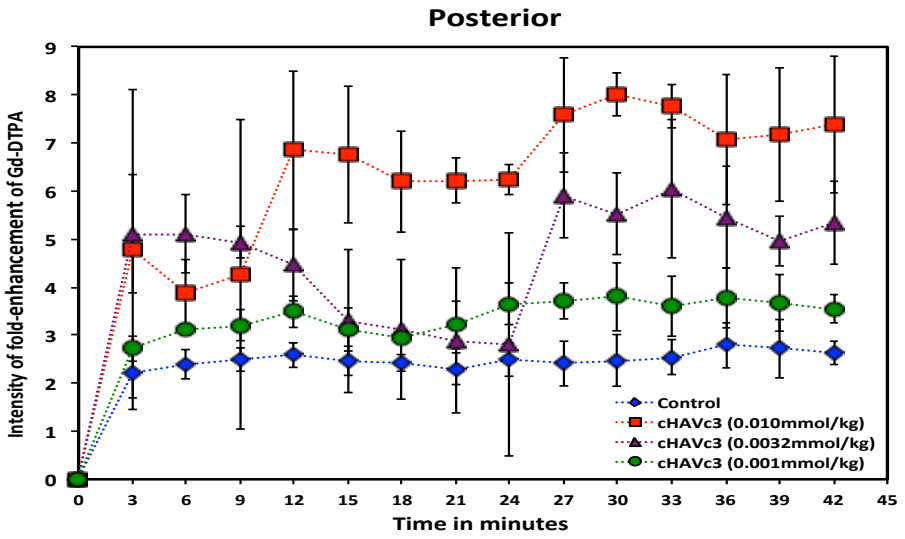

Figure 4F

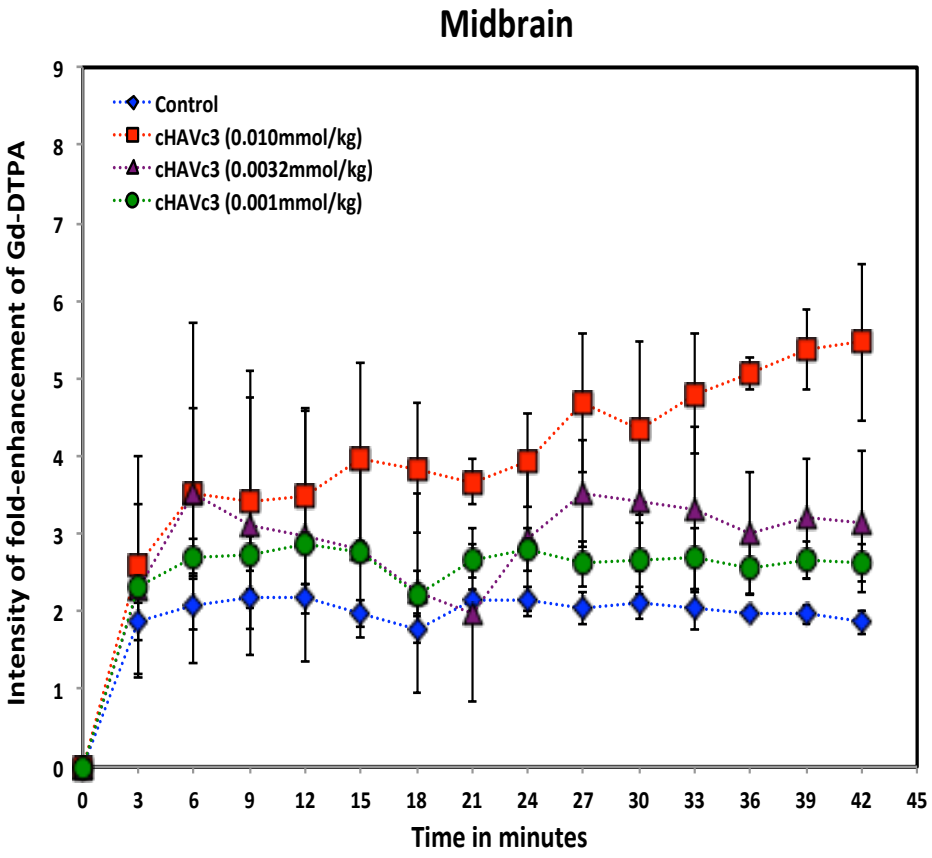
Midbrain
Control
cHAVc3 (0.010mmol/kg)
cHAVc3 (0.0032mmol/kg)
cHAVc3 (0.001mmol/kg)
Intensity of fold-enhancement of Gd-DTPA
Time in minutes
0
1
2
3
4
5
6
7
8
9
0
3
6
9
12
15
18
21
24
27
30
33
36
39
42
45

Figure 4G

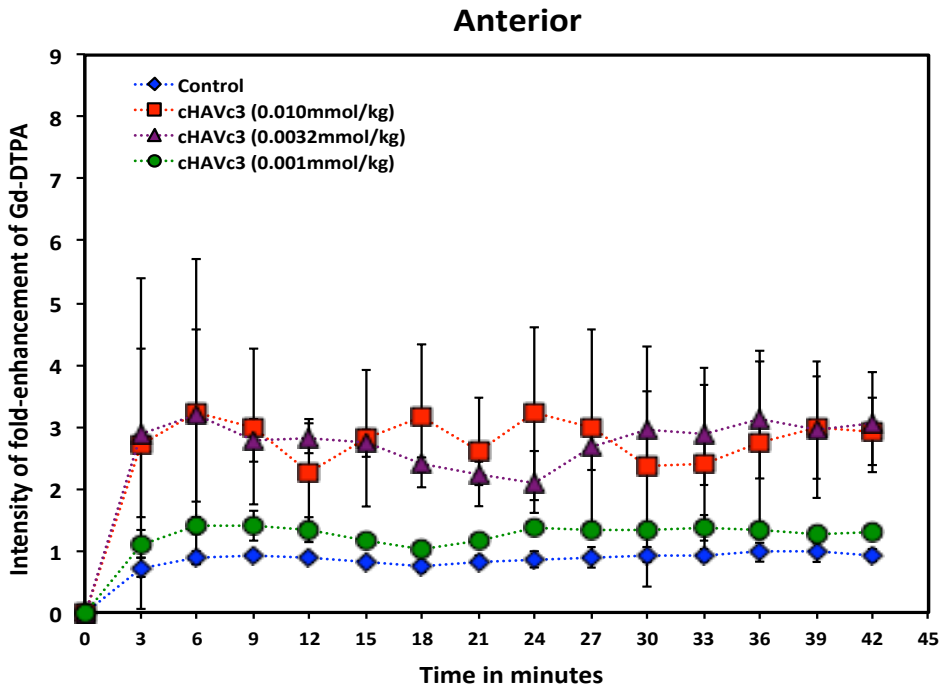

Figure 4: The effects of HAV4, cHAVc3, and vehicle on enhancing brain deposition of Gd-DTPA after i.v. administration in Balb/c mice. (A) Representatives of brain deposition of Gd-DTPA shown as T1-weighted MR images for the posterior region of the brain at 0- and 30-min time points after adminstration of Gd-DTPA (0.4 mmol/kg) with vehicle and 0.001 mmol/kg of peptides (HAV4 and cHAVc3). The red arrows indicate the brain depositions of the contrast agents. (B–G) The effects of (B–D) linear HAV4 peptide and (E–G) cyclic cHAVc3 peptide on the fold-enhancement of Gd-DTPA brain vs. time of imaging at (B, E) posterior, (C, F) midbrain, and (D, G) anterior regions.

The area under the curve (AUC) for Gd-DTPA contrast enhancement in the brain was used to compare the efficacy of HAV4 and cHAVc3 peptides compared to vehicle

(Figure 5). For HAV4 treatment group at the posterior and anterior regions, the AUCs of Gd-DTPA deposition were significantly higher than those of the vehicle group at all peptide doses examined; however, for the midbrain, only treatment with 0.01 mmol/kg showed significant enhancement compared to vehicle (Figure 5A). In addition, the effects of different HAV4 peptide doses could be distinguished in the anterior part of the brain but not in the other regions (i.e., posterior and midbrain). For cHAVc3 peptide, all peptide doses were significantly better than control in the posterior and midbrain regions. In the posterior region, the effect of each dose was significantly different from the others (Figure 5B). In the anterior region, only the highest peptide dose showed significantly enhanced delivery of contrast agent compared to vehicle.

Figure 5A

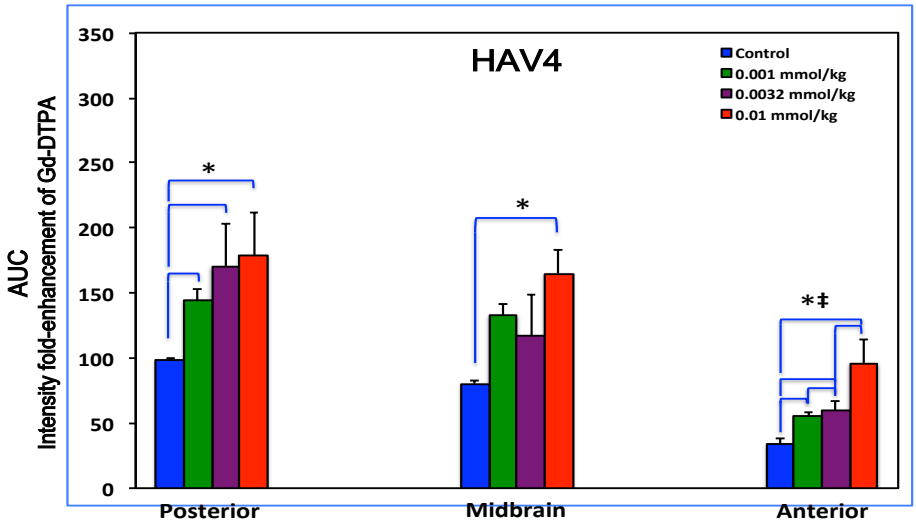

15

Figure 5B

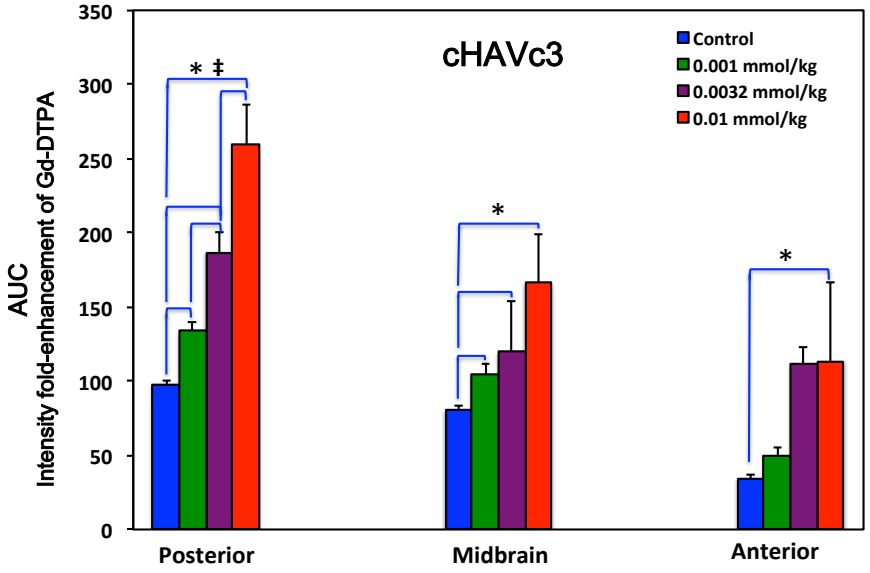

16

Figure 5C

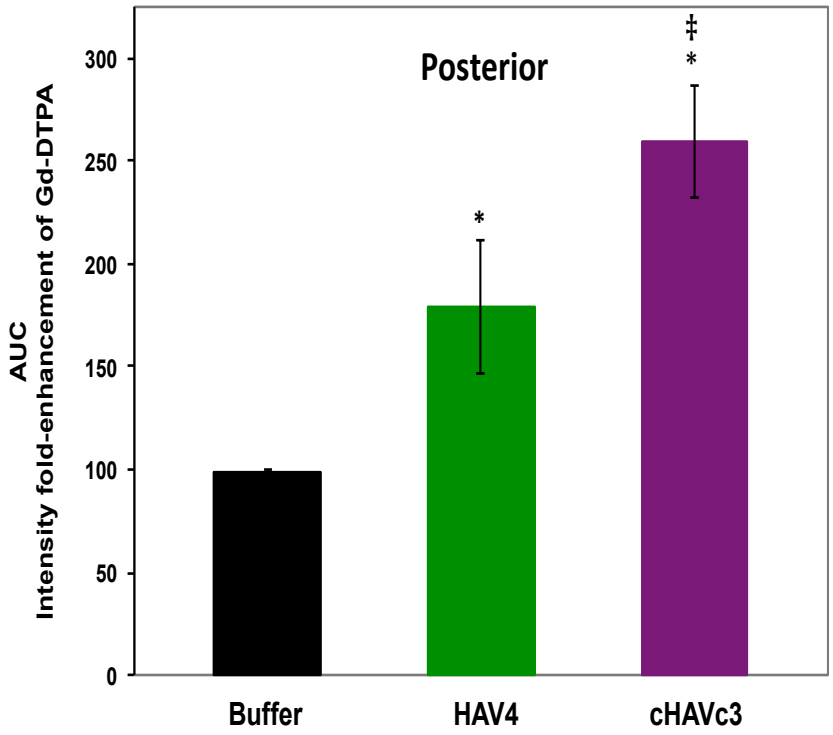

Figure 5: The effect of peptide dose (0.001, 0.0032, 0.01 mmol/kg) on the area under the curve (AUC) for Gd-DTPA fold-enhancement at the posterior, midbrain, and anterior regions for the entire 42-min session as a result of BBB modulation with (A) linear HAV4 and (B) cyclic cHAVc3 peptides (* represents $p < 0.05$ between peptide and vehicle; ‡ represents $p < 0.05$ between two different concentrations). (C) Comparison of AUC of Gd-DTPA in the brain posterior after treatment with HAV4 (0.01 mmol/kg), cHAVc3 (0.01 mmol/kg), and vehicle (* represents $p < 0.05$ between peptide and vehicle; ‡ represents $p < 0.05$ between two peptides).

2.3.5 Effect of Linear HAV4 and Cyclic cHAVc3 Peptides on the Duration of BBB Disruption

The duration of BBB disruption caused by each peptide was examined by administration of 0.01 mmol/kg of either HAV4 or cHAVc3 peptides at various pretreatment times (Figure 6). The AUCs of Gd-DTPA over a 42-min imaging period were plotted to compare the treatment effects following administration of vehicle, HAV4, or cHAVc3. When Gd-DTPA was delivered immediately after treatment with peptide or vehicle, there were clear increases in Gd-DTPA brain depositions in the posterior (Figure 6A), midbrain (Figure 6B), and anterior (Figure 6C) regions for both peptide treated groups (i.e., HAV4, cHAVc3) compared to the control group. However, administration of Gd-DTPA following a 1- or 2-h pretreatment with HAV4 did not produce any Gd-DTPA enhancement in any regions of the brain examined. In contrast, both the 1-h and 2-h cHAVc3 pretreatments caused significant enhancement of the Gd-DTPA contrast agent in all three brain regions. Only those mice receiving the 4-h pretreatment with cHAVc3 showed no significant increase in contrast enhancement compared to vehicle-treated control mice (Figure 6). These results demonstrate that the time frame for BBB modulation is longer for cHAVc3 than for HAV4 peptide.

The extent of BBB modulation with large macromolecules and drug efflux transport substrates was also examined using NIRF imaging agents IRdye800cw-PEG and R800, respectively. In these studies, mice were pretreated with the peptide and, after 5 min or 1 h, R800 and IRdye800cw-PEG were delivered and the brain deposition

of these molecules was quantitatively assessed using *ex vivo* brain images. Following 5-min pretreatment with both linear HAV4 and cyclic cHAVc3 peptides, the brain deposition of IRdye800cw-PEG was higher than in saline-treated controls (Figures 7A-B). However, the brain delivery of efflux pump substrate R800 was not enhanced by either peptide at the 5-min time point. After pretreatment with both peptides for 1 h, there were no significant differences in brain deposition of either IRdye800cw-PEG or R800 molecules (Figures 7C-D).

Figure 6A

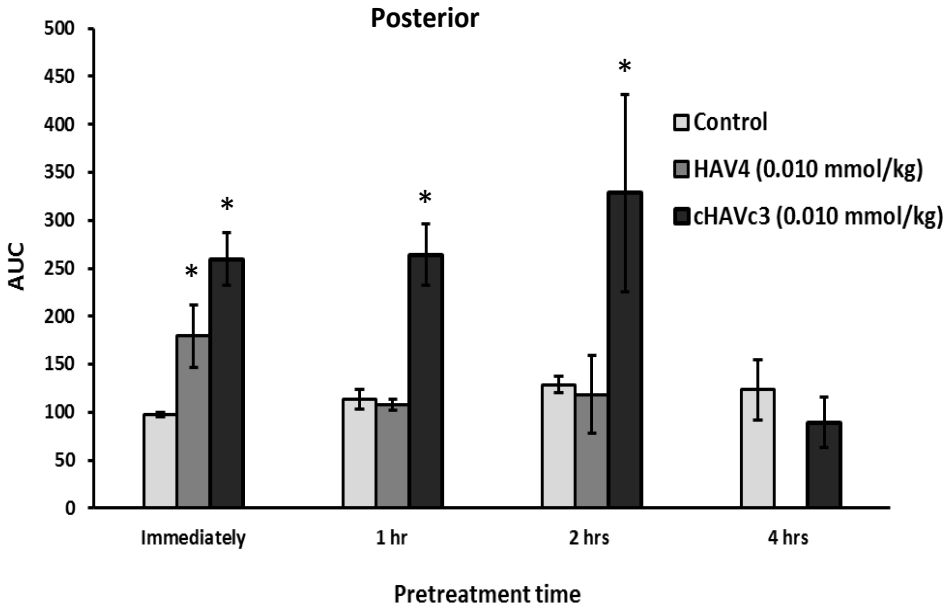

Figure 6B

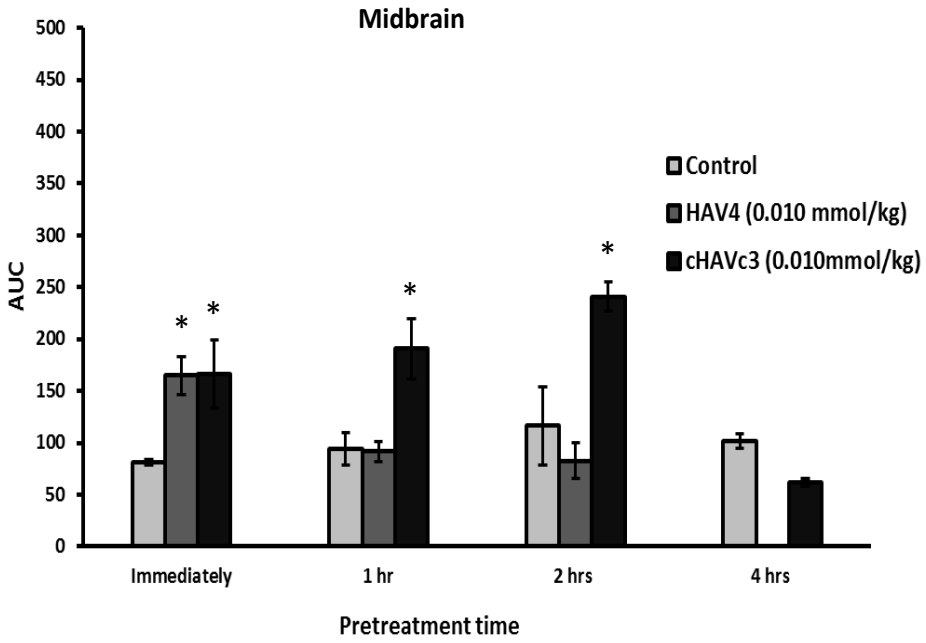

Figure 6C

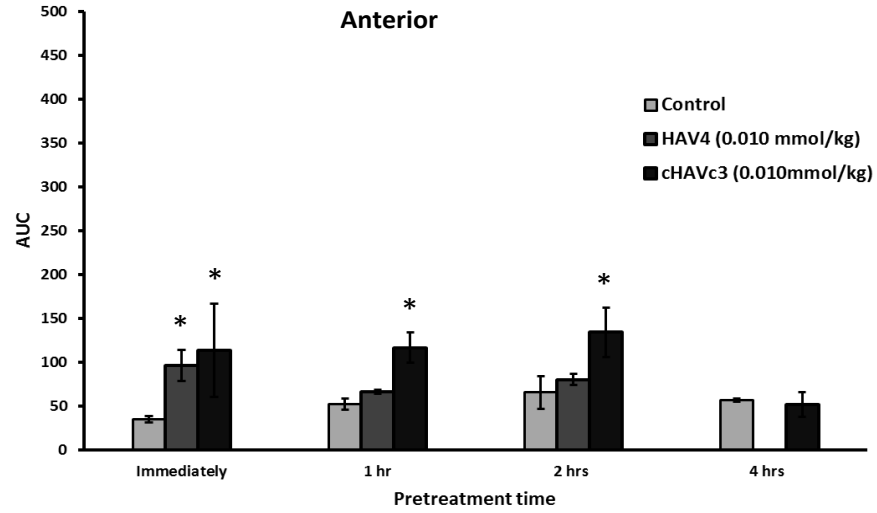

Figure 6: Comparison of length of BBB modulation by linear HAV4 and cyclic cHAVc2 peptides at 0.01 mmol/kg dose as measured by the AUC of Gd-DTPA brain deposition as a function of time in the (A) posterior, (B) midbrain, and (C) anterior regions. The brain depositions of Gd-DTPA were evaluated at different time points for HAV4 (immediately, and following 1-h, and 2-h pretreatment) and cHAVc3 (immediately, and following 1-h, 2-h, and 4-h pretreatment). * represents $p < 0.05$

Figure 7A

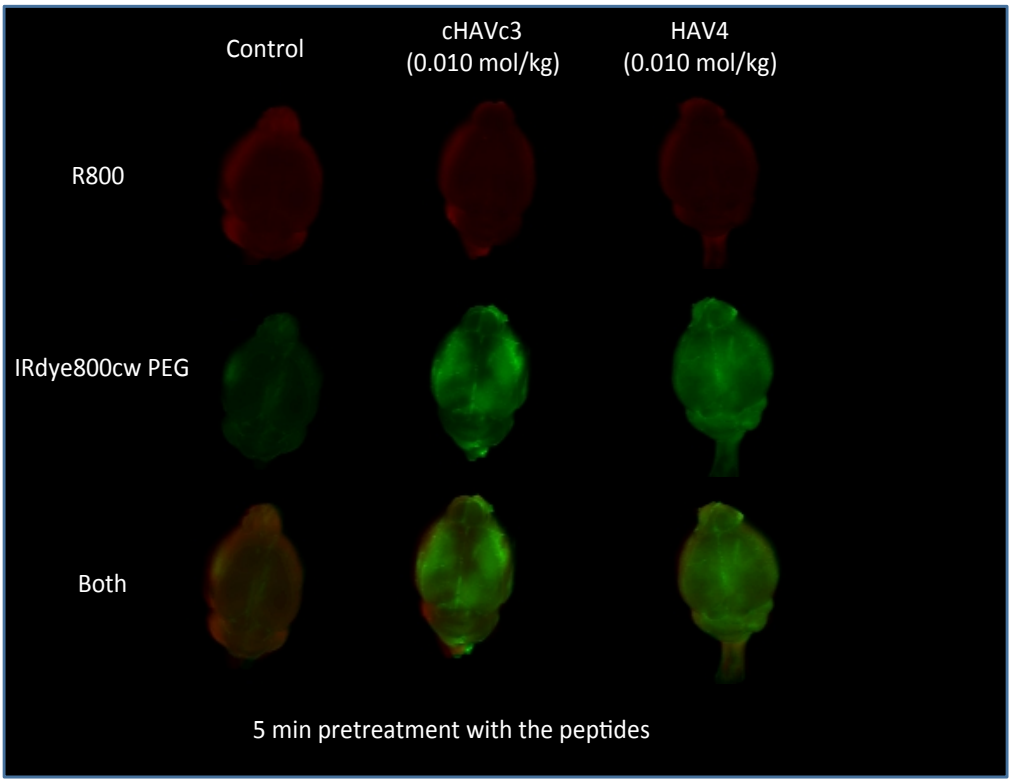

Figure 7B

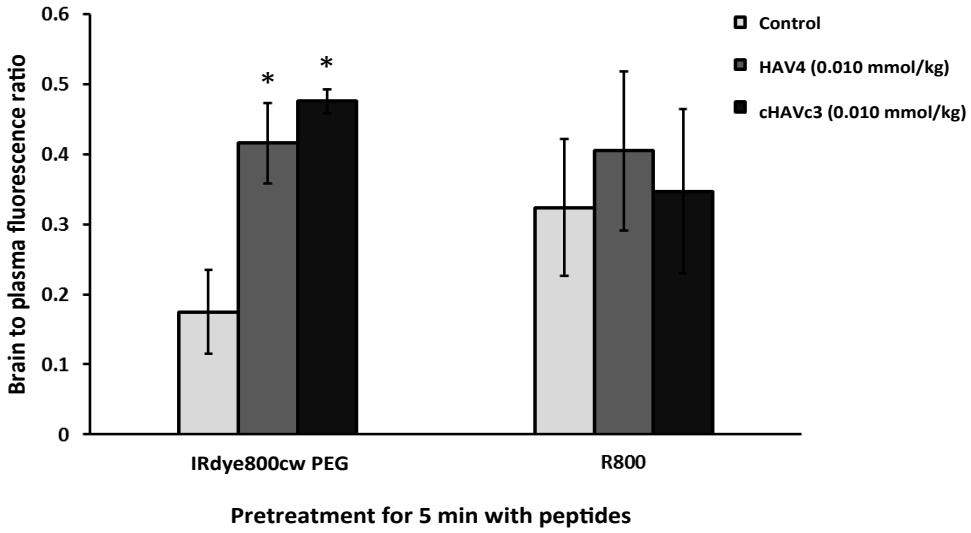
0.6
0.5
0.4
0.3
0.2
0.1
0
Brain to plasma fluorescence ratio
*
*
Control
HAV4 (0.010 mmol/kg)
cHAVc3 (0.010 mmol/kg)
IRdye800cw PEG
R800
Pretreatment for 5 min with peptides

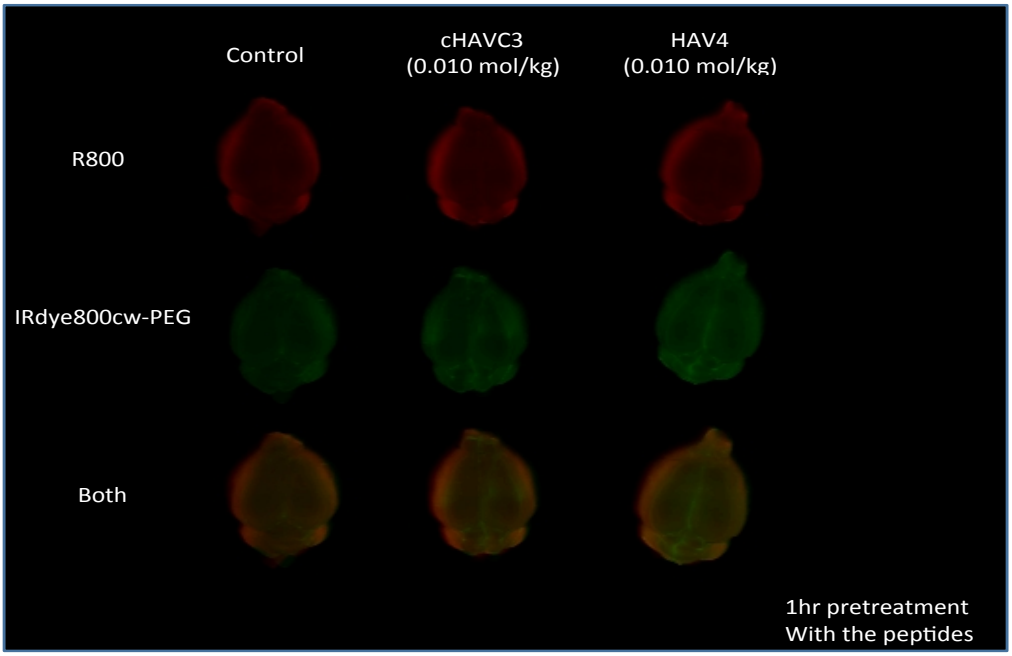
Control
cHAVC3
(0.010 mol/kg)
HAV4
(0.010 mol/kg)
R800
IRdye800cw-PEG
Both
1hr pretreatment
With the peptides

Figure 7D

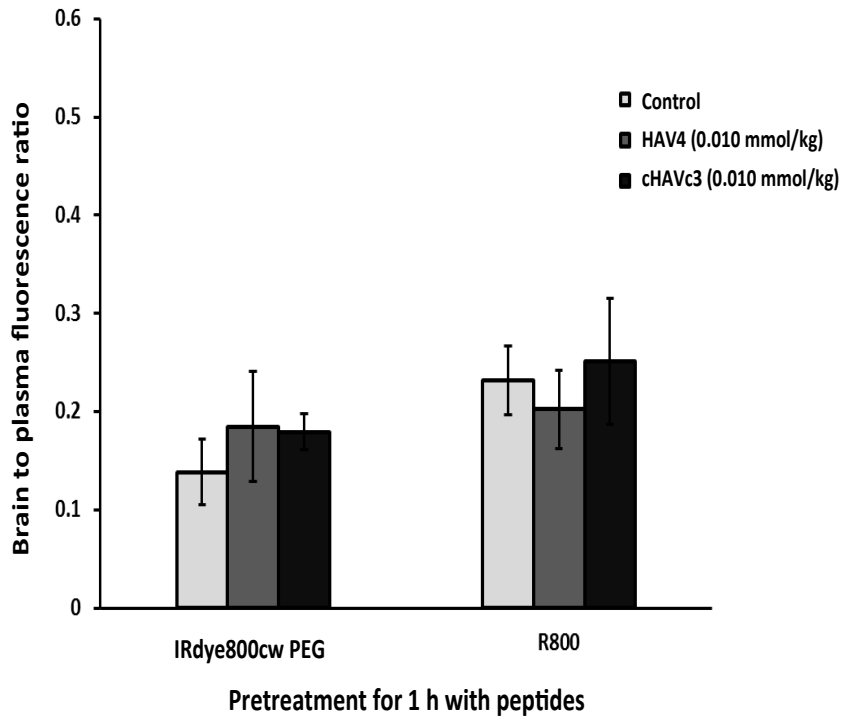

Figure 7: The effects of time and characteristics of marker molecules such as IR-dye-800cw PEG and R800 on their brain deposition when the BBB was modulated with HAV4 and cHAVc3 peptides (0.01 mmol/kg). The brain images (A, C) and brain-to-plasma fluorescence ratio (B, D) of marker molecules when the marker molecules were delivered 5 min (A, B) or 1 h (C, D) after the delivery of each peptide. * represents $p < 0.05$.

2.4 Discussion

The identification and development of methods to improve the delivery of molecules into the brain for diagnosis and treatment of brain diseases is a major challenge. This study was focused in evaluating the effect of linear (i.e., HAV4) and cyclic HAV peptides (i.e., cHAVc1 and cHAVc3) in modulating the intercellular adherens junctions using both *in vitro* cell culture models and *in vivo* BBB models. The hypothesis for these studies is that HAV peptides bind to E-cadherin and disrupt E-cadherin-mediated cell adhesion in the intercellular junctions, resulting in increased paracellular porosity of the BBB. HAV4 is a derivative of HAV6 in which the Ser5 residue in HAV6 was mutated with the Ala5 residue (Table 1) [22]. The sequence of HAV6 peptide was derived from the original sequence (SHAVSS) of extracellular 1 (EC1) domain of human E-cadherin. This original sequence is conserved in the E-cadherin from different species such as canine, human, murine and chicken [31, 32]. Based on the previous studies in MDCK monolayers, HAV4 displayed better modulation of the intercellular junctions of MDCK cell monolayers [22]. Similarly, HAV4 peptide enhanced the *in vivo* brain delivery of Gd-DTPA better than HAV6 in Balb/c mice as detected by MRI [26].

The formation of cyclic peptides has been shown to increase the peptide receptor binding selectivity and biological activity. For example, the antimicrobial activity of cyclic peptide BPC194 is higher than that of linear peptide BPC193 [33]. Similarly, a cyclic RGD peptide (e.g., cyclo(1,5)KRGDf) was specific toward integrin receptors $\alpha_v\beta_3$

and $\alpha_v\beta_5$ while a linear RGD peptide was not [34]. Furthermore, formation of cyclic peptide has been shown to improve chemical stability as well as plasma proteolytic stability of peptides. The chemical stability of cyclic RGD peptide was higher than linear RGD peptide in solution close to neutral pH = 7.0 [35]. In the present study, a cyclic peptide, derived from the linear HAV-based sequence, was formed to induce peptide backbone rigidity, increase binding selectivity to target the extracellular domain of the E-cadherin protein, and enhance BBB modulatory activity *in vitro* and *in vivo*.

Initially, the cyclic cHAVc1 peptide was designed and synthesized based on the linear HAV4 sequence with addition of cysteine residues at both N- and C-termini to make a cyclic octapeptide (Table 1). A disulfide bond was formed upon oxidation of thiol groups between the Cys1 and Cys8 residues. Examination of intracellular junction modulation in MDCK cell monolayers showed no significant difference in activity between cHAVc1 and HAV4 (Figure 1A). However, the cHAVc1 peptide did display concentration dependency with an IC_{50} of approximately 80 μM (Figure 1B). In this assay, the monolayers were first treated with Ca^{2+}-deficient medium to open the intercellular junctions and then exposed to the peptides and Ca^{2+}-containing medium to examine re-establishment of intracellular junctions and TEER values. Thus, although cHAVc1 could have better cadherin-binding affinity than HAV4, the larger size of cHAVc1 compared to HAV4 may have impeded its permeation through the tight junctions and influenced its ability to modulate the cadherin-cadherin interactions. However, as both the HAV4 and cHAVc1 peptides produced similar increases in the

BBB permeability of ^{14}C-mannitol in the *in-situ* rat brain perfusion experiments where the junctions are intact, differences in the abilities of the peptides to access the adherens junction appears unlikely. A more plausible explanation for the similar efficacies observed with the linear HAV4 and cyclic cHAVc1 peptides is that the large ring size of cyclic cHAVc1 did not impose sufficient backbone rigidity to enhance selectivity and affinity for targeting of E-cadherin protein.

In contrast to cHAVc1, cyclic cHAVc3 had better activity than linear HAV4 in inhibiting resealing of the intercellular junctions in MDCK cell monolayers (Figure 2A) and in modulating the intact MDCK cell monolayers (Figure 2B). Cyclic cHAVc3 was a derivative of cHAVc1 with deleted Ala6 and Ser7 residues; this deletion increased the backbone rigidity while reducing the size to a hexapeptide. It is interesting that cHAVc3 has previously been investigated and not found to inhibit the N-cadherin-mediated cell adhesion process [36]. This suggests that cHAVc3 peptide is selective for E-cadherin over N-cadherin. Thus, the conformational rigidity of cyclic cHAVc3 peptide may contribute to its activity and selectivity for E-cadherin compared to HAV4 and cHAVc1.

The BBB modulatory activities of cHAVc3 and HAV4 peptides were further compared in enhancing brain delivery of Gd-DTPA in Balb/c mice. The brain deposition of Gd-DTPA in mice was enhanced by both peptides in a concentration-dependent manner (Figures 4 and 5). Cyclic cHAVc3 had significantly higher activity than HAV4 in enhancing the delivery of Gd-DTPA. In the posterior region, cHAVc3 showed an eightfold enhancement of Gd-DTPA (Figure 4E) while HAV4 had only a

fivefold enhancement (Figures 4B). Increased activity of cHAVc3 was also supported by the AUC comparison of Gd-DTPA entry into the brain in the posterior region (Figure 5C). Taken together, both *in vitro* and *in vivo* studies indicated that cyclic cHAVc3 peptide had a greater ability to modulate the intercellular junctions than the linear HAV4 peptide.

The MRI studies measuring the brain deposition of Gd-DTPA showed regional differences in BBB permeability with the posterior having the greatest accumulation, followed by the mid-brain and anterior regions. Although not assessable with many of the methods used to measure BBB permeability, regional differences in both capillary density and permeability exist [37]. Despite these regional differences in basal BBB permeability, the cadherin peptides were able to modulate BBB permeability in all regions examined. These results were consistent with previous studies with other cadherin peptides such as HAV6 [25] and cyclic ADTC5 [26].

The dynamic range of BBB modulation with the cadherin peptides was evaluated with several different imaging agents. The effect of the cadherin peptides on BBB permeability was most evident for Gd-DTPA. As it is a hydrophilic compound of approximately 900 dalton size, there is limited BBB permeability of this agent under normal conditions. However, substantial increases (3-4-fold) in the brain delivery of Gd-DTPA were observed following both HAV4 and cHAVc3 treatments. While both cadherin peptides also increased the delivery of IRdye800cwPEG, an approximately 30,000 dalton near-infrared fluorescence contrast agent, maximal increases were only

around twofold in magnitude. The BBB permeability of the near-infrared fluorescent P-gp contrast agent R800 was not affected by either cadherin peptide. As R800 BBB permeability is influenced by transcellular diffusion and active drug efflux transport processes, the impact of the cadherin peptides on brain delivery of R800 was expected to be minimal.

The plasma stability of cHAVc3 was also better than that of HAV4 with $t_{1/2}$ = 12.95 h for cHAV3 and $t_{1/2}$ = 2.4 h for HAV4. This result suggests that cHAVc3 is more stable in systemic circulation than HAV4 after i.v. administration. The structural rigidity of cyclic cHAVc3 suppressed its rate of proteolysis in the blood compared to linear HAV4 peptide [35, 38]. Previous studies have shown that peptide cyclization prevented proteolytic degradation in plasma and improved the half-life of the peptide in systemic circulation [39]. The longer residence time of cyclic cHAVc3 peptide in the systemic circulation compared to the linear HAV4 peptide could influence the magnitude and duration of BBB modulation observed with the peptides.

The duration of BBB opening caused by both peptides was determined by measuring peptide response when given as a pretreatment. While both the linear and cyclic cadherin peptides were able to modulate BBB permeability, there were notable differences in the duration of BBB opening with the two peptides in terms of the size of delivered molecules. For Gd-DTPA, the small molecular weight paracellular marker, the duration of BBB modulation observed with HAV4 was less than 1 h (Figure 6). In contrast, based on the MRI studies examining effects of various pretreatment times,

cHAVc3 had a window of BBB opening from 2–4 h (Figure 6). These findings are similar to those of our previous studies with the cyclic cadherin peptide, ADTC5, in which BBB modulation was observed for 2 h, but was completely reversed by 4 h following treatment [26]. Such differences in duration of opening with the linear and cyclic cadherin peptides may be due to improved molecular interactions of the cyclic peptide with the extracellular domain of cadherin and/or improved plasma stability.

Interestingly, studies with IRdye800cw-PEG, the large molecular weight paracellular marker, indicated restoration of BBB permeability within 1 h for both peptides (Figure 7). For applications involving delivery of larger therapeutic molecules, infusions of cadherin peptide may be required to insure an adequate duration of BBB modulation. However, for small molecule brain delivery applications, the relatively limited duration of BBB modulation to the larger molecular weight molecules could be an advantage as it would reduce plasma protein deposition into the brain, which is a major contributor to toxicity observed with other BBB disruption methods. Our hypothesis is that the cadherin peptide modulates the BBB to create large, medium, and small size pores in the intercellular junctions as soon as the peptide is administered. As time progress, the large pores immediately collapse to medium and small size pores and followed by the collapse of medium pores to small pores. Finally, it leads to the resealing of the intercellular junctions to a normal condition. In other words, the rate of large pores disappearance (collapse) is faster than the rates of the collapse of medium and small size pores in the intercellular junctions. This could be the possible reason of

why a large molecule such as IRdye800cw-PEG could not be delivered after 1 h peptide pretreatment while a small molecule such as Gd-DTPA could be delivered after 1 h peptide pretreatment.

2.5 References

1. Pardridge WM 2007. Blood-brain barrier delivery. Drug Discov Today 12(1-2):54–61.
2. Di L, Kerns EH, Carter GT 2008. Strategies to assess blood-brain barrier penetration. Expert Opin Drug Discov 3(6):677–687.
3. Laksitorini M, Prasasty VD, Kiptoo PK, Siahaan TJ 2014. Pathways and progress in improving drug delivery through the intestinal mucosa and blood-brain barriers. Ther Deliv 5(10):1143–1163.
4. Pardridge WM 1983. Brain metabolism: A perspective from the blood-brain barrier. Physiol Rev 63(4):1481–1535.
5. McCaffrey G, Staatz WD, Sanchez-Covarrubias L, Finch JD, Demarco K, Laracuente ML, Ronaldson PT, Davis TP 2012. P-glycoprotein trafficking at the blood-brain barrier altered by peripheral inflammatory hyperalgesia. J Neurochem 122(5):962–975.
6. On NH, Miller DW 2014. Transporter-based delivery of anticancer drugs to the brain: Improving brain penetration by minimizing drug efflux at the blood-brain barrier. Curr Pharm Des 20(10):1499–1509.
7. Pardridge WM 2001. Crossing the blood-brain barrier: Are we getting it right? Drug Discov Today 6(1):1–2.
8. Isaacson LG, Saffran BN, Crutcher KA 1990. Intracerebral NGF infusion induces hyperinnervation of cerebral blood vessels. Neurobiol Aging 11(1):51–55.

9. Friden PM, Walus LR, Watson P, Doctrow SR, Kozarich JW, Backman C, Bergman H, Hoffer B, Bloom F, Granholm AC 1993. Blood-brain barrier penetration and in vivo activity of an NGF conjugate. Science 259(5093):373–377.

10. Hefti F, Weiner WJ 1986. Nerve growth factor and Alzheimer's disease. Ann Neurol 20(3):275–281.

11. Nosrat CA, Fried K, Ebendal T, Olson L 1998. NGF, BDNF, NT3, NT4 and GDNF in tooth development. Eur J Oral Sci 106 Suppl 1:94–99.

12. Pardridge WM, Kang YS, Buciak JL 1994. Transport of human recombinant brain-derived neurotrophic factor (BDNF) through the rat blood-brain barrier in vivo using vector-mediated peptide drug delivery. Pharm Res 11(5):738–746.

13. Zhang Y, Pardridge WM 2006. Blood-brain barrier targeting of BDNF improves motor function in rats with middle cerebral artery occlusion. Brain Res 1111(1):227–229.

14. Cloughesy TF, Black KL 1995. Pharmacological blood-brain barrier modification for selective drug delivery. J Neurooncol 26(2):125–132.

15. Neuwelt EA, Maravilla KR, Frenkel EP, Rapaport SI, Hill SA, Barnett PA 1979. Osmotic blood-brain barrier disruption. Computerized tomographic monitoring of chemotherapeutic agent delivery. J Clin Invest 64(2):684–688.

16. Neuwelt EA, Barnett PA, Bigner DD, Frenkel EP 1982. Effects of adrenal cortical steroids and osmotic blood-brain barrier opening on methotrexate delivery to

gliomas in the rodent: the factor of the blood-brain barrier. Proc Natl Acad Sci U S A 79(14):4420–4423.

17. Wong V, Gumbiner BM 1997. A synthetic peptide corresponding to the extracellular domain of occludin perturbs the tight junction permeability barrier. The Journal of cell biology 136(2):399–409.
18. Tavelin S, Hashimoto K, Malkinson J, Lazorova L, Toth I, Artursson P 2003. A new principle for tight junction modulation based on occludin peptides. Molecular pharmacology 64(6):1530–1540.
19. Zwanziger D, Hackel D, Staat C, Bocker A, Brack A, Beyermann M, Rittner H, Blasig IE 2012. A peptidomimetic tight junction modulator to improve regional analgesia. Mol Pharm 9(6):1785–1794.
20. Zwanziger D, Staat C, Andjelkovic AV, Blasig IE 2012. Claudin-derived peptides are internalized via specific endocytosis pathways. Ann N Y Acad Sci 1257:29–37.
21. Staata C, Coisneb C, Dabrowskia S, Stamatovicc SM, Andjelkovicc AV, Wolburgd H, Engelhardtb B, Blasiga IE 2014. Mode of action of claudin peptidomimetics in the transient opening of cellular tight junction barriers. Biomaterials 50:9–20.
22. Makagiansar IT, Avery M, Hu Y, Audus KL, Siahaan TJ 2001. Improving the selectivity of HAV-peptides in modulating E-cadherin-E-cadherin interactions in the intercellular junction of MDCK cell monolayers. Pharm Res 18(4):446–453.

23. Sinaga E, Jois SD, Avery M, Makagiansar IT, Tambunan US, Audus KL, Siahaan TJ 2002. Increasing paracellular porosity by E-cadherin peptides: discovery of bulge and groove regions in the EC1-domain of E-cadherin. Pharm Res 19(8):1170–1179.

24. Kiptoo P, Sinaga E, Calcagno AM, Zhao H, Kobayashi N, Tambunan US, Siahaan TJ 2011. Enhancement of drug absorption through the blood-brain barrier and inhibition of intercellular tight junction resealing by E-cadherin peptides. Mol Pharm 8(1):239–249.

25. On NH, Kiptoo P, Siahaan TJ, Miller DW 2014. Modulation of blood-brain barrier permeability in mice using synthetic E-cadherin peptide. Mol Pharm 11(3):974–981.

26. Laksitorini MD, Kiptoo PK, On NH, Thliveris JA, Miller DW, Siahaan TJ 2015. Modulation of Intercellular Junctions by Cyclic-ADT Peptides as a Method to Reversibly Increase Blood-Brain Barrier Permeability. J Pharm Sci 104(3):1065–1075.

27. Takasato Y, Rapoport SI, Smith QR 1984. An in situ brain perfusion technique to study cerebrovascular transport in the rat. Am J Physiol 247(3 Pt 2):H484–493.

28. On NH, Savant S, Toews M, Miller DW 2013. Rapid and reversible enhancement of blood-brain barrier permeability using lysophosphatidic acid. J Cereb Blood Flow Metab 33(12):1944–1954.

29. On NH, Mitchell R, Savant SD, Bachmeier CJ, Hatch GM, Miller DW 2013. Examination of blood-brain barrier (BBB) integrity in a mouse brain tumor model. J Neurooncol 111(2):133–143.

30. On NH, Chen F, Hinton M, Miller DW 2011. Assessment of P-glycoprotein activity in the Blood-Brain Barrier (BBB) using Near Infrared Fluorescence (NIRF) imaging techniques. Pharm Res 28(10):2505–2515.

31. Noe V, Willems J, Vandekerckhove J, Roy FV, Bruyneel E, Mareel M 1999. Inhibition of adhesion and induction of epithelial cell invasion by HAV-containing E-cadherin-specific peptides. J Cell Sci 112 (Pt 1):127–135.

32. Kister AE, Roytberg MA, Chothia C, Vasiliev JM, Gelfand IM 2001. The sequence determinants of cadherin molecules. Protein Sci 10(9):1801–1810.

33. Mika JT, Moiset G, Cirac AD, Feliu L, Bardaji E, Planas M, Sengupta D, Marrink SJ, Poolman B 2011. Structural basis for the enhanced activity of cyclic antimicrobial peptides: the case of BPC194. Biochim Biophys Acta 1808(9):2197–2205.

34. Cheng KT, Razkin J, Josserand V, Jin Z, Foillard S, Boturyn D, Favrot PMC, Dumy P, Coll JL. 2004. Self-quenched-regioselectively addressable functionalized template-[cyclo-(RGD-d-Phe-Lys)]4 peptide-Cy5-fluorescence quencher QSY21. Molecular Imaging and Contrast Agent Database (MICAD), Bethesda (MD).

35. Bogdanowich-Knipp SJ, Chakrabarti S, Williams TD, Dillman RK, Siahaan TJ 1999. Solution stability of linear vs. cyclic RGD peptides. J Pept Res 53(5):530–541.

36. Williams E, Williams G, Gour BJ, Blaschuk OW, Doherty P 2000. A novel family of cyclic peptide antagonists suggests that N-cadherin specificity is determined by amino acids that flank the HAV motif. J Biol Chem 275(6):4007–4012.

37. Phares TW, Kean RB, Mikheeva T, Hooper DC 2006. Regional differences in blood-brain barrier permeability changes and inflammation in the apathogenic clearance of virus from the central nervous system. J Immunol 176(12):7666–7675.

38. Bogdanowich-Knipp SJ, Jois DS, Siahaan TJ 1999. The effect of conformation on the solution stability of linear vs. cyclic RGD peptides. J Pept Res 53(5):523–529.

39. Pollaro L, Heinis C 2010. Strategies to prolong the plasma residence time of peptide drugs. MedChemComm 1(5):319–324.

CHAPTER 3

Probing the Interaction between cHAVc3 Peptide and the EC1 Domain of E-cadherin using NMR and Molecular Dynamics Simulations

3.1 Introduction

Brain diseases are difficult to treat because drug molecules cannot be easily transported from the bloodstream to the brain. The endothelial microvessels can deliver nutrients to the brain; however, these microvessels also comprise the blood-brain barrier (BBB), which is a selective barricade that prevents unwanted molecules from entering the brain from the bloodstream. Many drug and diagnostic molecules cannot cross the BBB; therefore, there is a need to develop new methods for delivery of drugs and diagnostic molecules across the BBB to treat diseases of the central nervous system (CNS). Only a very few methods, such as using brain osmotic solutions, have been successful in improving brain delivery in a non-invasive manner [1, 2]. In that approach, the hyperosmolarity of the osmotic solution used to deliver the drug modulates the intercellular junctions of the BBB by shrinking the vascular endothelial cells. Because the current choices are so limited, any new alternative and selective methods to deliver therapeutic and diagnostic molecules to the brain would help patients with brain diseases. Our group and others have developed peptides to enhance delivery of molecules to the brain by modulating protein-protein interactions (i.e., those of occludins, claudins, cadherins) in the intercellular junctions of the BBB [3, 4].

The HAV6 peptide (Ac-SHAVSS-NH_2) derived originally from the first domain (EC1) of E-cadherin enhances the brain delivery of a paracellular marker molecule (i.e., ^{14}C-mannitol) across *in vitro* cell culture monolayers of Madin-Darby canine

kidney cells (MDCK) [5]. The HAV6 peptide can also increase the brain delivery of ^{14}C-mannitol and ^{3}H-dounamycin in the *in-situ* rat brain perfusion model as well as Gd-DTPA, R800 near IR (NIR) dye, and R800cw-polyethylene glycol (25 kDa) in Balb/c mice *in vivo* upon intravenous (i.v.) administration [6, 7]. Recently, the cyclic cHAVc3 peptide (cyclo-(1,6)Ac-CSHAVC-NH_2) was shown to have better activity than linear HAV4 peptide (Ac-SHAVAS-NH_2) in modulating the intercellular junctions of MDCK cell monolayers and in enhancing *in vivo* brain delivery of Gd-DTPA in Balb/c mice. In addition, cyclic cHAVc3 has better plasma stability than the linear HAV4 peptide.

The proposed hypothesis for the general mechanism of action of synthetic HAV peptides is that they modulate the BBB via binding to the EC repeat domain(s) of E-cadherin; as a result, the peptides disrupt cadherin-cadherin interactions in the intercellular junctions of the BBB. The disruption of cadherin interactions increases pore sizes in the intercellular junctions of the BBB and enhances the penetration of molecules through the BBB. Because the EC1 domain is known to be one of the most important repeat domains in cadherins, we have proposed that HAV peptides bind to the EC1 domain to modulate E-cadherin homophilic interactions [8-10]. The results from this study will provide guidance in designing better BBB modulators for improving delivery of molecules into the brain.

In this study, the binding properties of the cHAVc3 peptide to the EC1 domain of human E-cadherin were evaluated using ^{1}H,-^{15}N-heteronuclear single quantum correlation (HSQC) NMR spectroscopy, molecular dynamics simulation, and molecular docking experiments [11, 12]. The amino acid assignments in the EC1 domain were completed previously using 3D NMR spectroscopy [13]. The EC1 domain was titrated with the peptide, and the NMR chemical shift perturbations (CSP) for the affected residues were monitored to determine the peptide-binding site on the EC1 domain [11]. CSP has also been used to estimate the dissociation constant (K_d) of cHAVc3 to the EC1 domain [14]. The conformations of cHAVc3 peptide and the EC1 domain were evaluated with molecular dynamics simulations, and the potential peptide-binding site was determined in molecular docking experiments using residues that were affected by the peptide titration.

3.2 Materials and Methods

3.2.1 Peptide Synthesis and Cyclization

The linear precursor of cyclic cHAVc3 peptide was synthesized using a solid-phase method with Fmoc chemistry in a peptide synthesizer (Pioneer, PerSeptive Biosystems). The linear peptide was cleaved from the resin and purified by reversed-phase HPLC using a C18 column. The cyclization reaction was done by bubbling air into a dilute solution of peptide in sodium bicarbonate buffer at pH

8.5 as previously described [15]. The peptide was purified with semi-preparative HPLC using a C18 column. Mass spectrometry was used to confirm the molecular weight of the cHAVc3 peptide [6].

3.2.2 Protein Expression and Purification

Expression and purification of the ^{15}N-labeled EC1 domain protein with 138 residues were accomplished using our previously published protocol [13]. The protein contains 110 residues from the EC1 domain and 28 residues at the C-terminus from the sequence of the EC2 domain. The N-terminus was connected to Streptag I sequence (WSHPQFEK) via a Factor Xa sequence (IEGR) for affinity purification using a Strep Tactin II column with size 5.0 × 0.6 cm (GE Healthcare Life Sciences, Pittsburgh, PA). The cDNA of the 138 residues protein (BlueHeron, Bothell, WA) was subcloned into pASK-IBA6 plasmid (Genosys, Woodland, TX). The cDNA vector of 2 μL was added in sterile technique to 100 μL of BL21 cells for 30 min in ice. Then the mixture was placed in a water bath at 42°C for 30 s to allow cDNA to enter the cells; this was followed by 3 min in ice. 200 μL of SOC medium (1.55 g yeast, 0.25 mL of 1M KCL, 0.5 mL of 1 M $MgCl_2$, 0.5 mL of 1 M $MgSO_4$, 1 mL of 1 M glucose in ddH_2O) was added to the mixture. The mixture was shaken at 250 RPM and 37°C for 0.5–1 h. Two aliquots of the mixture (50 and 100 μL) were added to different agar plates followed by incubation for 12–16 h at 37°C. One or two colonies were selected from either a 50- or 100-μL-plate and added to 10–20 mL of LB medium (10 g NaCl, 10 g peptone, 5 g yeast up to 1 L of dd H_2O). Ampicillin

solution (10–20 μL of 100 mg/mL) was added into the small-scale expression followed by overnight incubation at 37°C. The 20 mL LB medium was added to 1 L of 5× M9 medium (200 mL M9 minimal medium with ^{15}N-NH_4Cl as a nitrogen source, 2 mL of 1 M $MgSO_4$, 10 mL of 40% glucose, 0.5 mL of 1 M $CaCl_2$, 1 mL of 1% $FeSO_4$, 1 mL of 1% thiamine, 1 mL of antibiotic 100 mg/mL) until the cells density was 0.6–0.8 at OD_{600} nm. Cell growth was induced using 50 μL anhydrotetracycline (2 mg/mL, Promega Inc., Madison, WI) to express the ^{15}N-labeled EC1 followed by incubation for 6 h at 30°C. The resulting cells were harvested by centrifugation at 10000–12000 RPM, and cell pellets were immediately stored at –80°C.

Prior to the NMR experiment, the ^{15}N-labeled EC1-containing cells were taken from the –80°C freezer and subjected to lysing by sonication (Sonic Dismemberator) for 10 s every min for 30 min at 65 Hz in binging (or B) buffer (100 mM Tris, 150 mM NaCl, 1 M EDTA, 1 mM DTT, 0.02% NaN_3, pH 8). Then, the lysed cells were centrifuged at 14000 RPM for 1 h at 4°C. The supernatant was passed through a 0.2 μm sterile filter and concentrated by centrifugation using Amicon Ultra tubes (EMD Millipore, Billerica, MA) with 10,000 or 3,000 Da molecular weight cutoff. The concentrated ^{15}N-labeled EC1 was purified using a StrepTactin II column. The column was equilibrated and washed with B buffer before and after protein solution exposure to the column at 5 mL/min flow rate. Pure protein was then eluted from the column by elution buffer (B buffer + 2.5 mM desthiobiotin) at a low flow rate of 2 mL/min. Tris-Bis SDS-PAGE (4–12%) was used to check the

purity of the protein fractions. The protein was concentrated to 0.18–0.3 mM for NMR studies with Amicon Ultra tubes by centrifugation, and the protein concentration was monitored with a UV spectrophotometer at 280 nm using molar absorptivity of 19480 M^{-1} cm^{-1} [8]. The EC1 domain in elution buffer was dialyzed overnight with 20 mM phosphate buffer containing 5 mM DTT. Two hours before the NMR experiment, the DTT was removed from the EC1 buffer by dialysis using 20 mM phosphate buffer or by centrifuging with Amicon Ultra tubes with 3,000 Da molecular weight cutoff for 15–20 min. DTT was removed to prevent reduction of the disulfide bond in the cyclic cHAVc3 peptide during the titration procedure.

3.2.3 NMR Experiments for Titration of EC1 with cHAVc3 Peptide

Two-dimensional (2D) ^{1}H,-^{15}N-HSQC NMR experiments were carried out using a Bruker Avance 800 MHz NMR spectrometer (Billerica, MA) equipped with TCI cryoprobes. The effects of titration of cHAVc3 peptide on the ^{15}N-labeled EC1-domain were evaluated in buffer containing 10% D_2O. The HSQC NMR spectra were acquired with 10 or 16 scans, depending on the EC1 domain concentration. The peptide-to-protein ratios (cHAVc3: EC1) were from 0.3:1.0 to 2.5:1.0 for the low range and from 1:1 to 10:1 for the high range. The lower range titration ratios were used to estimate the K_d values of cHAVc3 peptide. For each titration point, 10 μL of cHAVc3 peptide was added to a sample of 500 μL of EC1. Then the data for each titration point were processed using NMRPipe program (nmrDraw and view2D.tcl). The chemical shift perturbation (CSP) and broadening of the ^{1}H or ^{15}N

peaks from the EC1 residues were used to determine the potential binding site and the dissociation constant (K_d) of the cHAVc3 peptide. The CSP was calculated using the following equations [16] :

$$\Delta F = [(\Delta\delta^{1}H^{*} (800.234 \text{ Hz/ppm}))^2 + (\Delta\delta^{15}N^{*} (81.096 \text{ Hz/ppm}))^2]^{1/2} \quad (1),$$

where ΔF represents fraction bound of protein and $\Delta\delta^{1}H$ or $\Delta\delta^{15}N$ represents the difference between free and bound protein for the EC1 domain for each NMR nucleus. Then, ΔF was plotted against the peptide concentration, and the K_d was calculated using non-linear regression for best fitting [14]:

$$\Delta_{obs} = \Delta_{max} ((P_o + K_d + L_o) - [(P_o + K_d + L_o)^2 - 4 P_o L_o]^{1/2})/2 P_o, \quad (2),$$

where Δ_{obs} is the difference between bound and free protein, Δ_{max} is the penultimate titration, and P_o and L_o are total EC1 concentration and total cHAVc3 concentration, respectively.

3.2.4 Molecular Dynamic Simulations

3.2.4.1 MD Simulation of the EC1 Domain

Molecular dynamics (MD) simulations were carried out to evaluate the dynamic movements of the EC1 domain and its C-terminal tail region. The X-ray structure of the EC1 domain (PDB file 2O72 from the Protein Data Bank) was used as the starting structure [17]. The EC1 structure was solvated in a cubic box of 35307 TIP3P water of size 10.27578 nm. To simulate the ionic strength to 0.15 M, 86 Cl^- and 98 Na^+ ions were added by replacing water molecules. Ionization states of titratable

residues were assigned corresponding to pH 7.0 conditions. After energy minimization, a brief constrained MD simulation and 100 ps unconstrained equilibration of EC1 were done. The EC1 structure was then subjected to an unconstrained MD simulation for 100 ns at a constant temperature of 300 K. The final structure from the MD simulations was used as a model for the solution structure of the EC1 domain and for molecular docking simulations with cHAVc3 peptide. The simulations were done using GROMACS 4.6 program [18, 19] with the CHARMM27 force field and nonbonded interactions. The long-range electrostatic interaction was computed by PME (not cutoff) with a distance of 1.3 nm for short-range non-bonded cutoff. The temperature of 300 K was maintained by the v-rescale method.

3.2.4.2 Replica Exchange Molecular Dynamic (REMD) Simulations for Linear HAVc3 and Cyclic cHAVc3

3.2.4.2.1 Simulation of the Linear HAVc3 Peptide as the Precursor of Cyclic cHAVc3

The linear HAVc3 peptide (Ac-CSHAVC-NH_2) was built using the CHARMM program [20] with acetylated N-terminus and amidated C-terminus. Both linear HAVc3 peptide without a disulfide bond and cyclic cHAVc3 peptide (cyclo(1,6)Ac-CSHAVC-NH_2) with a disulfide bond were simulated in a box of water (TIP3P) with eight ions (4 ions each for Cl^- and Na^+). REMD simulations were performed for HAVc3 with 15 replicas in a temperature range of 320–480 K over 50

ns. The rate for exchange attempts between neighboring replicas was every 1 ps; the observed exchange probabilities were in a range of 0.07–0.23 with cubic box size of 3.55578 nm and 1447 TIP3P waters. A GROMACS 4.5.6 program was used to simulate the peptide with CHARMM27 force field and non-bonded interactions as in the modeling of EC1. The structures sampled in the 320 K REMD were used to generate the cyclic peptide structure as described below.

3.2.4.2.2 Simulation of Cyclic cHAVc3

To allow HAVc3 peptide cyclization**, a brief constrained MD was done for HAVc3** peptide structures from REMD simulations **to bring** two sulfur atoms **to** a distance of <2 Å. After forming a disulfide bond to make cyclic cHAVc3, a 50 ns REMD simulation was performed with conditions analogous to those of linear HAVc3 (see above), and exchange probabilities in the range of 0.1–0.18 were observed. Clustering was performed from the 5000 conformations sampled in the 320 K replica trajectory of cHAVc3 using GROMOS algorithm [21]. The central structures from the five most populated clusters were selected to represent 95% of all sampled structures, and these structures were used for docking experiments with the EC1 domain of E-cadherin.

3.2.5 Docking of cHAVc3 to the EC1 Domain using HADDOCK

The coordinates for the human EC1 domain model were extracted from the final structure in the 100 ns EC1 MD simulation. Coordinates for five representative

structures of cHAVc3 from REMD simulations were used for the docking experiments. They were docked to the EC1 domain structure from the 100 ns EC1 structure using HADDOCK server with the Easy Interface option. Both blind and NMR-constraints docking experiments were performed. The blind docking was carried out using all 138 residues of the EC1 as the potential binding site, while NMR-constraints docking experiments were done using the C9, Y36, I38, T63, F77, S78, I94, D103, and V112 residues as constraints for the potential binding site(s). The NMR constraint residues were selected from the chemical shift perturbation data of peptide titration experiments, and the HADDOCK clusters of docking were selected based on the highest HADDOCK scores [22, 23].

3.3 Results

3.3.1 NMR Studies

3.3.1.1 Determination of the Binding Properties of cHAVc3 on the EC1 Domain

To identify the EC1 residues that showed CSP changes (i.e., interactions) when titrated with cHAVc3, the NMRPipe program was used to overlay the 2D ^{1}H,-^{15}N-HSQC NMR spectrum of the free and peptide-titrated EC1 domain (Figure 1). The peptide titration generated different magnitudes of CSP on the EC1 domain, including C9, N12, L21, Y36, S37, I38, I52, I53, T63, R68, F77, S78, H79, S82, S83, I94, D103, T109, V112, and F113 residues (Figure 1). These residues were selected based

on noticeable changes upon overlaying the NH crosspeaks of the free and titrated EC1 domain. The EC1 residues that have ΔF values higher than the total average ΔF value are considered to be residues that are involved in direct interactions with the peptide. The residues that had ΔF values higher than the total average ΔF were C9, Y36, I38, T63, F77, S78, I94, D103, and V112. The residues that had ΔF values lower than the total average were N12, L21, S37, I52, I53, R68, H79, S82, S83, T109, and F113, and these were considered to be insignificant changes. These residues were assumed not to be involved in direct binding, and the chemical shift changes (or CSP) were due to conformational changes in the EC1 domain away from the primary peptide-binding site.

Figure 1A

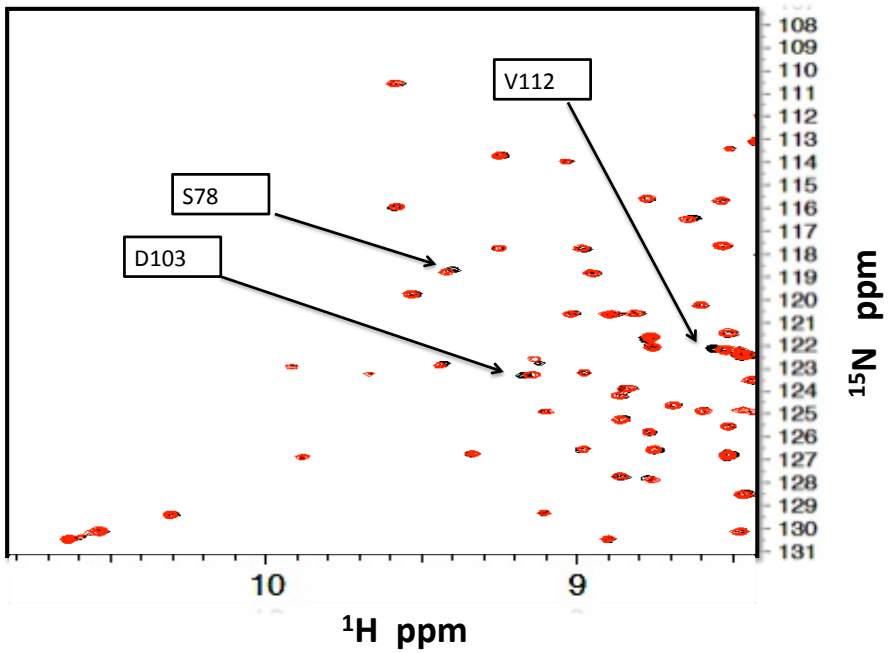

Figure 1B

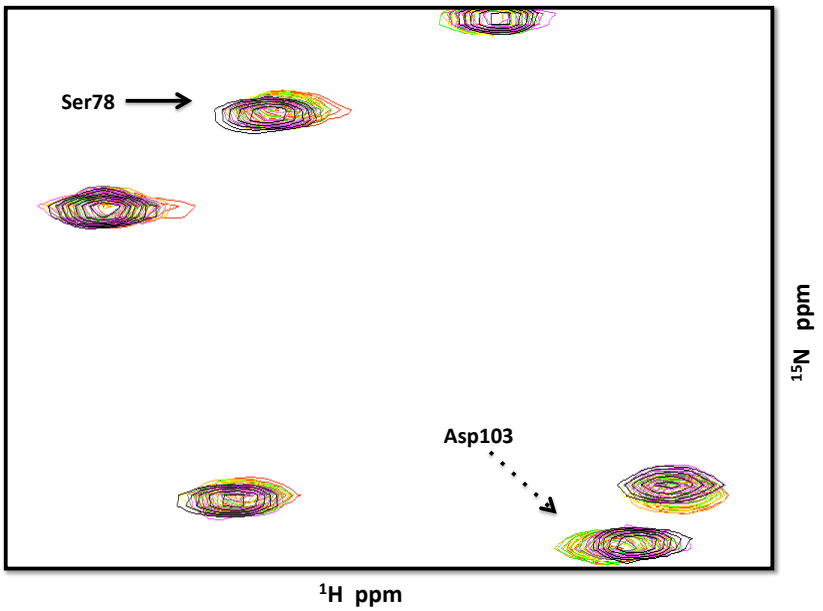

Figure 1C

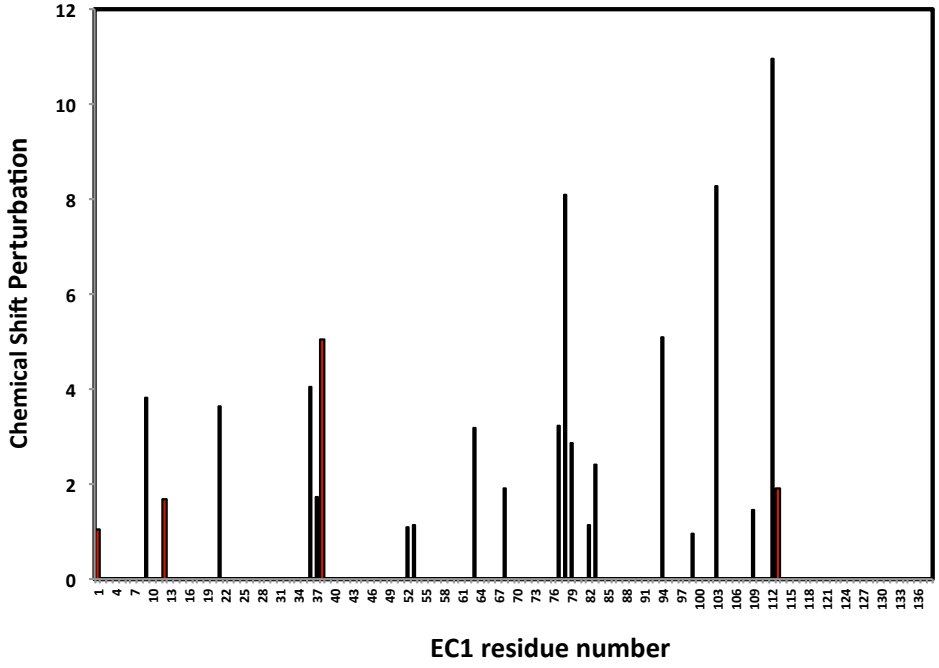

Figure 1D

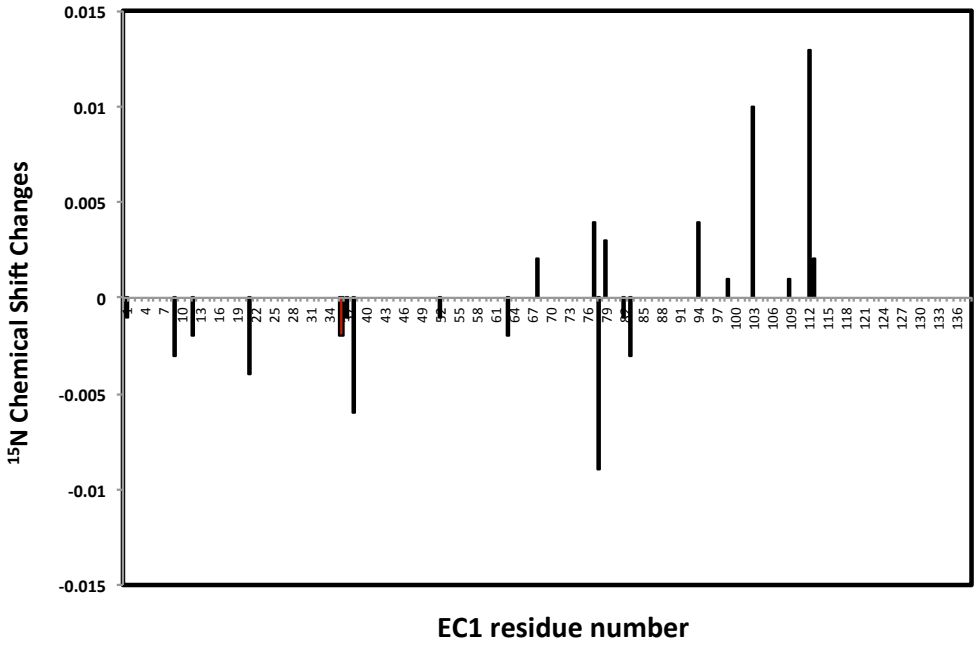

Figure 1. The chemical shift changes of residues in the 2D ^{1}H,-^{15}N-HSQC NMR spectra of the free and peptide-titrated EC1 domain collected using Bruker Avance 800 MHz spectrometer. (A) The overlay of partial 2D NMR spectrum of the EC1 domain (red) and titrated EC-1 domain at the highest peptide concentration (black). (B) The overlay of crosspeak shifts from the NH of Ser78 (S78, left) and Asp103 (D103, right) upon titration with cHAVc3 peptide from 0.3:1 to 2.5:1 peptide-to-protein molar ratios. (C) The observed chemical shift perturbation (CSP) of the EC1 residues weighted for both ^{1}H, and ^{15}N using equation 1 when titrated with cHAVc3 peptide at a peptide/protein ratio of 2.5:1. (D) The ^{15}N chemical shift changes in the EC1 residues upon titration with 2.5:1 peptide/protein ratio.

3.3.1.2 Determination of Dissociation Constant (K_d) of cHAVc3 to the EC1 domain

The dissociation constant (K_d) of cHAVc3 peptide to the EC1 domain was determined using NMR data from the peptide titration experiments at the peptide-to-protein ratios of 0.3:1 to 2.5:1. The estimated K_d values were determined using Δ_{obs} and Δ_{max} using equation 2 on different residues (i.e., C9, R68, F77, S78, I94, D103, and V112) with ΔF values (Equation 1) as represented by the F77, S78, and V112 residues in Figure 2. The K_d values of the R68 and I94 residues were measured using only the chemical shift changes in ^{15}N nucleus: $\Delta\delta^{15}N = \delta^{15}N_{obs} - \delta^{15}N_{free}$. The calculated K_d values from various residues ranged from 0.5×10^{-5} to 7.0×10^{-5} M (Table 1).

Figure 2A

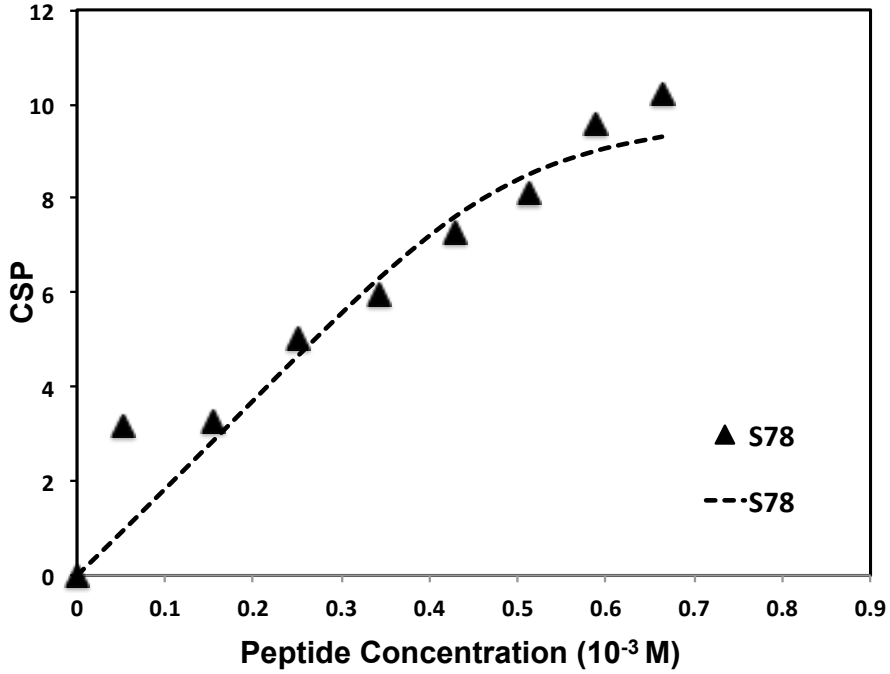
12
10
8
6
4
2
0
CSP
0
0.1
0.2
0.3
0.4
0.5
0.6
0.7
0.8
0.9
Peptide Concentration (10-3 M)
S78
S78

Figure 2B

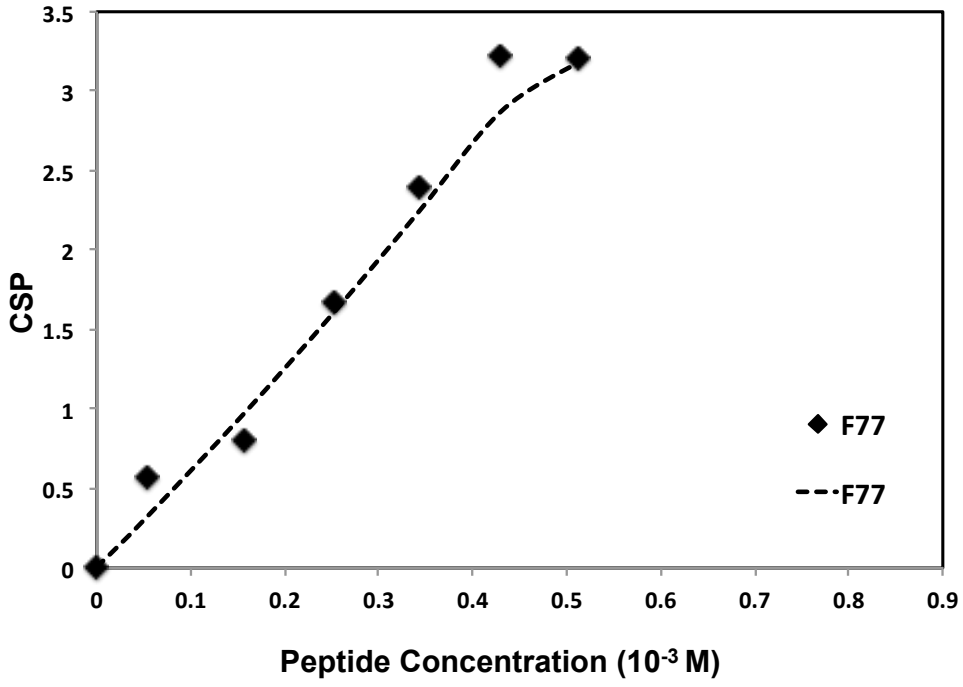
3.5
3
2.5
2
1.5
1
0.5
0
CSP
0
0.1
0.2
0.3
0.4
0.5
0.6
0.7
0.8
0.9
Peptide Concentration (10-3 M)
F77
F77

Figure 2C

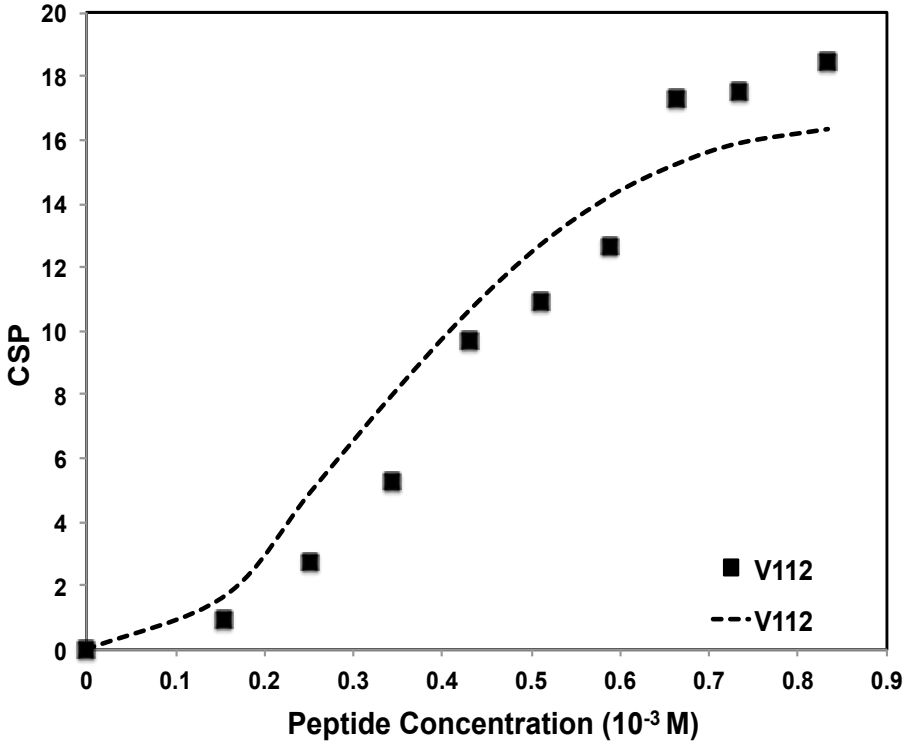

Figure 2. The ^{1}H,-^{15}N-weighted CSP changes (ΔF) from the NMR spectrum as a function of peptide/protein ratios for representative residues in the EC1 domain: **(A)** S78, **(B)** V112, and **(C)** F77. The K_d was estimated using nonlinear regression for the simulated curve (-.-.-). The saturation point was estimated because of small changes in chemical shift between the last and penultimate titration points.

Table 1. The estimated K_d values of binding between cHAVc3 and the EC1 domain of E-cadherin determined using ^{1}H,-^{15}N CSP of different residues upon peptide titration with cHAVc3:EC1 ratios of 0.3:1 to 2.5:1.	
Residue of Protein	**K_d (1×10^{-5} M)**
S78	2.5
F77	0.5
C9	1.0
*I94	7.0
*R68	1.0
V112	4.5
D103	0.5

3.3.3 Molecular Modeling Studies of Binding between cHAVc3 and the EC1 domain

3.3.3.1 Molecular Dynamics for the EC1 domain

To evaluate the dynamic properties of the EC1 domain used in the NMR studies, the starting structure had 138 amino acid residues that are derived from the sequence of the EC1 domain (110 residues as the "head region") plus 28 residues from the EC2 domain sequence of the "tail region." Because the starting structure was derived from the X-ray structure of the EC1-EC2 domains of human E-cadherin, the tail region extended away from the head EC1 domain (Figure 3A). At 100 ns MD simulations, the tail region moved closer to and interacted with the head

region (EC1, Figure 3B). The movement of the tail group was due to the absence of crystal packing in the starting X-ray structure. The starting structure and the final MD structure were overlaid using the C-alpha of the backbone residues 1 to 90. This comparison showed a root-mean-square-deviation (RMSD) of 0.746 Å (Figure 3C), indicating a stable head region. This study suggests that the EC1 structure in solution has the head region retained in its folded structure while the flexible tail region moves closer to the head region.

Figure 3

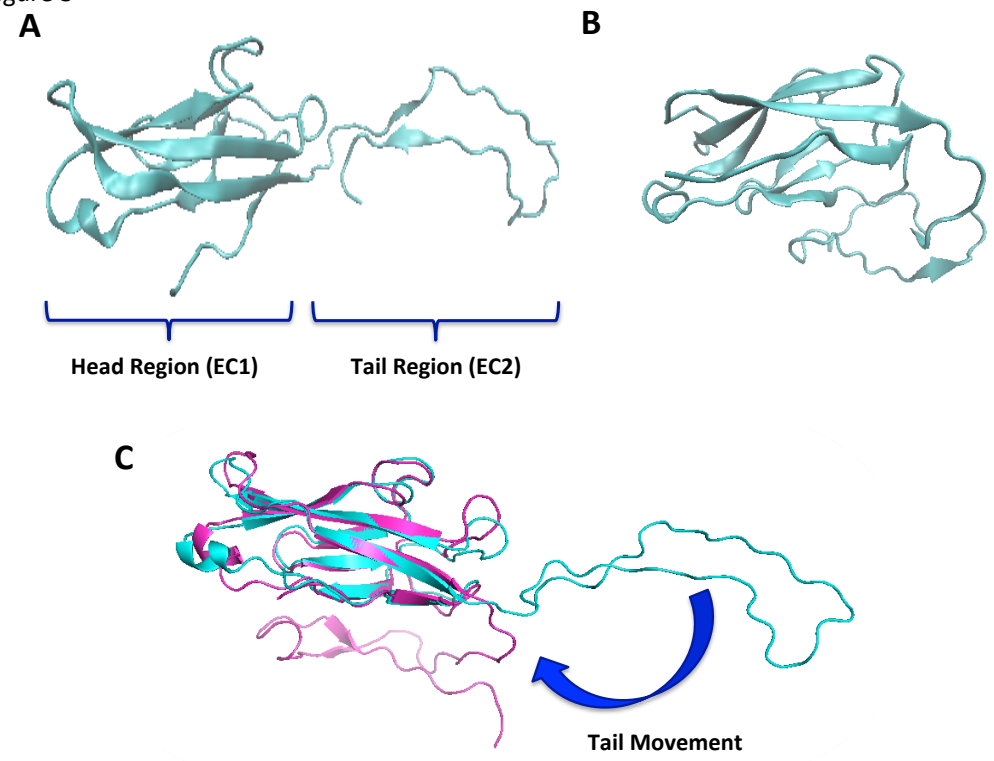

Figure 3. The comparison between **(A)** the starting structure, taken from the X-ray structure of the EC1 domain with a small fragment from the EC2 domain, and **(B)** the

final structure after 100 ns molecular dynamics simulations. **(C)** The overlay of the starting structure (magenta) and the final structure from MD simulations (pink). The structure from the MD simulations shows the C-terminal tail that swings into the main region of the EC1 domain as indicated by the curved arrow. After MD simulations, the alignment of the residues 1 to 90 between the X-ray structure and the MS simulation structure has RMSD < 1.0 and the tail is close to the head part of the protein.

3.3.3.2 Molecular Dynamics of cHAVc3

For docking studies, the structure of cyclic cHAVc3 was generated using CHARMM from the structure of linear HAVc3, which was subjected to 100 ps REMD simulations in a box of water molecules. The resulting structures of linear HAVc3 have an RMSD of 0.1Å, which was close to that of the initial structure. Then, a 50 ns REMD was carried out on linear HAVc3 with increasing constraints to pull the two sulfur atoms of the Cys residues to a distance of less than 0.2 nm. A disulfide bond was formed between two sulfur atoms of the cysteine residues of linear HAVc3 to make the cyclic cHAVc3 structure, followed by energy minimization. The cyclic cHAVc3 structure was then subjected to 100 ps REMD simulations to give acceptable probability exchange. A 50 ns REMD simulation at 320 K was carried out to provide the top five structural clusters, and the central conformer from each cluster was used to represent each cluster (Figure 4). The phi

and psi angles of each residue are shown in Table 1. The structures in both clusters 1 and 2 contain type-I and type-VII β-turns, respectively, at His3-Ala4-Val5-Cys6, with a potential hydrogen bond from the NH of Cys6 to the C=O of His3. The structures in clusters 3 and 5 have type-I and type-I' β-turns, respectively, at Cys1-Ser2-His3-Ala4, with a potential hydrogen bond from the NH of Ala4 to the C=O of Cys1. Finally, cluster 4 has structures with a γ-turn at Ala4-Val5-Cys6 with a potential hydrogen bond from the NH of Cys6 to the C=O of Ala4.

Figure 4

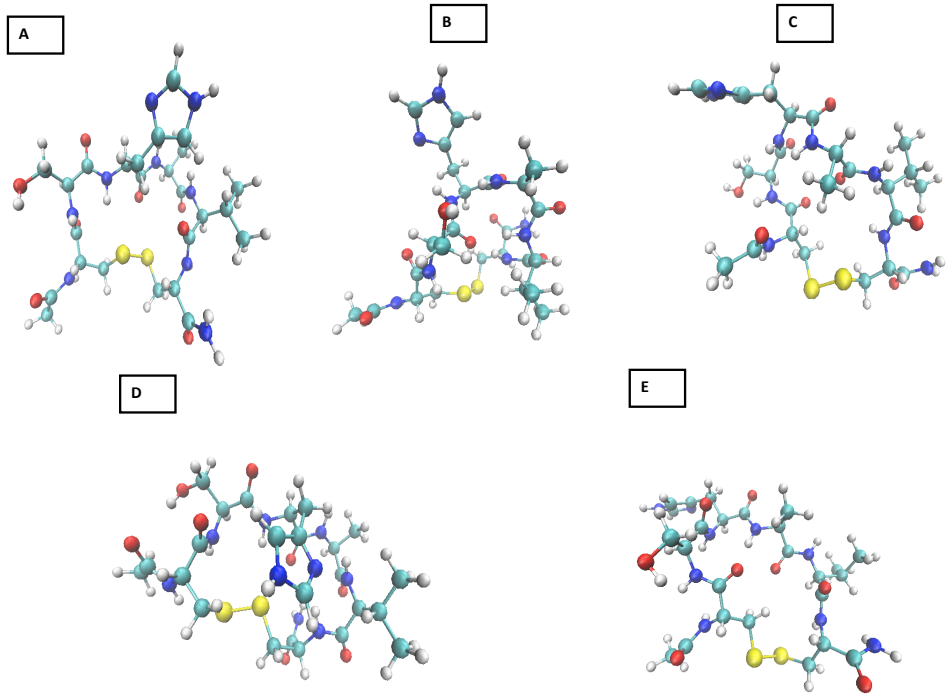

Figure 4. The results from MD simulations to generate stable cyclic structures of cHAVc3 peptide. There are five different clusters of structures of cyclic cHAVc3 (A to

E). Conformation A has the highest number of structures in a cluster, suggesting that it is the closest to the solution conformation of cHAVc3. Conformation A was used for docking experiments with the EC1 structure for the MD simulation. Other conformers (B–E) were also used for molecular docking with the EC1 domain, and they gave docking results on the EC1 domain similar to those of conformation A.

3.3.4 Molecular Docking of cHAVc3 to the EC1 Domain

The purpose of the docking studies was to propose a working model of binding between the cHAVc3 peptide and the EC1 domain. The potential binding site(s) was searched with the help of experimental data from peptide titration observed by 2D-NMR. The NMR-constraints docking experiment showed that the cHAVc3 structures with the highest HADDOCK scores were clustered around the F77 and S78 residues on the EC1 domain. This suggests that the region around F77 and S78 residues is the potential binding site for cyclic cHAVc3 peptide (Figure 5). The second highest docking score was found in a cluster of molecules that were docked on the tail region around the V112 residue. Finally, the third highest docking score was in a cluster of molecules that docked on the region around the K105 and D103 residues. The NMR data from titration experiments showed that the highest ΔF value was from the residue S78, supporting the suggestion that the potential binding site of cHAVc3 is around the S78 and F77 residues (Figure 5). The

detailed interaction between cHAVc3 on the EC1 around both F77 and S78 is shown in Figure 5, where hydrophobic pockets bind to the Ala and the disulfide bond of the cHAVc3 peptide, respectively. For the blind docking experiments, the highest scoring clusters were found around the K105/D103 residues. Finally, the third cluster was found around the V112 residue region (supplementary).

Figure 5A

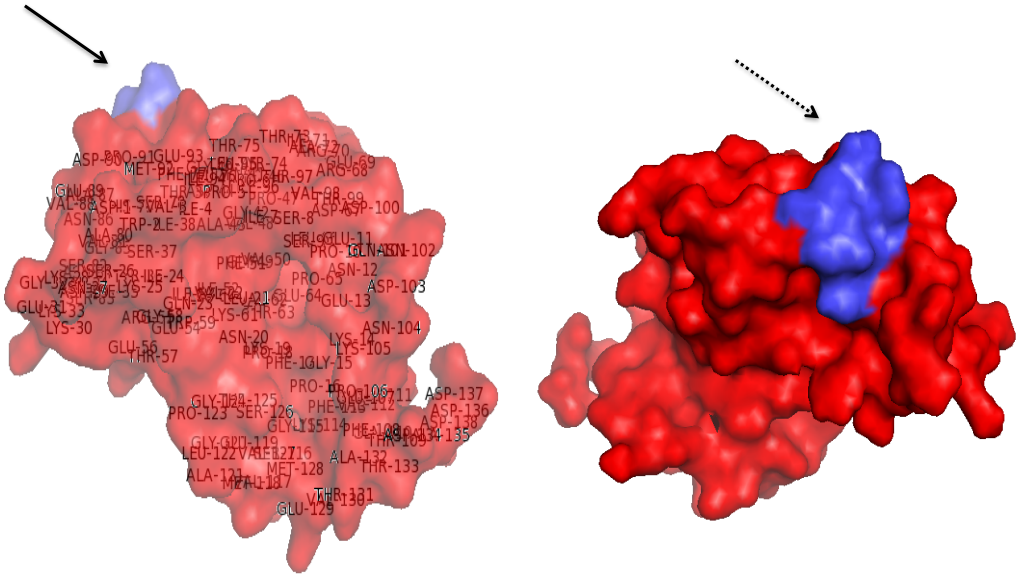

Figure 5B

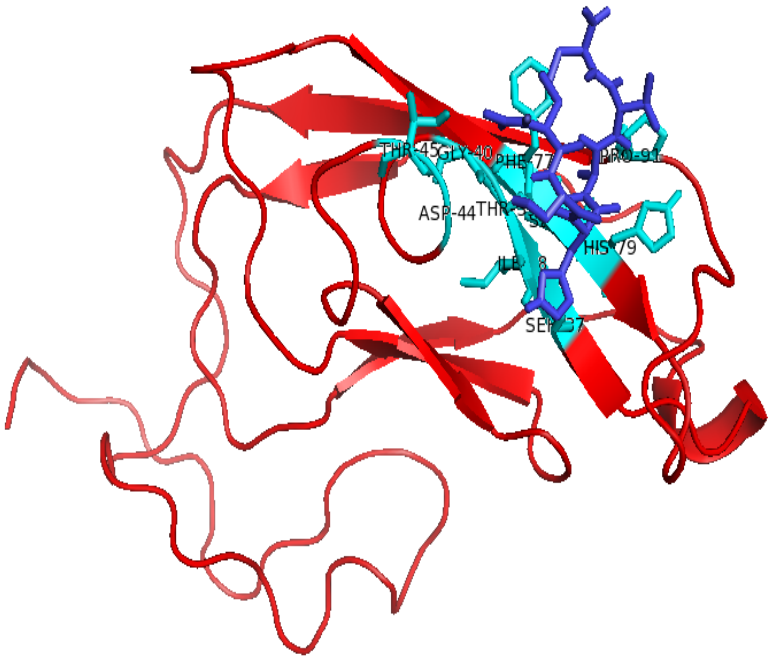

Figure 5C

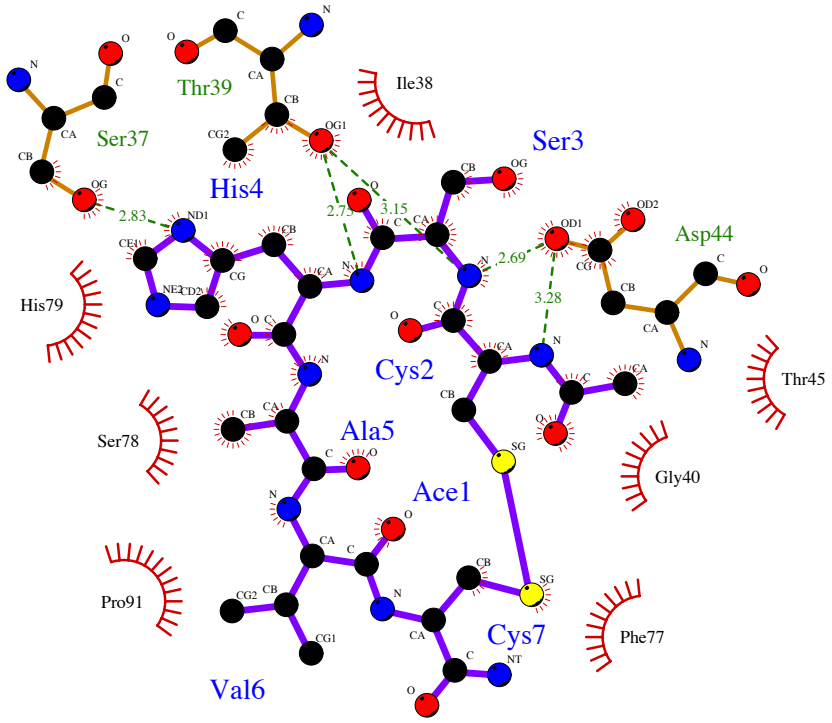

Figure 5. **(A)** The docking model of conformation A of cHAVc3 to the EC1 domain (black arrow) to indicate the potential binding site of cHAVc3 peptide in EC1. **(B)** The interaction region of cHAVc3 (blue) on the residues of EC1 (cyan). The S78 residue has a hydrophobic pocket that interacts with the Ala4 residue of cHAVc3 peptide. The F77 residue has the same type of interaction with the disulfide bond of the peptide. **(C)** The interaction network between cHAVc3 peptide and the EC1 domain from the docking structure.

3.4 Discussion

The NMR assignments of amino acids in the EC1 domain of human E-cadherin (h-E-cadherin) were done using the ^{15}N-labeled and $^{13}C/^{15}N$-labeled EC1 domain [13]. These assignments were accomplished with the help of the NMR assignments of the EC1 domain of mouse E-cadherin [13, 24]. The difference between the human EC1 (h-EC1) domain studied here and the mouse EC1 (m-EC1) domain is that the h-EC1 domain has an additional 28 amino acid residues from the EC2 domain at the C-terminal, which is called the tail region. The function of the tail region is to stabilize the conformation of the h-EC1 domain. Although the CD spectrum of the h-EC1 domain without the tail region showed a folded structure with a high beta-sheet secondary structure [25, 26], the NMR spectrum of the EC1 domain did not show well-spread crosspeaks in the HSQC spectrum. This suggests that without this tail region the structure of the EC1 domain is folded but rather dynamic in nature. Many attempts to change the solution conditions (i.e., pH, ionic strengths, various buffers) to stabilize the EC1 domain without the tail region for NMR study were not successful [25, 26]. In contrast, the m-EC1 domain has a stable conformation in solution and produces well-spread crosspeaks in the NMR spectrum for structural determination [24].

Here, MD simulations were done to observe the dynamic behavior of the EC1 molecule, especially the role of the tail region in stabilizing the structure of EC1. The starting structure of the EC1 domain was from the X-ray structure of h-E-

cadherin with the extended tail region derived from the sequence of the EC2 domain and without interaction with the head region. Because the NMR data showed that the tail region was important in stabilizing the solution structure of the head region of EC1, molecular dynamic simulations were carried out in an explicit water environment. The results showed that the tail region swings into and interacts with the head region of EC1 as indicated by the dramatic changes of the RMSD of the tail residues (Figure 3C). This indicates that these interactions stabilize the structure of the EC1 domain in solution. After MD simulations, the RMSD was determined using alignments of C-alpha backbone from residues 1–90 for EC1 from MD simulation and X-ray as well as m-EC1 from the NMR study (Figure 3C). The results show a small magnitude of the RMSD, indicating that there is limited change in the head region of the h-EC1 domain during MD simulations. The majority of the change occurred in the tail region that swung closer to and interacted with the head region of EC1.

The structure of the EC1 domain from MD simulations was used to determine the binding site of cHAVc3 by implementing the NMR constraints from the CSP data upon peptide titration. The observed CSP could also be the result of local conformational changes in the EC1 as a consequence of peptide binding [12, 27, 28]. Although the magnitude of CSP varied from residue to residue, the residues that have CSP values higher than average are C9, Y36, I38, T63, F77, S78, I94, D103, and V112. The high CSP changes were attributed to binding to the EC1 domain,

and these were used as NMR-constraints in the docking experiments to search for binding site(s) of the peptide [27]. The docking model shows that the cHAVc3 peptide interacts with residues Y36, I38, F77, S78, and I94 with CSP values higher than average, as well as with S37, I53, and H79 with CSP values lower than average (Figure 7). This binding site has high consistency with the NMR data (Figure 1C). Free docking calculations yielded several possible models for cHAVc3:EC1 complexes. However, the availability of NMR CSP data allowed generation of more reliable microscopic models by docking with NMR-constraints.

There are also residues with low and high CSP values that are far away from the binding site; these residues include D103, T109, V112, and F113 (Figure 7). The observed CSPs in these residues were attributed to conformational changes on the tail region of EC1 during peptide binding. It is interesting to find that the large change in chemical shift of D103 can be attributed to the conformational swing of the tail region to stabilize its interaction with the head region (i.e., EC1) (Figure 3C). The D103 residue can be categorized as the hinge residue for the dynamic movement of the tail region to interact with the head region. The dihedral angle measurement (ϕ; ψ) of D103 from 0 ns (X-ray structure) to 100 ns (MD structure) showed that the ψ of D103 changed dramatically (Figure 6). In the other hand, the ψ measurements of D100 and N104, flanking residues around D103, did not change dramatically during the MD run (Figure 6). This suggests that the D103 residue behaves as a hinge residue to move the tail region closer to the head region of EC1

(Figure 3C). In addition, the CSP comparison among the S78, D103, and V122 residues at the initial titration points shows that the CSP values of the D103 and V112 residues are less sensitive than that of S78 when titrated with the peptide, suggesting that cHAVc3 more likely binds to the region of the S78 residue. T109, V112, and F113 from the tail region were additional residues that were affected by peptide titration (Figure 7); these residues from the tail region are clearly interacting with the head region of the protein. The observed CSP values in the tail region are due to the conformational changes in the tail region upon peptide binding. This result also supports the idea that the tail region folded into the head region of EC1 as indicated by the MD simulation results.

The K_d values were estimated by curve fitting simulations using NMR data of chemical shift changes from several residues (i.e., C9, F77, S78, I94, D103, and V112) at different peptide:protein ratios (<2.5:1.0). The low range K_ds of cHAVc3 binding to EC1 were estimated to be around 0.5×10^{-5} – 1.0×10^{-5} M using the F77, C9, R68, and D103 residues (Table 1). The medium range K_d was estimated using the S78 residue, and the high range K_ds were estimated from the V112 and I94 residues. For the R68 and I94 residues, the chemical shift changes in ^{15}N as [PL] complex ($\Delta\delta^{15}N$; 1D) was fitted in the titration curve.

The calcium-binding region in E-cadherin was found at the interface between the EC1 and EC2 domains, and the D103 and the tail region of EC1 studied here contained part of the calcium-binding site. It has been shown previously that

cadherin molecules form a rod-like structure (or extended structure) due to the coordination of calcium at the interface region. In the absence of calcium, the rod-like structure collapses into a globular cadherin structure. In this study, the tail region swinging to interact with the head region of EC1 could be a natural behavior of this protein in the absence of calcium, and it is reasonable to speculate that the D103 residue is also involved in the dynamic conversion of a rod-like structure in the presence of calcium to a globular structure of cadherin in the absence of calcium.

Figure 6A

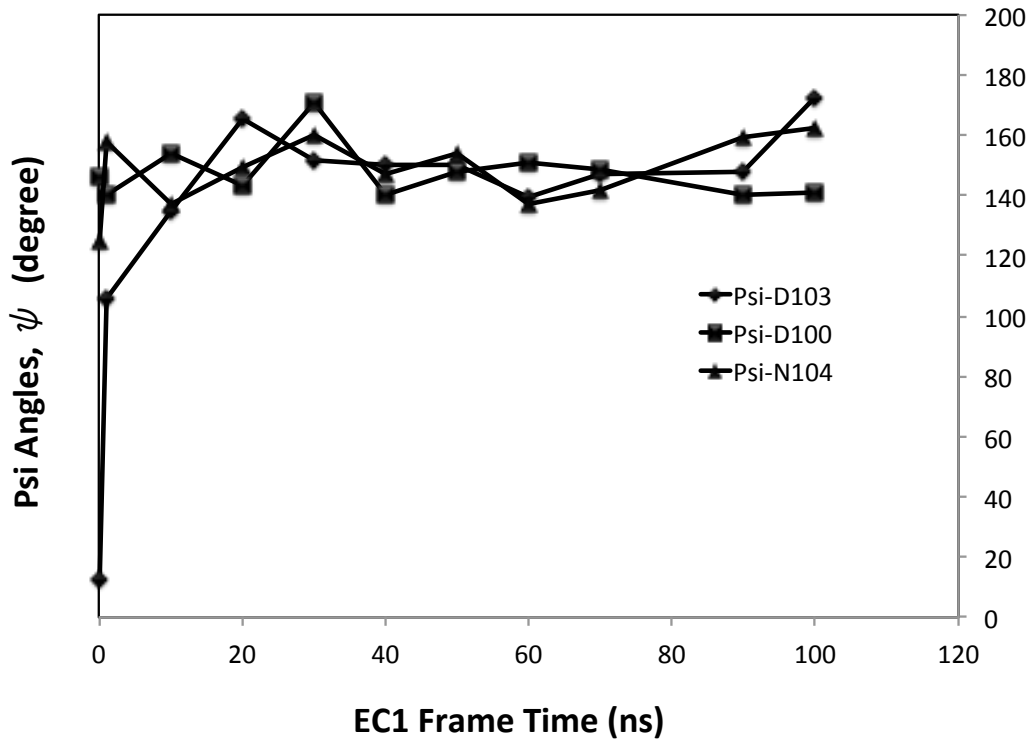

Figure 6B

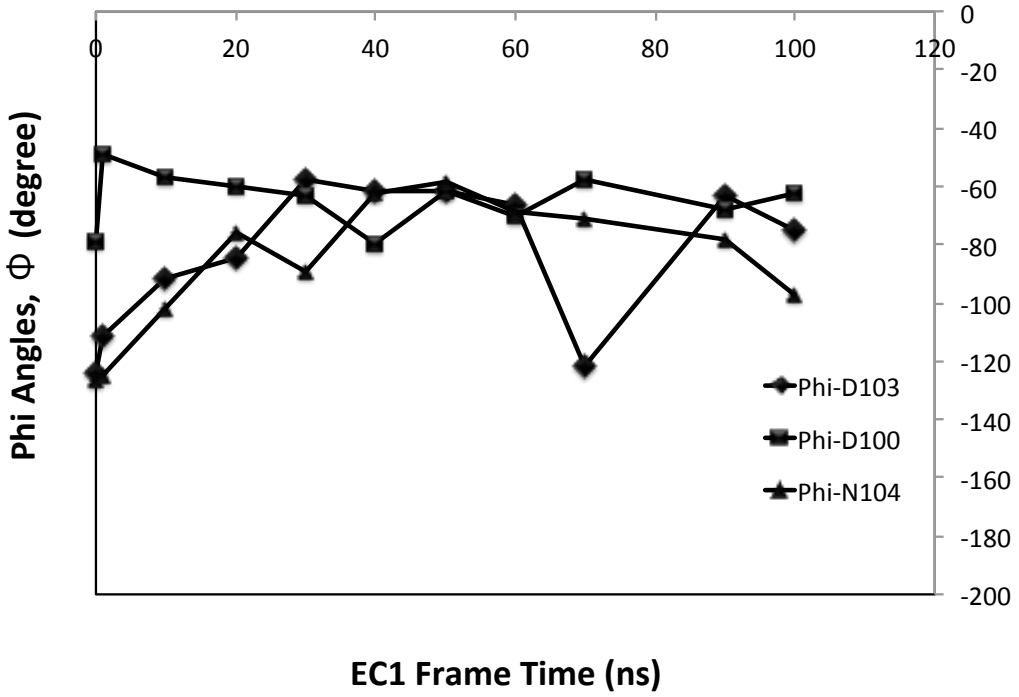
0
20
40
60
80
100
120
0
-20
-40
-60
-80
-100
-120
-140
-160
-180
-200
Phi Angles, Φ (degree)
EC1 Frame Time (ns)
Phi-D103
Phi-D100
Phi-N104

Figure 6C

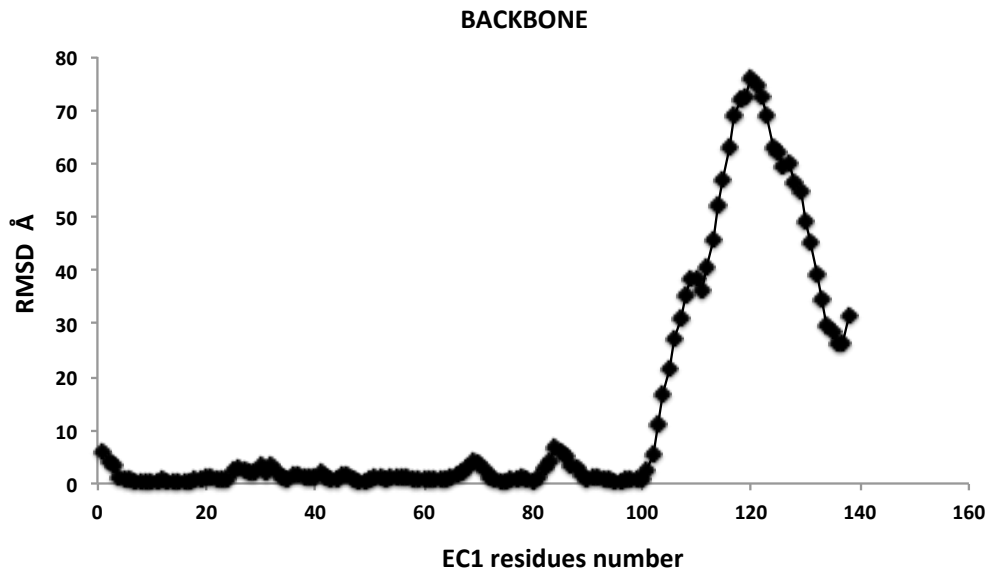

Figure 6. (A) The changes in psi (ψ) angle of D103 (◆), D100 (■) and N104 (▲) residues during the molecular dynamics run of EC1 domain in water. Comparing to the ψ^{D103} in the X-ray structure (0 ns) shows dramatic changes during the MD run. The ψ angles of D100 and N104 (flanking residues of D103) showed no dramatic changes between the X-ray and MD structures in comparison to ψ^{D103}. **(B)** The changes in phi (Φ) angles of D103 (◆), D100 (■) and N104 (▲) residues in which Φ^{D103}, Φ^{D100} and Φ^{N104} experienced similar changes during the MD run. **(C)** The RMSD per residues between the X-ray and MD structures of the EC1 domain as RMSD > 10 Å are accounted for mostly by tail residues.

Figure 7

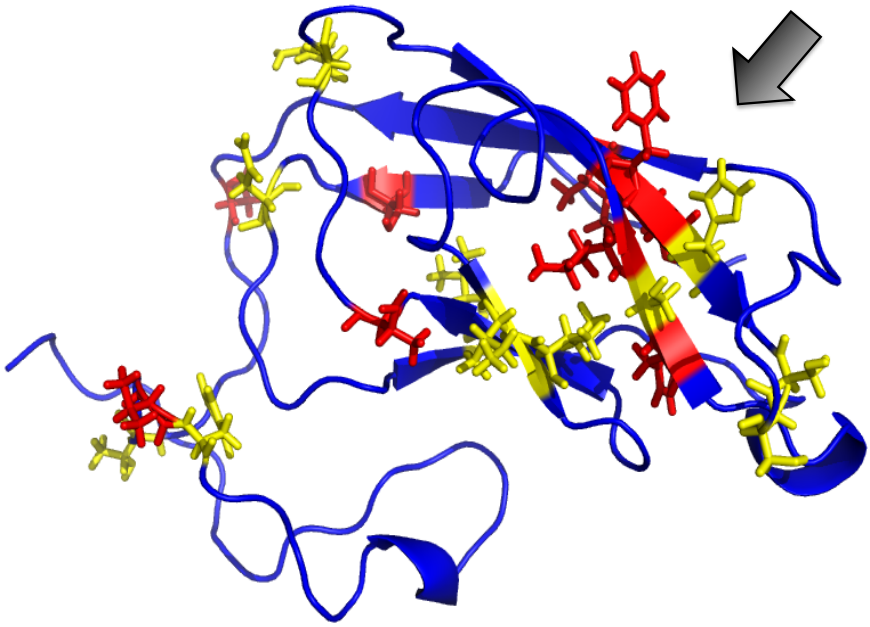

Figure 7. The MD structure of the EC1 domain showing residues that had higher ΔF values (red) and residues with lower ΔF values (yellow) when the EC1 domain was titrated with cHAVc3 peptide. The pocket for cHAVc3 peptide in EC1 domain is represented by S78, F77, H79, Y36, S37, and I38, along with the surrounding I94 and I53 residues. Most chemical shift changes (red and yellow colors) are closed to the binding pocket of cHAVc3, indicating the binding region of cHAVc3 peptide. The chemical shift changes of the tail residues, including the D103 residue, can be attributed to the dramatic conformational changes of the tail region.

Table 2. The phi and psi angles for amino acid residues of cHAVc3 peptide in different stable clusters of conformers from MD simulations. Secondary structure(s) for each cluster were determined by phi and psi angles and either H-bond network

Cluster Number	Dihedral Angles	Residues						Secondary Structure
		Cys1	Ser2	His3	Ala 4	Val5	Cys6	
Cluster 1	phi	–106.1	–108.5	–121.9	–63.5	–95.1	–124.9	βI-turn at H3-C6
	psi	144.2	139.0	–6.5	–39.9	–58.1	84.2	
Cluster 2	phi	–70.8	–70.5	–84.4	–59.5	–92.8	–73.6	βVII-turn at H3-C6 and Inv. γ-turn at C6
	psi	137.2	3.9	160.5	–41.3	126.7	77.4	
Cluster 3	phi	–116.3	–70.8	–107.5	–77.3	–108.3	–104.5	βI-turn at C1-A4
	psi	21.4	–41.5	–27.8	162.3	110.2	74.1	
Cluster 4	phi	–68.1	68.0	–145.9	–59.3	72.1	–67.6	γ-turn at V5
	psi	–36.2	43.3	169.3	–34.4	–47.3	–19.0	
Cluster 5	phi	–112.9	61.1	60.8	–141.5	–52.1	–84.9	βI'-turn at C1-A4
	psi	14.4	48.1	28.5	164.3	146.7	–7.3	

3.5 References

1. Neuwelt, E.A., et al., *Osmotic blood-brain barrier disruption. Computerized tomographic monitoring of chemotherapeutic agent delivery.* J Clin Invest, 1979. **64**(2): p. 684-8.
2. Dean, R.L., et al., *Cereport (RMP-7) increases carboplatin levels in brain tumors after pretreatment with dexamethasone.* Neuro Oncol, 1999. **1**(4): p. 268-74.
3. Laksitorini, M., et al., *Pathways and progress in improving drug delivery through the intestinal mucosa and blood-brain barriers.* Ther Deliv, 2014. **5**(10): p. 1143-63.
4. Zwanziger, D., et al., *A peptidomimetic tight junction modulator to improve regional analgesia.* Mol Pharm, 2012. **9**(6): p. 1785-94.
5. Makagiansar, I., et al., *Improving the selectivity of HAV-peptides in modulating E-cadherin-E-cadherin interactions in the intercellular junction of MDCK cell monolayers.* Pharm. Res., 2001. **18**: p. 446–553.
6. Kiptoo, P., et al., *Enhancement of drug absorption through the blood-brain barrier and inhibition of intercellular tight junction resealing by E-cadherin peptides.* Mol Pharm, 2011. **8**(1): p. 239-49.
7. On, N.H., et al., *Modulation of blood-brain barrier permeability in mice using synthetic E-cadherin peptide.* Mol Pharm, 2014. **11**(3): p. 974-81.
8. Makagiansar, I.T., et al., *Localized production of human E-cadherin-derived first repeat in Escherichia coli.* Protein Expr Purif, 2002. **26**(3): p. 449-54.
9. Lutz, K.L., et al., *Structure, function and modulation of E-cadherins as mediators of cell-cell adhesion.* Curr. Top. Pept. Prot. Res., 1997. **2**: p. 69–82.

10. Zheng, K., M. Trivedi, and T.J. Siahaan, *Structure and function of the intercellular junctions: barrier of paracellular drug delivery.* Curr Pharm Des, 2006. **12**: p. 2813–24.

11. Williamson, M.P., *Using chemical shift perturbation to characterise ligand binding.* Prog Nucl Magn Reson Spectrosc, 2013. **73**: p. 1-16.

12. Stark, J.L. and R. Powers, *Application of NMR and molecular docking in structure-based drug discovery.* Top Curr Chem, 2012. **326**: p. 1-34.

13. Prasasty, V.D., et al., *(1)H, (13)C and (15)N backbone assignment of the EC-1 domain of human E-cadherin.* Biomol NMR Assign, 2015. **9**(1): p. 31-5.

14. Fielding, L., *NMR methods for the determination of protein-ligand dissociation constants.* Curr Top Med Chem, 2003. **3**(1): p. 39-53.

15. A.Alaofi, N.O., P.Kiptoo, T. Williams, D. W. Miller, T. Siahaan, *Comparison of Linear and Cyclic HAV Peptides in Modulating the Blood-Brain Barrier Permeability: Impact on Delivery of Molecules to the Brain.* Journal of Pharmaceutical Sciences, 2015.

16. Skinner, A.L. and J.S. Laurence, *Probing residue-specific interactions in the stabilization of proteins using high-resolution NMR: a study of disulfide bond compensation.* J Pharm Sci, 2010. **99**(6): p. 2643-54.

17. Parisini, E., et al., *The crystal structure of human E-cadherin domains 1 and 2, and comparison with other cadherins in the context of adhesion mechanism.* J Mol Biol, 2007. **373**(2): p. 401-11.

18. Berendsen, H.J., D. van der Spoel, and R. van Drunen, *GROMACS: A message-passing parallel molecular dynamics implementation.* Computer Physics Communications, 1995. **91**(1): p. 43-56.

19. Hess, B., et al., *GROMACS 4: algorithms for highly efficient, load-balanced, and scalable molecular simulation.* Journal of chemical theory and computation, 2008. **4**(3): p. 435-447.

20. Brooks, B.R., et al., *CHARMM: The biomolecular simulation program.* Journal of Computational Chemistry, 2009. **30**(10): p. 1545-1614.

21. Daura, X., et al., *Peptide folding: when simulation meets experiment.* Angewandte Chemie International Edition, 1999. **38**(1-2): p. 236-240.

22. de Vries, S.J., M. van Dijk, and A.M. Bonvin, *The HADDOCK web server for data-driven biomolecular docking.* Nat Protoc, 2010. **5**(5): p. 883-97.

23. Wassenaar, T.A., et al., *WeNMR: Structural Biology on the Grid.* Journal of Grid Computing, 2012. **10**(4): p. 743-767.

24. Overduin, M., et al., *Solution structure of the epithelial cadherin domain responsible for selective cell adhesion.* Science, 1995. **267**(5196): p. 386-9.

25. Trivedi, M., et al., *Improving the stability of the EC1 domain of E-cadherin by thiol alkylation of the cysteine residue.* Int J Pharm, 2012. **431**(1-2): p. 16-25.

26. Trivedi, M., et al., *The role of covalent dimerization on the physical and chemical stability of the EC1 domain of human E-cadherin.* J Pharm Sci, 2009. **98**(10): p. 3562-74.

27. Cui, Y., et al., *Interaction between calcium-free calmodulin and IQ motif of neurogranin studied by nuclear magnetic resonance spectroscopy.* Anal Biochem, 2003. **315**(2): p. 175-82.

28. Williamson, R.A., et al., *Mapping the binding site for matrix metalloproteinase on the N-terminal domain of the tissue inhibitor of metalloproteinases-2 by NMR chemical shift perturbation.* Biochemistry, 1997. **36**(45): p. 13882-9.

CHAPTER 4

Discovery of Binding Pockets for Cadherin Peptides on the EC1 Domain of human E-cadherin

4.1 Introduction

The intercellular junctions of the blood-brain barrier (BBB) are mediated by protein-protein interactions form apposing cell membranes. The adheren junction of the BBB is partly mediated by calcium dependent cadherin-cadherin interactions (i.e., E- and VE-cadherins) and calcium independent Nectin interactions [1]. The primary structure cadherin include a C-terminal cytoplasmic domain, a single transmembrane domain, and an extracellular (EC) N-terminal domain. The EC domain composed of five repeat domains, which are designated as EC1, EC2, EC3, EC4, and EC5 domains. Three calcium ions with different Kds bind at the interface between two EC domains (between EC1 and EC2) [2]. These calcium ions are responsible to maintain the rod-like structure of the entire EC domain and the EC domain will fold to form a globular structure in the absence of calcium ions [2].

The mechanisms of cadherin-cadherin interactions have been studied using various methods, including using cell-adhesion assays and structural studies with X-ray crystallography and NMR spectroscopy using intact and truncated EC domains of cadherins. The similarity in EC domains of classical cadherin was shown using NMR, X-ray, and site-mutagenesis assays [3]. To form cell-cell adhesion at the intercellular junctions of biological barriers, several mechanisms of cadherin interactions have been proposed [4]. One proposed mechanism involves a homophilic interaction (*trans*-interaction) between EC1 domains form two apposite cell membranes (i.e., EC1-to-EC1 interaction) [5-7]. A second mechanism is called a

"zipper model" in which a *cis*-interacting dimer of two EC1 domains from one cell membrane forms a *trans*-interaction with another *cis*- dimer of EC1 domains from the opposing cell membrane. The *trans*-interaction involves domain swapping of the N-terminal of EC1 to a hydrophobic pocket of the opposing EC1 domain [4, 8]. The X-ray structure of C-cadherin shows a domain swapping mechanism of the EC1 domain in trans-interaction as well as a *cis*-interaction between EC1 of one cadherin molecule to EC2 of a parallel neighboring molecule [9]. The involvement of all five EC domains to form strong intercellular of E-cadherin has also been proposed after studying E-cadherin with truncated domain(s) using cell adhesion assays [6, 10, 11]. The C-terminal intracellular region of E-cadherin interacts with to β-catenin that binds to F-actin cytoskeleton complex via α-catenin. The monomeric α-catenin is essential to bind to β-catenin and then to cytoplasmic domain of E-cadherin; the dimeric form of α-catenin cannot bind to β-catenin. The cytoplasmic domain of E-cadherin also binds to p120ctn that is essential for E-cadherin function [6].

Previously, ADT and HAV peptides (Table 1) from the EC1 domain of human E-cadherin (hE-cadherin) have been shown to modulate the intercellular junctions of Madin-Darby Canine Kidney (MDCK) cell monolayers and enhance paracelluar transport of ^{14}C-mannitol across the cell monolayers [12, 13]. HAV6 peptide (Ac-SHAVSS-NH_2) enhanced transport of fluorescence-labeled dextran (MW = 4,400 Da) across the bovine brain microvessel endothelial cell (BBMEC) cell

monolayers [14]. Recently, linear and cyclic HAV (i.e., HAV6, HAV4, cHAVc3) and ADT (i.e., ADTC5) peptides were shown to increase the brain delivery of various molecules including paracellular markers (i.e., ^{14}C-mannitol, R800-cw-PEG 25 kDa), magnetic resonance imaging (MRI) contrast agent (Gadopentic acid or Gd-DTPA), near IR (NIR) dyes (R800) and anticancer drug (^{3}H-daunomycin) using in-situ rat brain perfusion model as well as in vivo Balb/c mouse model [15-18]. It is proposed that the mechanism of activity of HAV and ADT peptides is via binding to the EC1 domain of E-cadherin to inhibit cadherin-cadherin interactions and increase the pore size of paracellular pathway of the BBB.

In this study, the binding properties of HAV6, ADTC5, ADTC7, ADTC9 peptides to the EC1 domain of hE-cadherin were investigated using NMR data and molecular docking simulations. The ^{15}N-labeled EC1 domain was titrated with each peptide and the chemical shift perturbations (CSP) in the spectra of ^{1}H,-^{15}N-heteronuclear single quantum correlation (HSQC) NMR experiments were monitored for each residue of the EC1 domain. The docking experiments were conducted using NMR data constraints to determine the potential binding site of each peptide on the EC1 domain. The CSP values from NMR data of peptide titration experiments were used to estimate the dissociation constant (K_d) of each peptide to the EC1 domain.

4.2 Material and Methods

4.2.1 Dynamic Structure of EC1 Domain

The structure of EC1 domain used here was obtained from molecular dynamic (MD) simulations in a box of water using the X-ray structure of free EC1 domain (PDB code; 2O72) as the starting structure [19]. The studied EC1 domain has a total of 138 amino acid residues, which includes a flexible tail of 28 residues from the EC2 domain. The entire MD structure of EC1 at 100 ns was then compared to the standard X-ray structure from which a small RMSD value of 0.781 was obtained as described previously [20] .

4.2.2 Cadherin Peptide Structures

The PDB files of ADTc5, ADTc7, ADTc9 and HAV6 cadherin peptides were obtained using InsightII Program and their energy minimizations performed using CVFF91 force field (Accelrys, Inc. San Diego, CA) [21, 22] .

4.2.3 NMR-Constrained Docking Experiments

ADT and HAV peptides were docked onto the EC1 structure from MD simulations using HADDOCK program with Easy Interface option. The "active amino acids residues" of EC1 were selected based on chemical shift perturbation (CSP) analysis of NMR data for ADTc5, ADTc7, ADTc9 or HAV6 peptides [21, 22]. Residues of EC1 that showed noticeable chemical shift changes upon titration ADTc5, ADTc7, ADTc9, or HAV6 peptides to EC1 domain were selected as "active"

residues. Active residues were submitted as NMR constraints to HADDOCK program as docking simulations.

For ADTc5 peptide, the submitted active residues on the EC1 domain were selected from residues with large CSP values such as the I4, Y36, G58, R68, V98, T97, D103, and F113 residues. The active residues used for docking of ADTc9 were I4, L21, V48, I53, T97, V98, D103, F113, G115, E119 and T133 residues. For ADTc7 peptide, the active residues used for docking experiments were similar to those in ADTc9 titration with addition of the I38 residue. For the HAV6 peptide, the submitted active residues on the EC1 domain were S78, V48, T98, I53, and D103. After docking experiment for each peptide (i.e., ADTc5, ADTc7, ADTc9, and HAV6), the top three highest scoring clusters were selected and analyzed as working models for peptide binding.

4.2.4 Blind Docking Experiments

To validate the NMR-constrained docking experiments, "blind docking" experiments were performed. In this simulation, all 138 residues of the EC1 domain were considered active and submitted to HADDOCK. As in previous simulations, the top three HADDOCK-scoring clusters were selected and analyzed.

4.2.6 Structural Analysis of Docking Clusters

Each cluster file (PDB file) revealed interactions between EC1 domain and the peptide. LigPlus program was used to view the two-dimensional diagram of

interactions between the EC1 domain and each peptide as reported by HADDOCK. PyMOL program (PyMOL Molecular Graphics System, Version 1.3, Schrödinger, LLC.) was used for plotting and visualizing the interactions in 3D [23, 24].

4.3 Results

4.3.1 Binding Characteristics of ADTc5 Peptide to the EC1 Domain:

There were eight cluster models found during the docking experiment of ADTc5 peptide and all but one cluster models were approximately in close proximity to each other (Table 2). Clusters #5 and #8 have the top-two high HADDOCK scores and these clusters were used to represent binding characteristics of ADTc5 peptide to the EC1 domain (Figure 1A). In cluster #5, ADTc5 interacts with the following residues: P6, S8, S9, T97, T99, P10, D100, Q101, D103, and K105; while in cluster #8, it interacts with the following residues: P6, S8, P10, T99, D103, and K105 (Table 2). Thus, the P6, S8, P10, T99, D103 and K105 residues were the common residues in both clusters #5 and #8 (Figure 2A). The NMR data from peptide titration indicated that the T97, V98, and D103 residues had the high CSP values, which were consistent with the seven clusters found in docking experiment. Cluster #6 was located in a different region from the other seven clusters, which might not be a favorable binding site. The K_d values of ADTc5 (Table 3) were estimated using titration curves with high and saturable CSP values of EC1

residues (Figure 3A). The I24, I53, G58, G115, E119, and T133 residues have K_d values around 9–47 μM (Table 3).

4.3.2 Binding Characteristics of ADTc7 Peptide to the EC1 Domain:

Docking experiments of ADTc7 on the EC1 domain produced seven cluster models and all except one of the cluster models were approximately close regions except one model (Table 2). The top two clusters with high HADDOCK scores (cluster #1 and cluster #7) were used to represent the six cluster models of ADTc7 peptide. Both clusters bind to the N20, L21, and K105 residues on the EC1 domain, suggesting these residues defined the binding pocket for ADTc7 (Figure 1B). For cluster #1, ADTc7 interacts with residues E13, K19, N20, L21, K105, P106, G124, S126, and T125 in the EC1 domain. Similarly for cluster #7, the peptide interacts with residues I4, P5, I7, S8, P10, N20, L21, V22, Q23, W59, and K105 on the EC1 domain (Figure 2B). The I4 and L21 residues in EC1 showed considerable high CSP values in the NMR data upon titration with ADTc7. Finally, cluster#6 represents the docking of ADTc7 to the tail region of the EC1 domain. It has been shown previously that the tail region moved upon titration with cadherin peptides, which was also reflected by the change in CSP values. The accepted titration curves for the EC1 residues (Figure 3B) that involved in the binding site of ADTc7 peptide to EC1 were used to report K_d values (Table 3). The estimated K_d values using residues V98, I4, and T97 were 10, 10, and 22 μM, respectively (Table 3).

4.3.3 Binding Characteristics of ADTc9 Peptide to the EC1 Domain:

The results from docking of ADTc9 peptide to the EC1 domain produced six clusters and all the clusters were found located close to each other on EC1 domain (Table 2). The two cluster models with the top HADDOCK scores were cluster #1 and cluster #2; these clusters were used to represent the docking regions for ADTc9 peptide (Figure 1C). The residues on the EC1 domain that involved in binding or the binding pocket for both cluster models were at the S9, P10, E13, N20, L21, K105, P106, T125, G124, S126 residues (Figure 2C). In cluster #1 docking model, the residues of EC1 that interact with ADTc9 peptide are S9, P10, E13, K19, N20, L21, K105, P106, G124, T125, and S126 (Figure 2C). In parallel, the residues that interact with the EC1 domain in cluster #2 are residues S9, P10, E13, P16, N20, L21, W59, K105, F108, P106, G124, T125, and S126. Titration of EC1 with ADTc9 peptide generated considerable CSP on the NMR spectrum of L21 and this residue also interacted with the peptide in both cluster #1 and #2 models. The CSPs from several EC1 residues were followed during the titration and the titration curves from these residues were used to estimate the K_d values of ADTc9 to EC1 (Figure 3C). The result from the titration curve of L21 has Kd of 190 μM while the titration curve results form I53 and V98 gave K_ds of 403 μM and 480 μM, respectively (Table 3). Overall, the K_d values of ADTc9 peptide were between 190 to 500 μM, indicating a weak-binding property of ADTc9 peptide to EC1.

4.3.4 Binding Characteristics of HAV6 Peptide to the EC1 Domain:

There were a total of four clusters found in docking of HAV6 peptide to EC1 domain (Table 2). Cluster #1 (Figure 1D) and cluster #3 (Figure 1E) with the top HADDOCK scores were used to represent the binding of HAV6 peptide to EC1**.** The EC1 residues that are involved in binding to cluster #1 are the T39, G40, D44, T45, F77, H79, A87, and P91 (Figure 2D) and cluster#3 are T39, G40, D44, T45, F77, and H79. This suggests that the binding pocket for HAV6 consists of residues T39, G40, D44, T45, F77, and H79 in the EC1 domain. The EC1 residues were affected by titration with HAV6 and showed good titration curves were used to estimate the K_d values of HAV6 (Figure 3D). K_d values of HAV6 estimated using residues T97, I4, V98, and V48 were 182, 225, 410, and 520 μM (Table 3).

4.4 Discussion

The goal of this study was to determine the binding properties of ADTc5, ADTc7, ADTc9, and HAV6 peptides to the EC1 domain of h-E-cadherin because ADT and HAV peptides have been shown to modulate the intercellular junctions the BBB to improve brain delivery of molecules *in vivo*. The hypothesis is that these peptides bind to the extracellular domain of E-cadherin to modulate cadherin-cadherin interactions. Thus, the binding properties of ADT and HAV peptides to the EC1 domain of E-cadherin were evaluated because the X-ray and NMR structures of E-, N-, and C-cadherins have shown that the EC1 and EC2 domains

were involved in cadherin-cadherin interactions [9, 19, 25]. In the absence of X-ray data, a combination of NMR experimental data and molecular modeling methods (i.e., molecular dynamics and docking simulations) is a powerful tool to study ligand-receptor complexes for evaluating potential mechanisms of action of the ligand in biological systems [26, 27]. The EC1 domain used in this study contains a head EC1 domain with seven β-strand and two short α-helices and a tail region derived from a 28 amino acid sequence from the EC2 domain. In this study, the starting structure was derived from the X-ray structure h-E-cadherin with the extended tail region. Molecular dynamic simulations were carried out to the EC1 starting structure and the final structure from MD simulations showed the tail domain swings into the head part to EC1 to form interactions [28].

The cyclic ADTc5 peptide has been shown to improve the brain delivery of marker molecules in vivo. Thus, this study was done to evaluate its binding properties to the EC1 domain of E-cadherin. Furthermore, ADTc7 and ADTc9 peptides were designed as derivatives of ADTc5 in an attempt to understand role of the Val6 residue for its activity and design derivatives with better BBB modulatory activity. Mutation of Val6 residue was carried out because it was found previously to be important for peptide activity. In this study, the Val6 residue in ADTc5 was replaced with a negatively charged Glu6 in ADTc7 and an aromatic Tyr6 residue in ADTc9. Thus, the effects of these mutations were evaluated to the binding properties of ADTc7 and ADTc9 peptides to EC1. For ADTc5, seven out of eight

clusters from NMR-constrained molecular docking simulations bind to P6, S8, P10, T99, D103 and K105 residues (Figures 1A & 2A); the binding site for these clusters was consistent with the NMR data for chemical shift changes of the binding site residues. One out of eight clusters showed found ADTc5 bind to another a region around the Q23, N27, K30, Y36, and G58 residues. This region was different from the binding pocket of seven other clusters and was supported by the NMR data.

The mutation of Val6 to Glu6 in ADTc7 peptide shifts the binding site of ADTc7 slightly to a binding pocket involving residues I4, N20, L21 and K105 (Figures 1B and 2B); the CSP NMR data showed considerable CSP on the I4 and L21 residues (Figure 2B). There was an overlap between the binding region of ADTc5 and ADTc7. The docking experiments indicated that ADTc9 has a binding site defined by S9, E13, N20, L21, K105, P106, T125, and S126 residues (Figures 1C & 2C). ADTc9 peptide had strong influence the L21 residue with considerable high CSP values upon peptide titration. There is binding region overlap between ADTc9 and ADTc7 and slight overlap with ADTc5 binding site (Figure 4A).

The differences in binding pockets of different ADT peptides on the EC1 domain could influence in the binding affinity (i.e., K_d values). The mechanism activity of ADT peptides is proposed to be due to inhibition of domain swapping in the *trans*-dimer of two EC1 domains during cadherin-cadherin interaction. It has been shown that the domain swapping in C-cadherin domain is generated by

swapping W2 residues between the N-termini β-sheets of one EC1 domain to another EC1 domain. As in the C-cadherin, we also propose that the N-terminal residues of E-cadherin such W2, V3, I4, P5, P6 are involved in the domain swapping between two EC1 domains, in which the W2 side-chain interacts with the I24, Y36, S78, and A80 residues on the the hydrophobic pocket of another EC1 [9]. In order to perform domain swapping, the N-terminal β-sheet should be moved away from the current interactions within its EC1 domain (Figure 4C). However, the ADT peptide bind to the I4, P5 and P6 residues in this β-sheet; thus, this binding prevents the β-sheet to move away from its current interaction for performing domain swapping. Another possible mechanism is that the binding of ADT peptides to the EC1 could prevent *cis*-dimer formation from the EC1 domain of one protein to the EC2-domain of a neighboring protein from the same cell membranes.

The blind docking HADDOCK experiments has been done as a control for NMR-constrain docking. In the blind HADDOCK experiments, all three cyclic ADT peptides showed consistency with NMR-constrained docking results (Figure 4B). The blind docking results showed cyclic ADT peptides clusters dock close to the "hot spot" region of EC1 (Figure 4B).

The HAV6 peptide binds to the region of residues T39, T45, F77 and H79 on the EC1 domain (Figures 1D & 2D), which is a different binding site than those of ADT peptides (Figure 4A). The binding site of HAV6 was similar to the binding site

of cyclic cHAVc3 peptide (Cyclo(1,6)Ac-CSHAVC-NH_2), which is a more potent peptide than HAV6 in modulating the BBB in vivo. The cyclic cHAVc3 peptide binds to the F77 and S78 residue on the EC1 domain [28].

The affinities of cyclic ADT and HAV6 peptides to human EC1 domain were determined using CSP values of the residues of EC1 upon peptide titrations. In general, the K_d values for ADT and HAV peptides fall in weak binding category (μM) to the EC1 domain (Table 3). The lowest estimated K_d values of ADTc5 (9 μM) and ADTc7 (10 μM) were lower than the lowest estimated K_d values of ADTc9 (190 μM) (Table 3). In other words, ADTc7 and ADTc5 peptides have higher affinity to than ADTc9 peptide to the EC1 domain. The affinity of HAV6 peptide to the EC1 domain (lowest K_d = 182 μM) was comparable to ADTc9 (190 μM). The cyclic cHAVc3 peptide has stronger binding affinity (K_d values = 5–20 μM) than linear HAV6 (Kd = 182 μM) [28] and these result is consistent with the in vivo data [18].

The activity of ADTc5 to modulate the BBB in vivo in Balb/c mice was higher than HAV6 peptide. With the same dose of ADTc5 and HAV6 (0.001 mmol/kg), the ADTc5 has higher enhancement of the brain deposition of Gd-DTPA than that of HAV6 in the brain of Balb/c mice [17]. At the same dose (0.01 mmol/kg), ADTc5 modulates the BBB for 2 h to allow the delivery of Gd-DTPA to the brain while the opening of the BBB is less than 1 h for HAV6 for delivering Gd-DTPA to the brain [17]. The in vivo activity of cyclic cHAVc3 to deliver Gd-DTPA

to the brain was also better than linear HAV6 peptide. Cyclic cHAVc3 peptide activity to modulate the BBB was comparable to ADTc5 peptide and it modulates the BBB opening for 2 h time frame. Thus, the in vivo data were congruent with the EC1 binding data [17]. These results also indicate that the Val6 residue is an important residue in ADT peptide and replacing it can have impact on the binding affinity and binding site location on the EC1 domain.

As shown in titration of the EC1 domain of with cyclic cHAVc3, the titration with ADT peptides (i.e., ADTc5, ADTc7, and ADTc9) and the linear HAV6 peptide also showed dramatic changes in the CSP in the D103 residue as well as other tail residues such as T125, G124, S126 (Figure 5). These changes presumably were due to conformational changes in the tail region upon peptide binding. The observed strong and medium CSP values upon titration with each peptide were shown in Figure 5. The molecular dynamic studies showed a dramatic change on the tail region from extended form away from the head EC1 domain to a folded form into the head EC1 to form globular structure. From our previous study, it is proposed that the D103 residue acts as a hinge for swinging the tail domain into the head EC1 domain (Figure 5, see arrow). The D103 residue is also involved with clusters of calcium binding residues (i.e., PENE, DQND and LDRE) at the interface between EC1 and EC2; the presence of calcium ions at the interface between domains (e.g., between EC1–EC2, EC2–EC3) causes cadherin to convert from a globular structure

with folded EC domains to a rod-like structure where the domains form an extended rod of extracellular domain of cadherin [2, 10, 29].

In conclusion, ADT peptides (ADTc5, ADTc7, ADTc9) bind to a different region than HAV peptides (e.g., HAV6 and cHAVc3) on the EC1 domain. Mutation of Val6 residue in ADTc5 can influence the binding properties of ADT peptides. ADTc5 and ADTc7 have better binding properties than ADTc9 and HAV6 peptide, which is consistent with the in vivo studies. This study suggest that the NMR and molecular modeling methods can be used to improve the BBB modulatory activity of ADT and HAV peptides before their evaluation in the in vitro and in vivo BBB models.

Table 1. Synthetic cadherin peptides sequences	
Name	**Sequence**
ADTc9	Ac-CDTPPYC-NH_2
ADTc7	Ac-CDTPPEC-NH_2
ADTc5	Ac-CDTPPVC-NH_2
HAV6	Ac-SHAVSS-NH_2

Table 2. Interacting EC1 residues for each HADDOCK cluster per peptide	
ADTc9	*Cluster#1* S9, P10, E13, K19, N20, L21, K105, P106, T125, G124, S126 *Cluster#2* S9, P10, E13, P16, N20, L21, W59, K105, F108, P106, T125, G124, S126 *Cluster#3* E13, P16, K19, N20, L21, K105, P106, T125, G124, Ser126 *Cluster#4* I4, P5, P6, I7, S8, P10, N20, L21, V22, W59, K105 *Cluster#5* P16, K19, N20, K105, P106, E107, F108, T125, S126, A132 *Cluster#6* P5, P6, I7, S8, P10, E13, N20, L21, D103, K105
ADTc7	*Cluster#1* E13, K19, N20, L21, K105, P106, G124, S126, T125 *Cluster#2* I7, P10, E13, K19, N20, L21, K105, P106, T125, S126 *Cluster#3* G15, P18, K19, N20, L21, P106, Glu107, F108, T125, S126, A132 *Cluster#4* I4, P5, P6, I7, S8 L21K105, V122 *Cluster#5* I7, S8, E13, K19, N20, L21, W59 K105, P106, T125 *Cluster#6** T109, F113, K114, G115, S116, M128, V130 *Cluster#7* I4, P5, I7, S8, P10, N20, L21, V22, Q23, K105, W59
ADTc5	*Cluster#1* S8, S9, P10, T99, D100, Q101, N102, D103, K105, *Cluster#2* P6, R68, T73, L95, T97, V98, T99, D100 *Cluster#3* P5, P6, I7, S8, P10, L21, T99 K105 *Cluster#4* I7, S8, S9, P10 T99, D100, Q101, N102, D103, N104, K105 *Cluster#5* P6, S8, S9, P10, T97, T99, D100, Q101, D103, K105 *Cluster#6** Q23, K25, E56, G58, S26, N27, Y36, I24, D29, K30 *Cluster#7* W2, V3, P5, P6, I7, S8, L21, V22, Q23, W59 *Cluster#8* P6, S8, P10, T99D103, K105
HAV6	*Cluster#1* T39, G40, D44, T45, F77, H79, A87, P91 *Cluster#2* T39, G40, D44, T45, F77, H79, A87, P91

	Cluster#3 T39, G40, D44, T45, F77, H79 *Cluster#4* T39, G40, D44, T45, F77, H79, T75, N93.

* Represent models that were dock differently from the other models for ADTc7 or ADTc5 peptides.

Table 3. K_d values in μM for each peptide for some EC1 residues				
Residues	**ADTc5**	**ADTc7**	**ADTc9**	**HAV6**
I4		10	255	225
L21			190	
I24	20			
I53	10		403	
V48		16	500*	520
G58	47			
T97		22		182
V98		10	480	410
G115	11	18		280
E119	38			250
T133	9	15		

Figure 1A

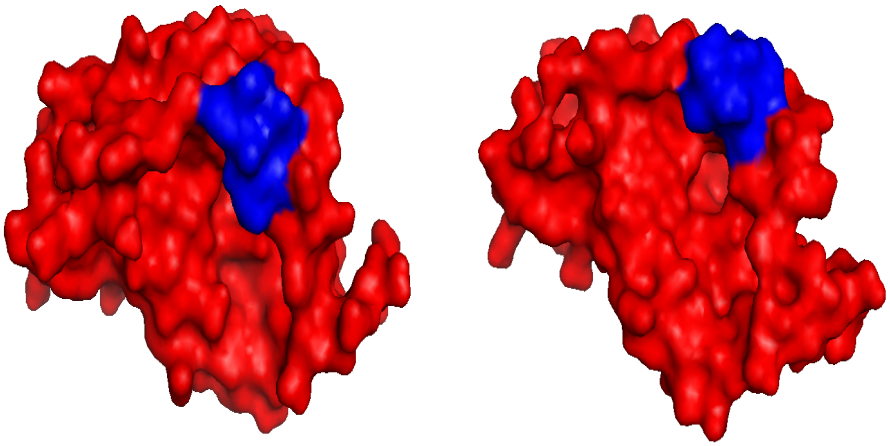

Cluster #5 **ADTc5** **Cluster #8**

Figure 1B

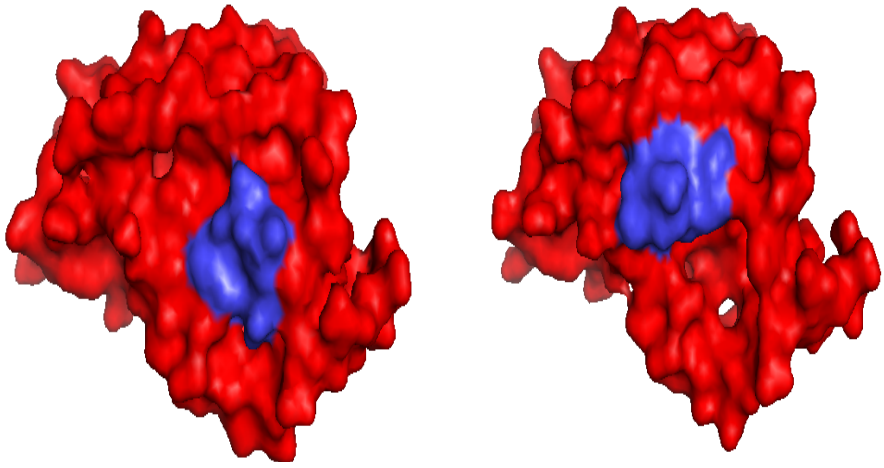

Cluster #1 **ADTc7** **Cluster #7**

Figure 1C

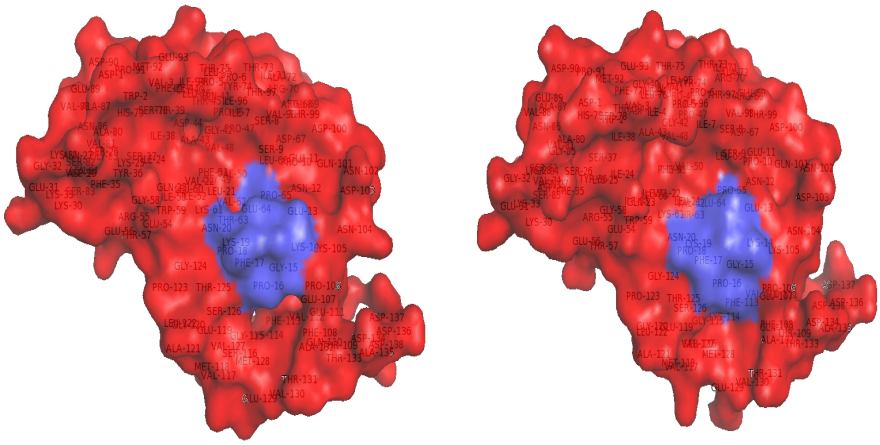

Cluster #1 **ADTc9** **Cluster #2**

Figure 1D

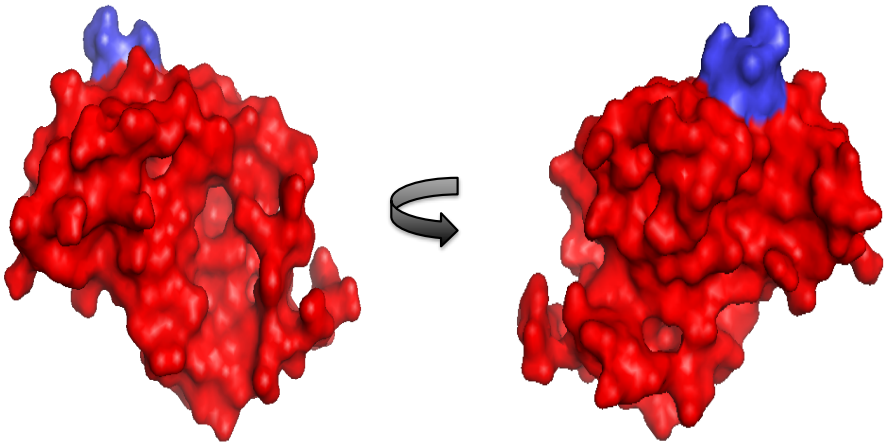

Cluster #1 **HAV6** **90° rotation cluster #1**

Figure 1E

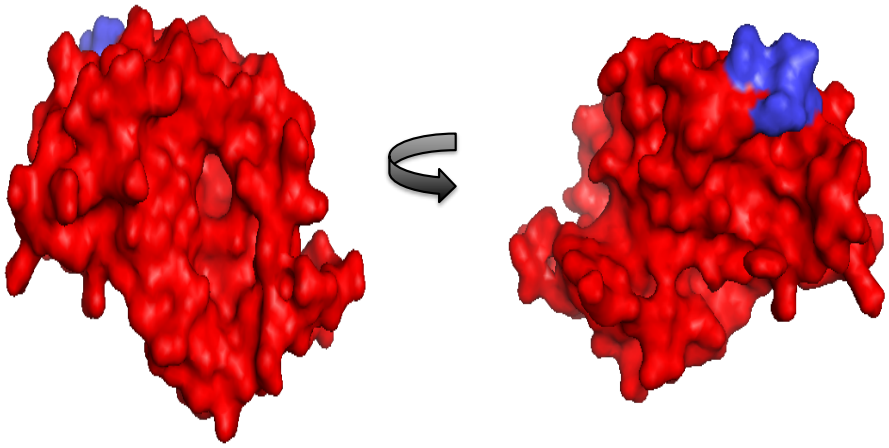

Cluster #3 **HAV6** **90° rotation cluster #1**

Figure 1. The blue colors indicate where **(A)** ADTc9, **(B)** ATDc7, **(C)** ADTc5 or **(D & E)** HAV6 peptides dock to the EC1 domain. A potential binding site for **(A)** ADTc5 on the EC1 domain as represented by clusters #5 and #8 with a common binding site around P6, S8, S9, T97, T99, P10, D100, Q101, D103, and K105 residues; **(B)** ADTc7 to the EC1 domain as represented by clusters #1 and #7 with a common binding site around E13, K19, N20, L21, K105, P106, G124, S126, and T125; **(C)** ADTc9 to the EC1 domain as represented by cluster #1 and cluster #2 with common binding site around S9, P10, E13, K19, N20, L21, K105, P106, G124, T125, and S126 residues; and **(D & E)** HAV6 to the EC1 domain as represented by cluster #1 and #3 with common binding site around T39, G40, D44, T45, F77, H79, A87, and P91 residues.

Figure 2A

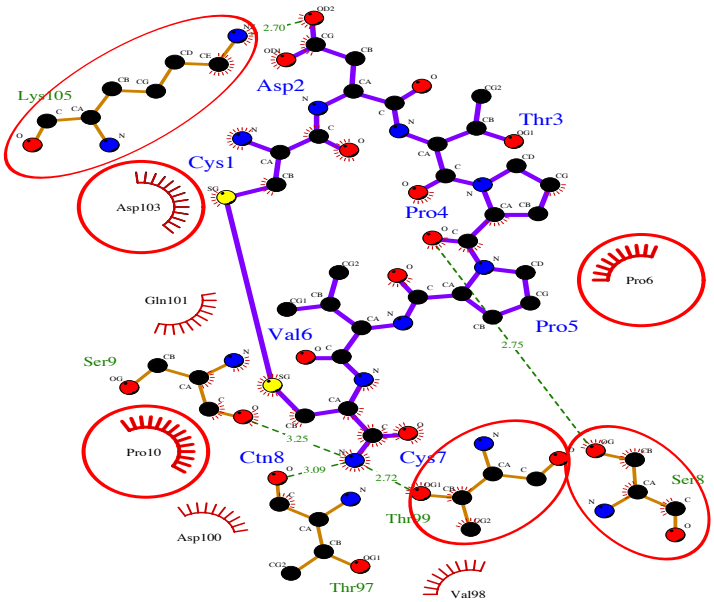

ADTc5 Cluster #5

Figure 2B

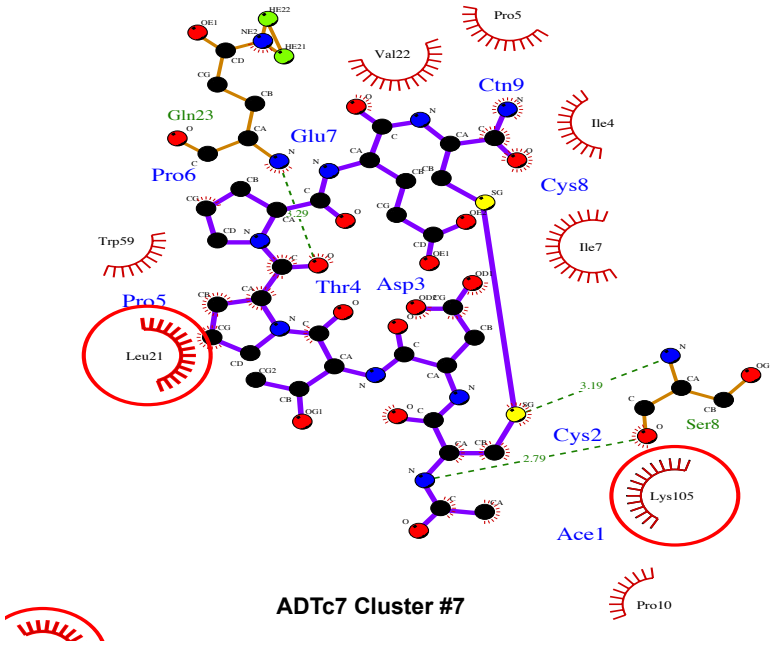

ADTc7 Cluster #7

Figure 2C

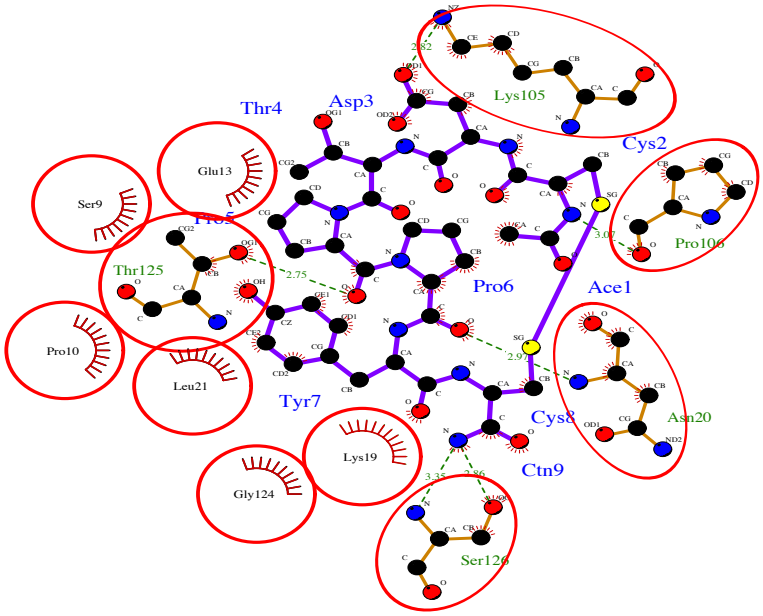

ADTc9 Cluster #1

Figure 2D

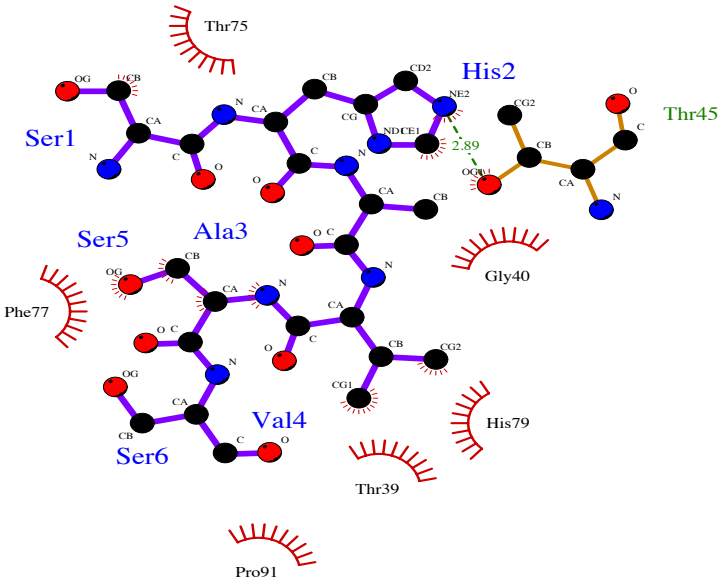

HAV6 Cluster #1

Figure 2. Shows the interaction of amino acids of each peptide with the residues on the EC1 domain for **(A)** ADTc5 cluster #5, **(B)** ATDc7 cluster #7, **(C)** ADTc9 cluster #1, and **(D)** HAV6 cluster #1. For simplicity only one cluster for each peptide was used to represent peptide-to-EC1 interaction.

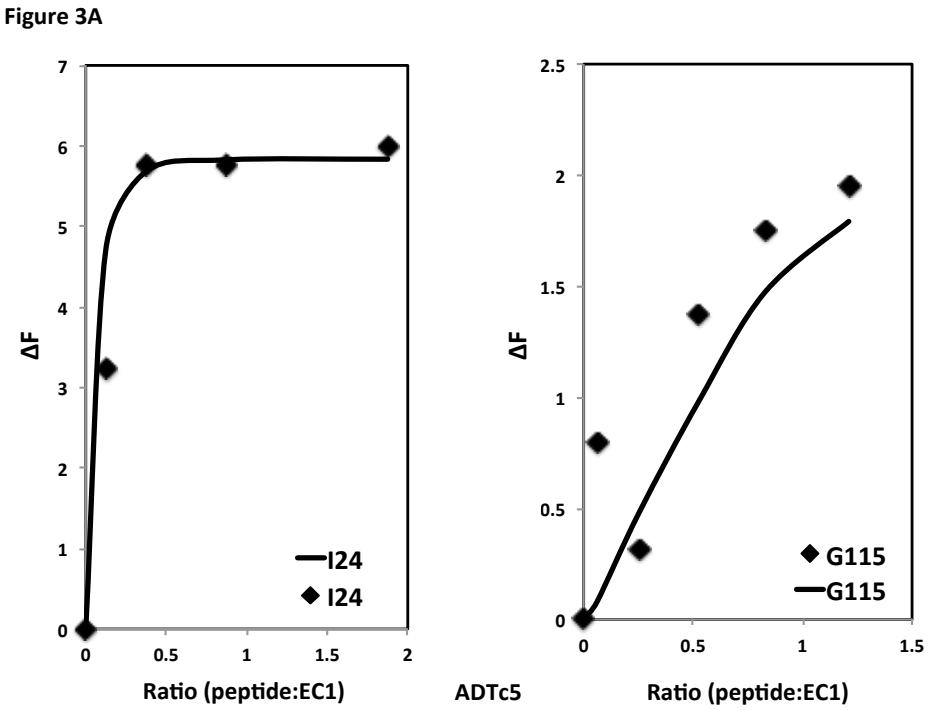

Figure 3B

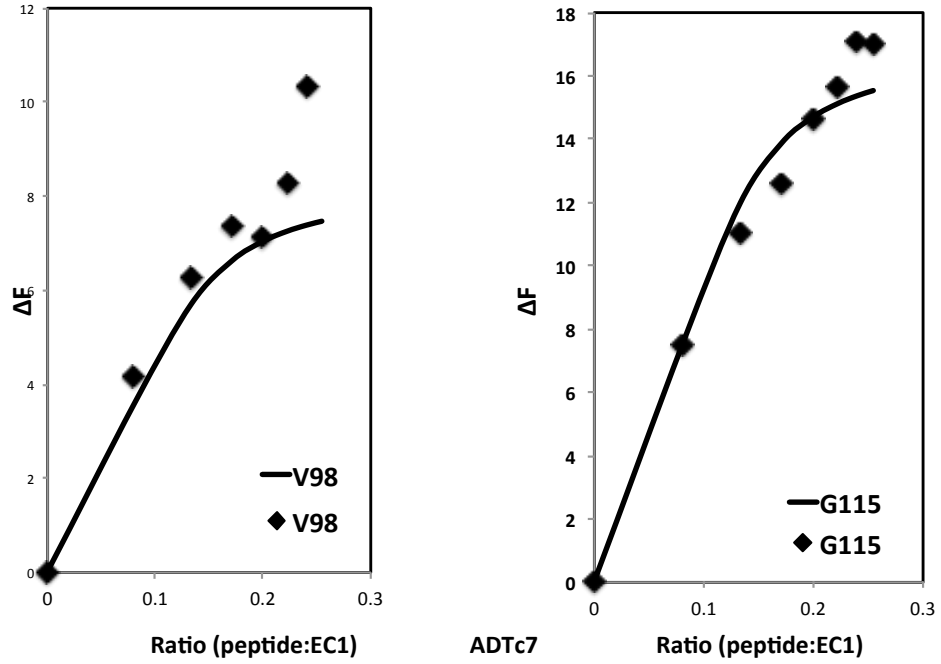

Figure 3C

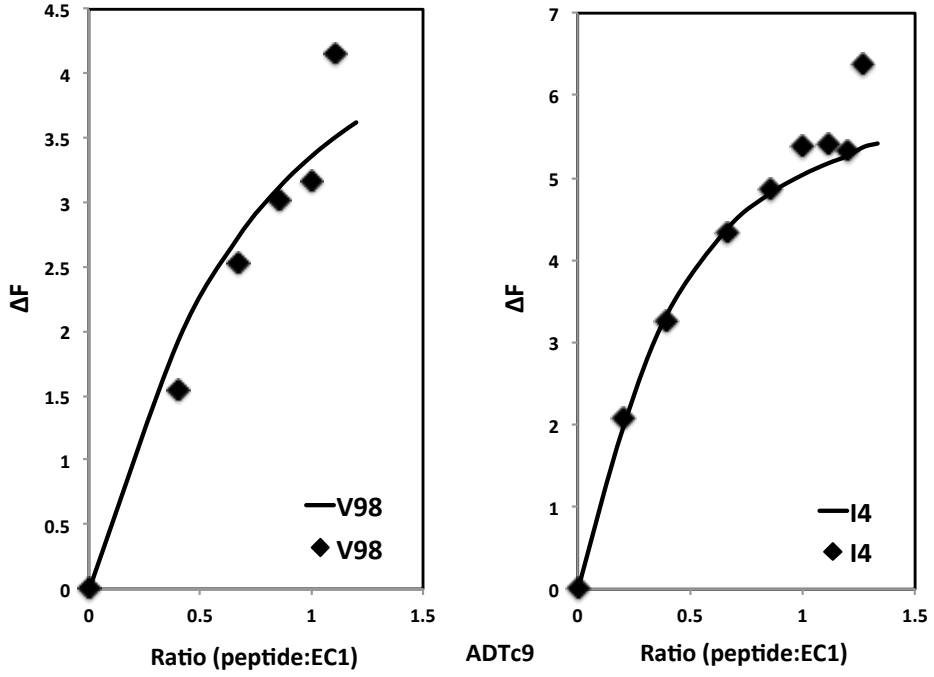

Figure 3D

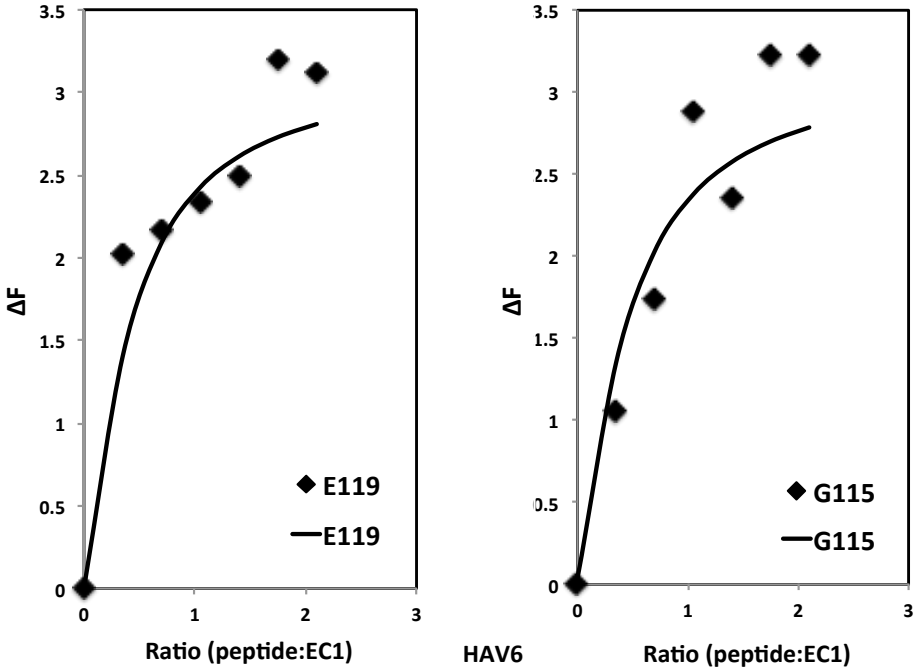

Figure 3. Representatives of the best curve fitting of EC1 titration to estimate Kd values of binding for each peptide, including **(A)** ADTc5, **(B)** ADTc7, **(C)** ADTc9, and **(D)** HAV6. Titration curves were plotted as peptide-to-EC1 ratio *vs.* ΔF (ΔF = $[(\Delta\delta^{1}H^{*}\ (800.234\ Hz/ppm))^{2} + (\Delta\delta^{15}N^{*}\ (81.096\ Hz/ppm))^{2}]^{1/2}$). Kd values were estimated using simulated curve obtained by the following equation: $\Delta_{obs} = \Delta_{max}\ ((P_o + K_d + L_o) - [(P_o + K_d + L_o)^2 - 4\ P_oL_o]^{1/2})/2\ P_o$.

Figure 4A

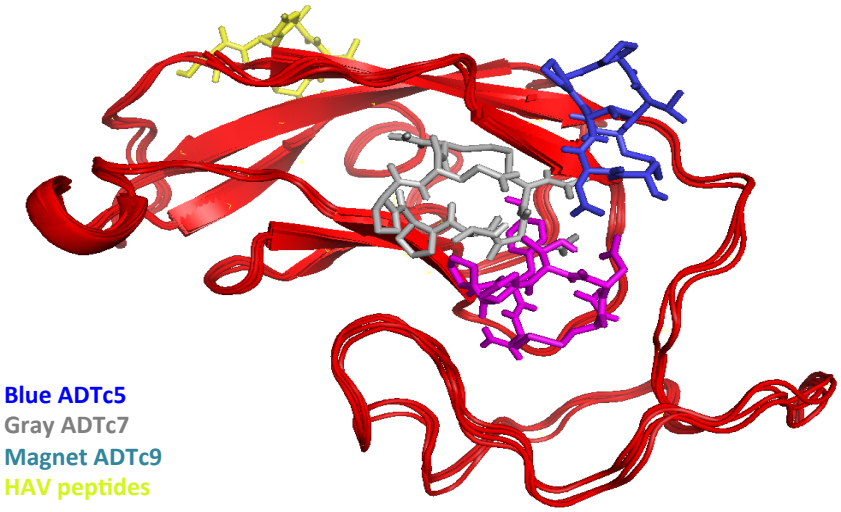

Figure 4B

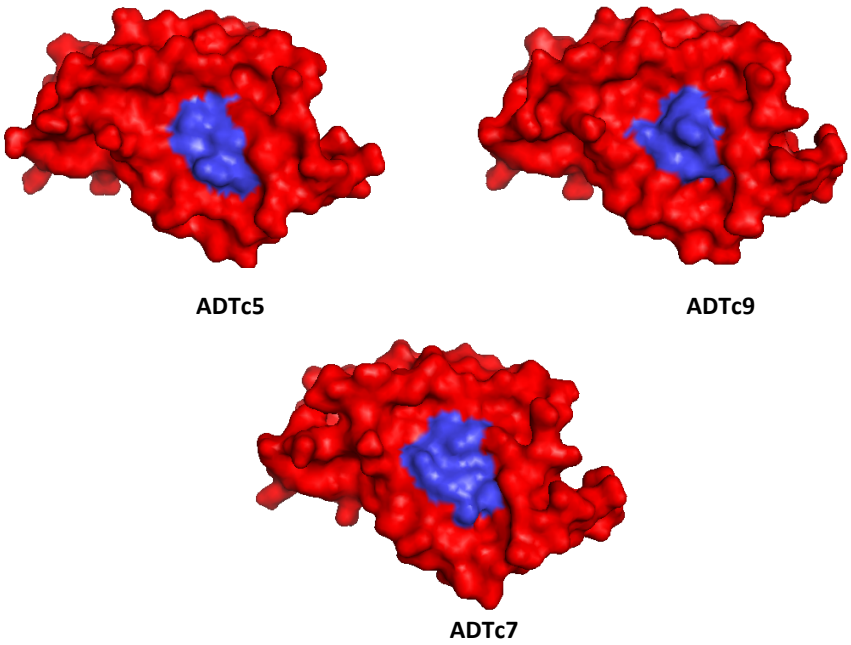

Figure 4C

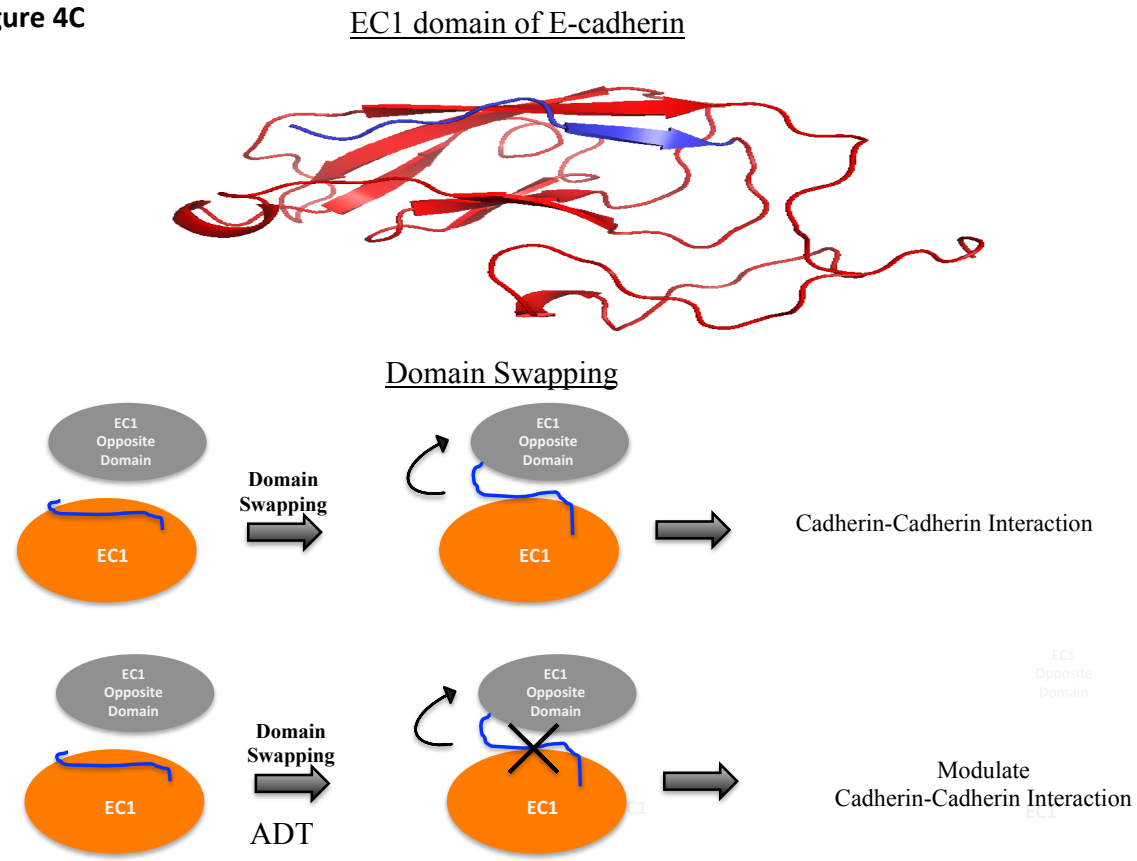

Figure 4. (A) Comparison for favorable binding sites for ADT and HAV peptides on the EC1 domain: ADTc5 (blue), ADTc7 (gray), ADTc9 (magnet), and HAV6 peptide (yellow). Cyclic ADT peptides showed a binding site different from the HAV6 peptide. **(B)** A common binding site for ADTc5, ADTc7, and ADTc9 on the EC1 domain from a blind docking molecular docking experiment with HADDOCK. **(C)** Shows (upper) MD structure of E-cadherin domain with N-terminus β-sheet labeled in blue color and (lower) diagrams for domain swapping mechanism with

N-terminus β-sheet of EC1 domain labeled in blue color, too. In domain swapping, the β-sheet of EC1 domain (red-filled circle) should move to let its W2 binds to its hydrophobic pocket on the opposite EC1 domain (green-filled circle). ADT peptides bind to I4, P5 and P6 residues (Table 3). The hypothesis for ADT peptides activity is preventing the β-sheet movement from EC1 (red-filled circle) by binding to β-sheet I4, P5 and P6 residues. Thus, modulate the E-cadherin-E-cadherin interaction.

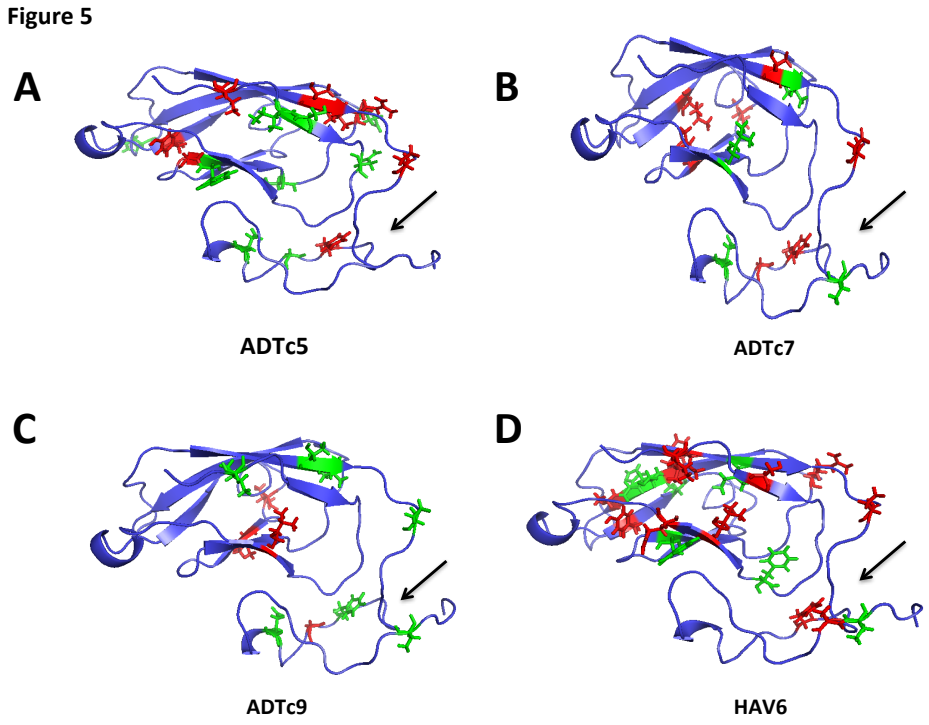

Figure 5. The MD structure of EC1 domain showing residues with high (red) and low (green) ΔF values when titrated with **(A)** ADTc5, **(B)** ATDc7, **(C)** ADTc9, and **(D)** HAV6 peptides. The favorable binding site for each peptide showed more residue experience large CSP (red) and low CSP presumably due to the

conformational change. All peptides showed chemical shift changes in tail residues (black arrows) that may result from dynamic behavior of the EC1 tail when it titrated with the peptide and not from direct binding events.

4.5 References:

1. Pal, D., K.L. Audus, and T.J. Siahaan, *Modulation of cellular adhesion in bovine brain microvessel endothelial cells by a decapeptide.* Brain Res, 1997. **747**(1): p. 103-13.
2. Makagiansar, I., et al., *Roles of E-cadherin and β-catenin in cell adhesion, signaling and possible therapeutic applications.* Curr Top Biochem Res, 2000. **2**: p. 51-61.
3. Tamura, K., et al., *Structure-function analysis of cell adhesion by neural (N-) cadherin.* Neuron, 1998. **20**(6): p. 1153-63.
4. Zheng, K., M. Trivedi, and T.J. Siahaan, *Structure and function of the intercellular junctions: barrier of paracellular drug delivery.* Curr Pharm Des, 2006. **12**(22): p. 2813-24.
5. Wheelock, M.J., et al., *Cadherin switching.* Journal of cell science, 2008. **121**(6): p. 727-735.
6. van Roy, F. and G. Berx, *The cell-cell adhesion molecule E-cadherin.* Cell Mol Life Sci, 2008. **65**(23): p. 3756-88.
7. Angst, B.D., C. Marcozzi, and A.I. Magee, *The cadherin superfamily: diversity in form and function.* Journal of cell science, 2001. **114**(4): p. 629-641.
8. Koch, A.W., K.L. Manzur, and W. Shan, *Structure-based models of cadherin-mediated cell adhesion: the evolution continues.* Cell Mol Life Sci, 2004. **61**(15): p. 1884-95.
9. Boggon, T.J., et al., *C-cadherin ectodomain structure and implications for cell adhesion mechanisms.* Science, 2002. **296**(5571): p. 1308-13.
10. Overduin, M., et al., *Solution structure of the epithelial cadherin domain responsible for selective cell adhesion.* Science, 1995. **267**(5196): p. 386-9.
11. Chappuis-Flament, S., et al., *Multiple cadherin extracellular repeats mediate homophilic binding and adhesion.* J Cell Biol, 2001. **154**(1): p. 231-43.

12. Makagiansar, I.T., et al., *Improving the selectivity of HAV-peptides in modulating E-cadherin-E-cadherin interactions in the intercellular junction of MDCK cell monolayers.* Pharm Res, 2001. **18**(4): p. 446-53.

13. Sinaga, E., et al., *Increasing paracellular porosity by E-cadherin peptides: discovery of bulge and groove regions in the EC1-domain of E-cadherin.* Pharm Res, 2002. **19**(8): p. 1170-9.

14. Lutz, K.L., et al., *Inhibition of E-cadherin-mediated cell-cell adhesion by cadherin peptides*, in *Peptides: Frontiers of Peptide Science*, J.P. Tam and P.T.P. Kaumaya, Editors. 1997, Kluwer Academic Publisher: Dordreccht/Boston/London. p. 753–754.

15. On, N.H., et al., *Modulation of blood-brain barrier permeability in mice using synthetic E-cadherin peptide.* Mol Pharm, 2014. **11**(3): p. 974-81.

16. Kiptoo, P., et al., *Enhancement of drug absorption through the blood-brain barrier and inhibition of intercellular tight junction resealing by E-cadherin peptides.* Mol Pharm, 2011. **8**(1): p. 239-49.

17. Laksitorini, M.D., et al., *Modulation of intercellular junctions by cyclic-ADT peptides as a method to reversibly increase blood-brain barrier permeability.* J Pharm Sci, 2015. **104**(3): p. 1065-75.

18. A.Alaofi, N.O., P.Kiptoo, T. Williams, D. W. Miller, T. Siahaan, *Comparison of Linear and Cyclic HAV Peptides in Modulating the Blood-Brain Barrier Permeability: Impact on Delivery of Molecules to the Brain.* Journal of Pharmaceutical Sciences, 2015(Accepted).

19. Parisini, E., et al., *The crystal structure of human E-cadherin domains 1 and 2, and comparison with other cadherins in the context of adhesion mechanism.* J Mol Biol, 2007. **373**(2): p. 401-11.

20. A. Alaofi, E.F., V. Prasasty, A. Anbanandam, K. Kuczera, J. Laurence, T. Siahaan, *Probing the Interaction between cHAVc3 Peptide and the EC1 domain of E-cadherin using NMR and*

Molecular Dynamics Simulations. J. Biomolecular Structure and Dynamics, 2015.

Submitted.

21. Farokhi E. , L.J., T.Siahaan *Determination of Binding Sites of CAdherin Peptides on th EC1 domain of E-cadherin using NMR Spectroscopy.* Master Thesis, 2014.
22. Vivitri D. Prasasty, M.E.K., Elinaz Farokhi, Asokan Anbanandam, Seetharama Jois, Usman S.F. Tambunan, Jennifer Laurence, and Teruna J. Siahaan, *Determination of Binding Sites of Cadherin Peptides on the EC1 domain of E-cadherin: Modulators of the Blood-Brain Barrier.* PhD Thesis, 2013.
23. de Vries, S.J., M. van Dijk, and A.M. Bonvin, *The HADDOCK web server for data-driven biomolecular docking.* Nat Protoc, 2010. **5**(5): p. 883-97.
24. Wassenaar, T.A., et al., *WeNMR: Structural Biology on the Grid.* Journal of Grid Computing, 2012. **10**(4): p. 743-767.
25. Hetényi, C. and D. van der Spoel, *Efficient docking of peptides to proteins without prior knowledge of the binding site.* Protein science, 2002. **11**(7): p. 1729-1737.
26. Stark, J.L. and R. Powers, *Application of NMR and molecular docking in structure-based drug discovery.* Top Curr Chem, 2012. **326**: p. 1-34.
27. Nagar, B., et al., *Structural basis of calcium-induced E-cadherin rigidification and dimerization.* Nature, 1996. **380**(6572): p. 360-4.
28. Lutz, K., et al., *Structure, function and modulation of E-cadherins as mediators of cell-cell adhesion.* Curr. Top. in Pept. Prot. Res, 1997. **2**: p. 69-82.

CHAPTER 5

Summary, Conclusions and Future Directions

5.1 Summary and Conclusions

The objectives of this project were to modulate the blood-brain barrier (BBB) for brain deliver of molecules using cadherin peptides and to understand the mechanism of action of cadherin peptides. Although drug or diagnostic molecules might be available for treatment or diagnosis of brain diseases, the BBB acts as physical and enzymatical barriers to limit molecules from entering the brain with a sufficient and effective dose for pharmacological activity [1]. Thus, it makes the treatment of brain diseases challenging as well as contributing to high health care costs.

The second chapter showed that cyclic HAVc3 peptide had better activity than linear HAV (HAV4) peptide in enhancing the delivery of marker molecules to the brain using in vitro and in vivo models of the BBB. In the vitro model, cHAVc3 has shown better activity than HAV4 peptide in modulating the intercellular junctions of MDCK cell monolayers. In the vivo model, both peptides enhance the brain deposition of Gd-DTPA and cyclic cHAVc3 peptide also has better BBB modulatory activity than HAV4 peptide. The duration of BBB modulation in vivo for cHAVc3 was between 2–4 h while it was less than 1 h for HAV4 peptides. For a larger molecule, cHAVc3 and HAV4 peptides can only delivery an IR-dye-800cw PEG (25 kDa) to the brain when they delivered together without time delay. The stability of cHAVc3 in rat plasma is about five-times ($t_{1/2}$ = 12.9 h) higher compared to HAV4 peptide ($t_{1/2}$ = 2.4 h).

The hypothesis for the activity of cadherin peptides (HAV or ADT peptides) is that they bind to the EC1 domain to interrupt E-cadherin-to-E-cadherin interactions in

the intercellular junctions of the BBB. Using NMR and computational experiments, the binding sites and dissociation constants of cHAVc3 peptide were determined in Chapter 3. The NMR results showed that the cHAVc3 peptide binds to the EC1 domain of E-cadherin, providing support for the mechanism its BBB modulatory activity. The MD simulations data of EC1 showed that the tail part of the protein interacted with the head part of EC1 domain; this suggests that it mimicked the solution conformation of EC1. The tail part of the protein is sandwiched to the head of EC1 domain. The NMR titration data between cHAVc3 and EC1 showed that it bound to Y36, I38, F77, S78, and I94 residue on the EC1 domain and the K_d value of cHAVc3 peptide to EC1 domain was estimated to be around 0.5–7.0 X 10^{-5} M.

Protein-protein interaction is important for biological cellular functions such as adhesion or signaling function. This interaction usually involves large surface areas between two proteins (e.g. domains) but the effectiveness and specificity of the binding often include a small area or "hot spot" [2]. In Chapter 4, binding sites of cyclic ADT and linear HAV peptides to EC1 domain were investigated and compared. The finding shows that cyclic ADT peptides (ADTc5, ADTc7, and ADTc9) have a common overlapping binding region on the EC1 domain while the HAV6 peptide has a different binding site on the EC1 domain. ADTc5 and ADTc7 have similar affinity to the EC1 domain (K_d = 10 μM) and they have better affinity than ADTc9 and HAV6 peptides (Kd ~ 190 μM).

5.2 Future Directions

5.2.1 Optimization of Molecules being Delivery to the Brain

As the delivery of molecules across the BBB remains to be a major challenge for drug delivery to the brain, the distribution of molecules in the brain tissues can pose another challenge. Although our studies showed the enhancement of marker molecules (such as Gd-DTPA and IR-dye-800cw PEG) to the brain models using cHAVc3 peptide, less information is known about the distribution of marker molecules in the brain. The extravascular space of the brain is narrow and tortuous and less molecules can traverse the extravascular space and reach the target site(s). In the future, we would like to investigate the bioavailability and brain distribution of delivered molecules upon enhanced delivery by cadherin peptides. One of the precise methods to evaluate molecules distribution in the brain tissues is by utilizing the brain slice method. This method keeps much of the brain cellular component integrity allowing us to accurately measure the distribution of molecules in the brain.

5.2.2 Improving Specificity of HAV and ADT peptides

The current clinical methods for the brain delivery are either by medical surgeries of the brain or a prolonged disruption of the BBB using hyperosmotic solutions [3]. Using peptides as BBB modulators to promote delivery to the brain has some advantages compared to the current hyperosmotic solution method. The BBB modulation by synthetic E-cadherin peptides (as BBB modulators) may have benefited

compared to hyperosmotic modifiers such as 25% mannitol. The reason is that the chemistry of peptides allows one to do chemical modification on the peptides. For example, the specificity or potency of these peptides can be improved by mutation of residues flanking motif sequence (such as HAV) or making more rigid cyclic peptide using peptide bonds instead of disulfide bonds in cyclic HAV and ADT peptides. Another way to increase the specificity is by targeting a certain adhesion protein in the BBB such as the VE-cadherin [4]. Identifying the binding sites and dissociation constants for HAV and ADT peptides in EC1 domain or other domain of VE-cadherin may help to design molecules that bind specifically to VE-cadherin. This will increase targeting for endothelial cells and provide fewer tissues affected by synthetic E-cadherin peptide modulators.

5.2.3 Screening BBB modulators affinities

NMR techniques can provide binding information at atomic level in solution state. In addition, NMR methods can be used in high throughput (HP) drug design assays since it is a fast acquisition technique [5]. Thus, NMR can be used to explore the affinity peptide mutants from HAV or ADT peptides to enhance their potency and specificity to deliver drugs or molecules to the brain.

5.2.4 Brain Diseases: Treatment and Diagnosis

As cyclic cHAVc3 peptide enhanced the delivery of molecules (i.e. small and large molecules) to the brain; this suggests cHAVc3 peptide is able to increase drug or diagnostic molecules, either small or large, to brain models. In the future, cHAVc3 will be used deliver large protein molecules, such as brain-derived neurotrophic factor (BDNF) and nerve growth factor (NGF), to the brain of neurodegenerative diseases such as Alzheimer's and Parkinson's to stimulate neuroregeneration in the brain [6].

5.3 References

1. Pardridge, W.M., *The blood-brain barrier: bottleneck in brain drug development.* NeuroRx, 2005. **2**(1): p. 3-14.
2. Adler, M.J., A.G. Jamieson, and A.D. Hamilton, *Hydrogen-bonded synthetic mimics of protein secondary structure as disruptors of protein-protein interactions*, in *Small-Molecule Inhibitors of Protein-Protein Interactions*. 2011, Springer. p. 1-23.
3. Siegal, T., et al., *In vivo assessment of the window of barrier opening after osmotic blood-brain barrier disruption in humans.* J Neurosurg, 2000. **92**(4): p. 599-605.
4. Giannotta, M., M. Trani, and E. Dejana, *VE-cadherin and endothelial adherens junctions: active guardians of vascular integrity.* Developmental cell, 2013. **26**(5): p. 441-454.
5. Gao, G., J.G. Williams, and S.L. Campbell, *Protein-protein interaction analysis by nuclear magnetic resonance spectroscopy.* Methods Mol Biol, 2004. **261**: p. 79-92.
6. Scott, S.A. and K.A. Crutcher, *Nerve growth factor and Alzheimer's disease.* Rev Neurosci, 1994. **5**(3): p. 179-211.